AN EXAMINATION OF INFLUENZA IMMUNITY IN PIGS AND THEIR ROLE IN ASSESSING ANTIVIRAL THERAPIES FOR HUMANS

A Dissertation presented to

the Faculty of the Graduate School

at the University of Missouri-Columbia

In Partial Fulfillment

of the Requirements for the Degree

Doctor of Philosophy

By

DARLING MELANY DE CARVALHO MADRID

Dr. John Driver, Dissertation Supervisor

December 2022

The undersigned, appointed by the dean of the Graduate School, have examined the dissertation entitled

"An examination of influenza immunity in pigs and their role in assessing antiviral therapies for humans"

presented by Darling Melany de Carvalho Madrid,

a candidate for the degree of Doctorate of Philosophy

and hereby certify that, in their opinion, it is worthy of acceptance.

_____

Professor John Driver

_____

Professor Kiho Lee

_____

Professor Wenjun Ma

_____

Professor Wesley Warren

DEDICATION

To my family.

ACKNOWLEDGEMENTS

This work would not have been possible without the help of many individuals. Each of them contributed to my success in their own way. I'd like to express my gratitude to them. First, I would like to thank my major advisor, Dr John Driver, for his relentless support, dedication, and enormous patience. His valuable guidance always helped me grow both as a person and as a researcher. His enthusiasm for science and exploring new research directions is contagious.

I would like to extend my gratitude to the members of my committees both the University of Florida and the University of Missouri. They have provided me with guidance, useful critiques and mentoring during my research and development as a scientist. Thank you, Drs John Bromfield, David Pascual, Leah Reznikov, Kiho Lee, Wenjun Ma and Wes Warren. I would also like to thank our collaborators, the Dr Lednicky lab, Dr Castleman and Dr Ian Hawkins. A special thank you to the technical staff for excellent care of animals and for helping plan the animal experiments. To the past and present members of the Driver lab, thank you for helping me with the experiments, guiding me in my studies and sharing good moments. Thank you as well to my past and present fellow graduate students for making the program such a friendly and supporting place.

To my friends in my hometown and scattered around the globe, thank you for holding my hand, keeping my head high, and my heart light. And finally, to my family, both in Brazil and in the U.S., thank you for the patience, understanding, support, and love. Thank you for accommodating for all the times I could not be there. Thank you for always believing in me. A special thank you to my parents, for being my number one fan club, and for my husband, Dillan, who through thick and thin walked this path with me and was always there to lift me up.

Thank you all for believing in me and in my dreams.

TABLE OF CONTENTS

LIST OF TABLES

LIST OF FIGURES

NOMENCLATURE

AAL-2	Sphingosine-1-phosphate receptor agonist
AMCF-II	Macrophage chemotactic factor 2
BALF	Bronchoalveolar lavage fluid
BAM	Butorphanol, azaperone and medetomidine
CD62L	L-selectin
cDC1	Classical type 1 dendritic cell
cDC2	Classical type 2 dendritic cell
CTFR	Cystic fibrosis transmembrane conductance regulator
d.p.c	Days post contact
d.p.i	Days post infection
DC	Dendritic cell
DEG	Differentially expressed gene
EOMES	Eomesodermin
FASL	FAS ligand
FDR	False discovery rate
GO	Gene ontology
GO-BP	Gene ontology biological process
GO-CC	Gene ontology cellular component
GO-MF	Gene ontology molecular function
HA	Hemagglutinin

HBSS	Hank's Balanced Salt Solution
IACUC	Institutional Animal Care and Use Committee
IAV	Influenza A virus
IFN	Interferon
IFN-γ	Interferon gamma
IL	Interleukin
ILC	Innate lymphoid cell
iNKT	Invariant natural killer T cell
IP-10	Interferon gamma-induced protein 10
KEGG	Kyoto Encyclopedia of Genes and Genomes
LN	Lymph node
MAIT	Mucosal associated invariant T
MDA5	Melanoma differentiation-associated protein 5
MHC	Major histocompatibility complex
moDC	monocyte-derived dendritic cell
MR1	Major histocompatibility complex class I-related gene protein
NA	Neuraminidase
NAI	Neuraminidase inhibitor
NET	Neutrophil extracellular trap
NK	Natural killer
NKT	Natural killer T cell
PBS	Phosphate-buffered saline
pDC	Plasmacytoid dendritic cell

pdmH1N1	A/California/04/2009 H1N1
PI	Propidium iodide
PIM	Pulmonary intravascular macrophages
PR8	A/Puerto Rico/8/1934 H1N1
PU.1	Spi-1 proto-oncogene
RIG-I	Retinoic acid-inducible gene 1
RNA	Ribonucleic acid
ROR	Retinoid orphan receptor
RT-qPCR	Reverse Transcriptase real time PCR
SA	Sialic acid
scRNA-seq	Single-cell RNA sequencing
SEM	Standard error of mean
$TCID_{50}$	Median Tissue Culture Infectious Dose
T_{CM}	Central memory T cell
TCR	T cell receptor
T_{EM}	Effector memory T cell
Tfh	Follicular helper T cell
Th	T helper cell
TLR	Toll-like receptor
TNFα	Tumor necrosis factor alpha
TRAIL	Tumor necrosis factor-related apoptosis inducing ligand
T_{RM}	Tissue resident memory T cell
UMAP	Uniform manifold approximation and projection

WC1	Workshop cluster 1
WHO	World Health Organization

AN EXAMINATION OF INFLUENZA IMMUNITY IN PIGS AND THEIR ROLE IN ASSESSING ANTIVIRAL THERAPIES FOR HUMANS

Darling Melany de Carvalho Madrid

Dr. John Driver, Dissertation Supervisor

ABSTRACT

The lung is dynamic barrier organ with a complex cell population. Pulmonary immune cells must balance an effective and tolerogenic response to keep homeostasis. Due to numerous similarities to the human respiratory system, the pig is an excellent biomedical model for lung diseases, however many aspects of the porcine immune system remain poorly characterized. Moreover, influenza A viruses infect humans and pigs every year, causing major economic and health impacts. Nevertheless, there immunological mechanisms of influenza infection in the pig are not yet completely understood. Here we employ single-cell RNA sequencing (scRNA-seq) to create an immune atlas of the pig lung. Our data show conserved features as well as species-specific differences in cell states and cell types compared to mice and human pulmonary immune cells. We also investigate the impact an influenza infection on leukocytes, gene expression profiles and cell-cell communication of pig and mice. Our data provides important insights into the pig pulmonary immune response in healthy and influenza-infected animals at a higher resolution than was previously available.

CHAPTER ONE

REVIEW OF LITERATURE

Influenza

Influenza virus infections are a major burden for health care and the economy. Seasonal influenza is associated with 2% or almost 0.4 million deaths of respiratory causes each year (1, 2). Transmission is particularly prevalent in high-density areas and can occur year-round in warmer climates. However, in temperate regions it is considered a winter disease (3). The illness is characterized by fever, cough, headache, malaise, sore throat, and nasal secretions. Moreover, influenza infections can progress to secondary pneumonia, can trigger severe conditions such as asthma, and can increase mortality rate from other diseases (3, 4). Among adults, influenza is associated with over 5 million hospitalizations per year with the highest rates among those 65 years older (5). Among children under five years old, there is an estimated 10.1 million influenza-associated acute lower respiratory infection cases per year, leading to 870,000 hospitalizations globally(6).

Influenza viruses belong to the *Orthomyxoviridae* family and are currently classified into four genera (influenza A, B, C, and D). However, the influenza A virus (IAV) is the most common cause of human and animal epidemics worldwide (7, 8). IAV is an enveloped virus containing eight negative-sense RNA fragments and surface proteins hemagglutinin (HA) and neuraminidase (NA), which are used for classification into its distinct subtypes (9). IAVs enter the respiratory system of the host through direct mucosal contact, or through inhalation of droplets or aerosols and infect pulmonary epithelial cells by interaction of the viral HA with the cell sialic acid (SA)

receptors SAα2,6Gal and SAα2,3Gal. IAVs that infect humans preferably bind to SAα2,6Gal. In contrast, IAVs that infect avian species preferably recognize SAα2,3Gal (9).These SA receptors are differently distributed throughout the respiratory tract and may be linked to the tissue tropism of different IAV strains as regards whether they induce upper or lower respiratory tract infections (10, 11). The genomic IAV RNA is replicated by the viral polymerase complex within the cell nucleus. The transcripted viral proteins can also downregulate immune pathways in the host cell (12). Viral particles are then transported to the cell membrane where they assemble to form new IAV virions that bud off from the plasma membrane. The newly formed IAV virions are released from the cell by the NA protein, which is an enzyme that cleaves the SA bound HA complexes (13).

As with other RNA viruses, the process of IAV genome replication lacks proofreading-repair molecules, which results in high mutation rates (14). While many of the mutations lead to nonviable progeny or minor changes, mutations in the HA or NA proteins, or antigenic drift, can alter the antibody epitope binding regions and allow the virus to evade immune detection (15-19). A second mechanism that induces antigenic changes is viral reassortment, also known as antigenic shift. Rather than gradual changes, antigenic shift results in a complete new viral genome when a host cell is co-infected by two IAV with distinct genomes and during viral reproduction the parental strain segments may get mixed and produce a hybrid genotype (20). Reassortment of human and animal strains is particularly concerning as it can occasionally give rise to the emergence of IAV strains capable of causing pandemics (21, 22). Influenza pandemics represent a major global health threat as exemplified by the estimated 500 million infections and 50 million deaths worldwide in the 1918-1919 influenza pandemic (23). In livestock, influenza outbreaks can cause substantial disease that affects production and occasionally entire herds may be culled to

prevent the spread of infection (24, 25). The threat of pandemics continues to grow due to the increasing rate that new IAV virus variants with diverse epitopes are arising (19). This phenomenon makes it particularly challenging to develop efficient anti-influenza vaccines that offer long-lasting and/or heterologous protection (18, 26). Since human and livestock continue vulnerable to contracting influenza, due in part to inefficient IAV vaccines, there exists a growing need to be able to treat infected individuals with antiviral therapeutics in order to control the severity and spread of the disease.

Therapeutic strategies against influenza

There are four FDA-approved antiviral drugs recommended to treat seasonal influenza (27, 28). These include baloxavir marboxil, which inhibits the influenza RNA polymerase activity and prevents the transcription and replication of the viral genome and is approved for acute influenza and post-exposure prophylaxis (28, 29); and oseltamivir, peramivir, and zanamivir, which are neuraminidase inhibitors (NAI). NAIs interfere with the neuraminidase activity of the virus which prevents the release of new influenza virions from infected host cells (30). Oseltamivir is the most frequently prescribed NAI and the only NAI to be approved for prophylactic use (31, 32). Currently, there is strong clinical data to show that oseltamivir shortens the duration of flu symptoms. However, there is limited evidence that oseltamivir reduces influenza-induced disease complications, such as bronchitis, sinusitis, and ear infections (33, 34). Moreover, oseltamivir must be administered shortly after the onset of the disease to improve clinical signs (35, 36). Finally, there is some debate about whether oseltamivir can reduce hospitalizations and mortality (33, 34). Nevertheless, evidence supporting the positive effect of oseltamivir for influenza infections was strong enough that after the 2009 H1N1 influenza pandemic, the World Health Organization

(WHO) encouraged member states to stockpile oseltamivir preemptively as a protective measure against another influenza pandemic.

Due to the rapid mutation rate of IAV, there is a significant risk that resistance will arise against anti-influenza drugs making them obsolete. Indeed, amantadine and rimantadine, two M2 proton channel inhibitors approved by the FDA as anti-influenza drugs are no longer prescribed due to widespread resistance (30). Numerous influenza strains have also been reported to be oseltamivir resistant (37, 38) and even though baloxavir was only recently approved in 2018, a viral strain with a mutation in the PA subunit that confers resistant to baloxavir has been detected (39).

Despite the above-mentioned limitations and adverse effects, antivirals are still the main option to control existing IAV infection in humans. Therefore, there is substantial interest in discovering new anti-influenza compounds (40-42), and using existing antiviral drugs in combination. As regards the latter approach, several studies have demonstrated that combining various anti-influenza compounds can synergistically decrease viral load and influenza-induced clinical signs (43-45). This strategy appears to be particularly effective when anti-influenza drugs targeting viral proteins are combined with compounds targeting host factors that enhance antiviral immune responses since this approach mitigates virus replication through several independent pathways which is difficult to develop resistance against (46).

The host immune response plays an important role in determining the severity of disease from an IAV infection. Indeed, acute respiratory syndrome, which is caused by the pulmonary inflammation associated with excessive release of pro-inflammatory cytokines, is a major cause of patient death from influenza (47). Immunomodulatory drugs have been developed to counteract these effects, such as AAL-R which is an agonist for sphingosine-1-phosphate receptor, and

antagonists of pro-inflammatory cytokines such as interferon gamma-induced protein 10 (IP-10), interleukin 8 (IL-8) or CXCL8 receptors (48-50). In addition, broadly suppressive anti-inflammatory drugs such as corticosteroids have been shown to ameliorate lung injury in the mouse model (51). However, they may worsen patient outcomes in the clinic (52-54). A potential alternative is the stimulation of early innate immune defenses that in turn inhibit viral replication. This includes therapies that act by recruiting immune cells to the site of infection, which is an approach that has been tested in a number of mouse models of infectious diseases (55-58). This class of drugs includes derivatives of the glycolipid molecule α-galactosylceramide (α-GalCer).

The marine sponge-derived α-GalCer acts as a superagonist of natural killer T (NKT) cells, which are a minor immunoregulatory population of readily activated T cells that coordinate the early phases of immune responses (59-62). Unlike conventional T lymphocytes, NKT cells express a restricted T cell receptor (TCR) repertoire which recognizes a limited selection of lipid and glycolipid antigens presented by the non-polymorphic MHC class-I like CD1d molecule (60). Once activated, NKT cells rapidly stimulate both innate and adaptive immune responses that are important for controlling a wide range of infectious diseases (63, 64). This includes influenza infections as NKT cell-deficient mice develop much more severe infections compared to intact mice (65-68). Moreover, several studies have shown that *in vivo* treatment of mice with α-GalCer profoundly reduces the severity and duration of IAV infections (66, 68, 69).

The underlying mechanisms thought to mediate this protection were a migration of NKT cells and neutrophils into the lungs followed by the rapid release of cytokines including IL-2, IL-4, IL-12 and IFN-γ that stimulated innate defenses against influenza viruses. In addition, NKT cells provide a rapid source of IL-22 that protects airway epithelial cells from influenza-mediated destruction (67).

While these studies suggest that targeting the immunoregulatory activities of NKT cells is a promising strategy to reduce the severity and duration of influenza infections, they were conducted in mice, which are not a natural host of the influenza A virus. The translatability of influenza studies conducted on mice may be limited due to significant differences in host factors that can affect disease severity (70). The majority of influenza virus research in mice uses A/Puerto Rico/8/1934 (H1N1) (PR8) which is a mouse adapted influenza A virus strain that behaves differently to most circulating swine and human influenza viruses (71). Other differences are that, unlike humans, mice are uncapable of transmitting influenza infections and that influenza viruses usually cause much more severe disease in mice than in humans due to a dysfunctional murine Mx1 gene and because the virus usually infects the lower respiratory tract of mice (71).

Aside from differences in influenza infection susceptibility, there appear to be substantial differences in NKT cell frequency, subsets, and tissue localization between mice and humans, which may affect how these two species respond to NKT cell agonists, including α-GalCer (72, 73). In contrast, pigs are similar to humans for NKT cell frequency and tissue distribution (74-76). Moreover, the invariant T cell receptor chains expressed by pig NKT cells are homologous to the invariant chains expressed by human NKT cells (77). These observations suggest pigs may be a useful species to study the contribution of NKT cells to the human immune response, including how humans respond to NKT cell-based therapies.

We have demonstrated that α-GalCer can be administered as an adjuvant to enhance cellular and humoral immune responses induced by the influenza vaccines in pigs (78). In contrast, we found that α-GalCer had no effect on changing the course of an influenza infection in pigs pretreated 2 or 9 days before challenge, which expands NKT cells in the lungs (79). This may have been because the cytokine response induced by NKT cells had dissipated by the time pigs were

challenged with influenza or that the NKT cells had been rendered anergic by the intense stimulation. In another study, pigs that received an intranasal dose of α-GalCer at the time of influenza infection had reduced virus shedding, decreased viral replication in the lungs, and less lung inflammation compared to vehicle treated pigs (80). This study formed the basis of the current work which compared α-GalCer to oseltamivir for treating influenza virus infections in swine.

The pig as a biomedical model for IAV infection

Pigs are natural hosts of IAV and also susceptible to the same IAV subtypes that infect humans, namely H1N1, H1N2 and H3N2. They can also be infected by some avian IAV. Because of this susceptibility to co-infection by viruses of different origins, which occasionally leads to reassortment of novel IAVs, the pig is known as a "mixing vessel" of influenza viruses (81). There are reported cases of double and triple reassortant IAV isolated from pigs (82-84) and these new viruses have the potential to infect humans and cause pandemics. An example in the H1N1 2009 pandemic IAV which emerged from a reassortment of avian H1N1, swine H1N2 and human H3N2 (85-87). Influenza infections cause substantial economic losses for the swine industry since respiratory diseases are a major source of illness and IAV is readily transmitted high-density pig production system (88-91).

Pigs are considered an excellent model for studying human IAV infections. This is because pigs mirror humans for clinical signs of IAV infection; they present with coughing, sneezing, nasal discharge and dyspnea (92). Also parallel to humans, influenza infection induces a low mortality but can be aggravated by co-infections (88, 93). Furthermore, the anatomy of the respiratory tract between pigs and humans is much similar. Unlike rodents, pigs and humans possess tonsils that

are lymphoid structures that are involved in inducing immune responses against upper respiratory tract infections (94). Moreover, adult humans and pigs have similar lung size and anatomy, including that in both species the tracheobronchi have a tree-like structure (95). At the microscopic level, pigs and humans overlap for numerous immune and non-immune cell lineages, SA α2,3Gal and α2,6Gal receptor distribution and abundance, and their distribution of goblet cells, which produce a protective mucus layer. The mucus layer is formed by a mixture of mucins, or mucous glycoproteins, which contain SA that competitively inhibit virus infection by acting as decoy receptors (96). This similarity may explain why IAV usually cause upper respiratory tract infections in humans and pigs, whereas in mice influenza is primarily a lower respiratory tract infection (97).

Additional similarities include that the pig genome is of similar size, complexity and in general shows remarkable structural similarity to that of humans (98). Pigs and humans share approximately three times more similarities in genomic sequence identity than mice and humans (98, 99). Accordingly, the porcine and human immunomes are more similar to each other than the human and mouse immunomes (100). Furthermore, compared to other influenza animal models, pigs have a high degree of amino acid sequence similarity for human proteins related to the antiviral immune response, including Retinoic Acid-Inducible Gene 1 (RIG-I), Melanoma Differentiation-Associated protein 5 (MDA5), various Toll-Like Receptors (TLR) and TLR signaling molecules, interferon (IFN) and IFN receptors, Interferon Stimulated Genes (ISGs), and Inflammasome-associated proteins (93).

To fully understand the mechanisms that underly the anti-influenza immune response in pigs, it is critical to establish the role played by individual immune cell subsets during infection. This cannot be achieved using bulk analysis approaches that have commonly been used until now.

However, techniques like single cell RNA sequencing that can map the transcriptome of individual cells is beginning to provide a much clearer picture of the porcine immune system and how it reacts to perturbations, including viral infections.

The myeloid response against IAV

Different cell types orchestrate the response against IAV infection. They can be categorized according to the stage at which they participate in the immune response. Innate-type cells, many of which are from the myeloid lineage of hematopoietic cells, usually participate in the early stages of infection. In contrast, lymphocytes, including B cells and T cells, require time to develop effector functions and are usually involved at later stages of disease. The pig myeloid cell compartment is very similar to humans. The phenotype of pig polynucleated cells (neutrophils, basophils and eosinophils), also known as granulocytes, closely matches that of humans (101, 102).

Neutrophils are part of the initial response against infections and their secretion of CXCL12 is key to attracting virus-specific cytotoxic $CD8^+$ T cells into the infected tissue (103). However, IAV can induce neutrophil extracellular traps (NETs) which can cause damage to the lung epithelium. Indeed, a high quantity of NET production is correlated with IAV severity in patients (104). Excessive neutrophil migration to the lung has also been pointed out as one of the probable causes of why elderly patients are more prone to severe influenza, as that population presents a stronger neutrophil migration after infection (105).

Mast cells are innate sentinel-like cells present at various mucosal sites, including the lung. They are capable of producing multiple inflammatory cytokines, chemokines and proteases. It has

been shown that different strains of influenza, especially the more pathogenic avian types, are able to recruit mast cell progenitors to the site of infection (106). Once activated, mast cells produce proinflammatory mediators such as histamine and tryptase, which can contribute to virus-induced lung lesion (107). Moreover, different influenza strains can induce mast cell apoptosis, or programmed cell death, through intrinsic caspase-9 or extrinsic caspase-8 mediated pathway. While apoptosis can be a defense mechanism to limit viral replication, it has been suggested that virus-induced apoptosis can facilitate the spread of the virus (108). Additionally, mast cells over activation during IAV infection has been linked to the increased severity of lung diseases such as asthma (106). Apart from inducing pro-inflammatory responses that damage lung tissue, mast cells can produce the anti-inflammatory cytokine IL-10, that suppresses inflammation during the resolution phase of infection (109).

Monocytes are recruited to tissues during an infection differentiate into monocyte-derived dendritic cells or macrophages. Human monocytes can be divided into classical, intermediate, and nonclassical monocytes based on their expression of CD14 and CD16 markers. While most recruited monocytes are involved with inflammation and clearance of pathogens, nonclassical monocytes are long-lived and tend to patrol healthy tissues (110). Monocytes and monocyte-derived macrophages are susceptible to IAV infection, which may alter their ability to undergo phagocytosis and produce cytokines during an influenza infection (111). For example, $CD16^{+}$ monocytes have a more substantial proinflammatory role after IAV infection as they upregulate genes for cytokines *IL6* and *TNF*, signal transducer and activator of transcription *STAT1*/*2*/*3* and interferon regulatory factors *IRF1*/*2*/*7* (110). Pig monocytes can be subcategorized into $CX3CR1^{+/-}$ and $CCR2^{+/-}$, like the human counterparts (112), and their gene expression is more similar to humans than mouse monocytes (113). During influenza, $CCR2^{+}$ $CX3CR1^{+}$ monocytes are

considered pro-inflammatory as they can induce naive T cell proliferation and produce nitric oxide synthase 2 (114). Until recently, few studies have investigated the function of different monocytes in the swine biomedical model lung infections (115, 116).

Dendritic cells (DCs) are professional antigen presenting cells. They are located throughout the respiratory system where they constantly survey for pathogens and play a role in bridging the innate and adaptive immune response following an infection (117). During an influenza infection, there is an influx of DCs into the lungs where they can recognize the virus RNA through various antiviral sensors such as RIG-I and TLR7. Following viral recognition, they activate MyD88 or MAVS pathways for initial antiviral response, but to generate a protective adaptive immune response, the TLR7-MyD88 combination is necessary (118). Activated DCs phagocytosis virus and migrate to the draining lymph nodes where they present viral antigens to naïve T and B cells for their activation. Different subpopulations of DCs have been identified in pig lungs including classical type 1 dendritic cells (cDC1), classical type 2 dendritic cells (cDC2) and monocyte-derived dendritic cells (moDC) have been described. The primary role of all DC subtypes is to function as antigen presenting cells. However, each subtype makes a different contribution during an influenza infection. For example, cDC1 activate naïve T cells to mature to Th1 cells. cDC1 cells in humans reactivate memory CD8+ T cell. However, mouse and pig cDC1 are less effective than their human counterparts at performing this function (115).

Porcine and human cDC2 are localized close to pneumocytes of the alveoli and during influenza infections they induce naïve T cells to differentiate into Th2 cells (115). moDCs are derived from monocytes which migrate into the lung. This DC subset may play a pathological role in influenza infections by exacerbating inflammation (114).

Alveolar macrophages are a tissue-resident population of macrophages which are required for mice to survive influenza infections (119). Their functions include the maintenance of lung homeostasis, regulation of inflammation, phagocytosis of inhaled particles and debris clearance (120). As in humans and mice, pig lungs harbor an auto fluorescent $CD163^{high}$ population of alveolar macrophages (115). Alveolar macrophages are also considered critical for the control of influenza infections in swine as pigs depleted of alveolar macrophages by injection of liposome-encapsulated MDPCL2 suffered much higher mortality when infected by a human H1N1 virus compared to control pigs (121). In addition to alveolar macrophages, pigs and other members of the *Laurasiatheria* superorder harbor a unique population of lung resident macrophages, known as pulmonary intravascular macrophages (PIM), that inhabit the intravascular space (122). PIMs resemble alveolar macrophages in their gene expression and may be derived from the same lung precursor (116). Interestingly, a population of macrophages resembling PIMs was recently discovered in a humanized mouse model where immunodeficient MISTRG mice were reconstituted with human $CD34^+$ hematopoietic stem and progenitor cells, suggesting that humans may also express PIMs (123).

The lymphoid response against IAV

Like humans, pigs possess αβ T cells and γδ T cells. αβ T cells express a T cell receptor (TCR) comprised of α and β chains while γδ TCRs are composed of γ and δ chains. αβ T cells express the co-receptors CD4 or CD8. $CD4^+$ T cells have a phenotypic plasticity which allows them to differentiate and execute different effector functions in the immune system according to the different environmental cues and cytokines they encounter or cytokines. The two main CD4 T cell phenotypes are known as Th1 and Th2. Th1 cells produce IL-2, interferon gamma (IFN-γ),

and lymphotoxin-a, whereas Th2 cells produce IL-4 and other cytokines (124). Naïve CD4+ T cells can become polarized to become Th1 cells through exposure to inflammatory cytokines IL-2, IL-12, IFN-γ along with strong stimulation via TCR-MHC signaling. These stimuli induce CD4 T cells to express the transcription factors STAT1, STAT4 and T-bet, RUNX3 and T-bet paralog eomesdermin (EOMES). On the other hand, Th2 induction occurs in presence of IL-2, IL-4 and weak TCR signaling. This induces the expression of the transcription factors GATA3 and STAT6, which leads to the production of the cytokines IL-4, IL-5, and IL-13 (124). $CD4^+$ T cells can also differentiate into Th17 cells. This third type of $CD4^+$ T cell phenotype develops in an inflammatory environment that contains the cytokines IL-6, IL-21, IL-23, and TGFβ. These cells express the transcription factors retinoid orphan receptor (ROR)γt, STAT3 and the cytokines IL-17 and IL-22 (124, 125). IAV infections typically prime naïve $CD4^+$ T cells to become Th1 cells and the IFN-γ they produce is usually correlated with protective immune responses (125, 126). Th17 cells may also play a protective role in IAV infections as it was demonstrated that adoptive transfer of Th17 cells, but not Th2 cells, protected mice from a lethal IAV infection. Furthermore, Th17 cells also protected mice against a secondary bacterial pneumonia following an IAV infection (126). The specialized roles of Th1, Th2 and Th17 $CD4^+$ T cells allow them to migrate into the lung and modulate immune responses in innate effector cells and $CD8^+$ T cells (127).

Another role of the $CD4^+$ T is to provide cognate help necessary to B cells for affinity-maturation and antibody class-switching (127). In fact, a specialized lymph-node resident type of $CD4^+$ T known as follicular helper T (Tfh) cell produces high quantities of IL-21 and is essential for the formation of germinal center and B cell affinity-maturation and for the development of memory B cells (124, 128). Tfh cells undergo a multi-stage differentiation program that requires them to not receive cell signals for Th1, Th2 nor Th17 differentiation (128). Other unique $CD4^+$ T

subtype include Tregs, which are formed in the presence of IL-2 and TGFβ and express transcription factors FOXP3, STAT4 and produce IL-10 and TGFβ. Their function lies in regulating T cell priming and T cell function, but they also release cytokines which promote the effector functions of Tfh (124).

$CD8^+$ T cells, or cytotoxic T cells, are traditionally associated with antiviral immune responses since they specialize in eliminating virus-infected cells, which is critical for controlling virus infections. After antigen recognition, $CD8^+$ T cells become activated and undergo maturation. They then express the chemokine receptor CCR5 which allows them to migrate to the respiratory tissues where they can release IFN-γ and mediate cytotoxicity through the release of granules. They also induce apoptosis through MHC-TCR and Fas-Fas ligand (FasL) signaling (129, 130). Because of these effects, $CD8^+$ T cells are important to prevent or reduce the severity of IAV infections and IAV-associated symptoms (131). In fact, an early $CD8^+$ T cell response has been associated with improved outcomes in severe influenza infections in humans (132). Additionally, $CD8^+IFN\text{-}\gamma^+IL2^-$ T cells were associated with an overall reduction of disease severity and the control of viral shedding (130).

After antigen exposure, $CD4^+$ and $CD8^+$ T cells develop into long lived memory T cells which become resident within different tissues in the body. These cells are capable of orchestrating a rapid response during reinfection (133). Central memory T cells (T_{cm}) are (i) capable of rapid proliferation, (ii) they rapidly produce IL-2, and (iii) they circulate through secondary lymphoid tissues. Accordingly, central memory T cells express the lymph-node homing markers CCR7, L-selectin (CD62L), and S1pr1 (133, 134). The expression of transcription factors EOMES and T-bet as well as the chemokine receptor CCR5 appear to be important in preserving the T_{cm} phenotype (135). In addition to T_{cm} there are effector memory T cells (T_{em}). These cells circulate

through non-lymphoid tissues and are concentrated at pathogen entry sites, such as the mucosa and the skin, where they provide a rapid response against reoccurring infections and improve pathogen clearance. These effector memory cells lack traditional lymph node homing markers expression by T_{cm} (133, 134). In pigs the effector memory phenotype is characterized by the dual expression of CD4 and CD8α co-receptors on the T cell membrane (136). Another type of memory T cell is the tissue resident memory T cells (T_{rm}). T_{rm} are present in a wide variety of tissues after infection, due in part to their expression of the activation marker CD69 and the cell migration integrin CD103 and their downregulation of lymphoid homing molecule S1pr1 (133). They also express transcription factors Blimp1, Hobit, Nur77 and Runx3 which are necessary for maintaining an immunosurveillance phenotype (135). T_{rm} can represent the first line of defense as they exist in a poised effector state and can quickly release IL-4 and IFN-γ (137). It has been reported that a significant fraction of lung $CD4^+$ T_{rm} are derived from Th17 cell and are maintained in the lung by endothelial cells producing IL-7 (137).

During influenza infection or vaccination, B cell clones that recognize viral antigens become stimulated, expand, and differentiate into either short-lived B cells, long-lived affinity-maturated antibody-secreting B cells, or memory B cells (138). Antibodies produced by these B cells can protect the host from infection by neutralizing IAV particles directly or by enhancing the effector functions of other cells. Depending on their binding site, antibodies may neutralize the activity of surface viral proteins NA or HA (139). Understanding the contribution of B cells to IAV infections in pigs has been hindered by a lack of reliable immune reagents, including antibodies against common B cell markers such as CD19, CD20 and IgG isotypes that are used to characterize the distinct B cell subtypes (140). Nevertheless, it is known that pig B cells produce

specific anti-influenza antibodies which can help neutralize the virus and suppress viral replication (141, 142).

Another member of the lymphoid compartment, natural killer (NK) cells are innate immune cells important in the early response against influenza and other infections (143, 144). It has been shown in humans that lung resident NK cells are particularly hyperfunctional in response to influenza infection and may provide a first line of protection against viral infections (145). NK cells can directly recognize the influenza virus via the SAα2,6 motif present on natural cytotoxic receptors like NKp46 (146). Another cytotoxic receptor which recognizes viral HA, NKp44 (*NRC2*), is expressed by humans and pigs, but not mice (93, 147). The large amount of cytokines NK cells produce is also important for how these cells control IAV infections. These cells secrete particularly high quantities of IFN-γ and TNF that modulate the innate and adaptive immune compartments towards a pro-inflammatory response, which inhibits viral replication (145). The production of IFN-γ also induces B cells to secrete antibodies (148). In some instances, NK cells can have a detrimental effect on influenza infections. This is due their overproduction of inflammatory cytokines to the extent that they cause lung damage (149).

Like NK cells, innate lymphoid cells (ILCs) are a type of lymphocyte that lack T or B cell receptors. Three subsets of ILCs have been identified, ILC1, ILC2, and ILC3, which express the master transcription factors that engender the fate of Th1, Th2, and Th17 cells, respectively (150). While rare in lymphoid tissues, ILCs are enriched in mucosal surfaces, including the lung. ILCs are capable of rapidly secrete multiple cytokines which helps to shape the subsequent adaptive immune responses to an infection (151, 152). Along with NK cells, they express Hobit and Blimp1, which are transcription factors expressed by tissue resident T cells (135). ILC1 express transcription factors T-bet and ZNF683 and secrete IFN-γ and TNF when activated. ILC2 express

GATA3 and produce IL-13. Moreover, ILC2 effector functions are influenced by the tissue environment (151, 153). For example, in the lung ILC2 may express Galectin-1 but in the intestines they express Aiolos (153). Finally, ILC3 express CCR6, IL-23R, and c-Kit. Humans harbor two populations of ILC3 that are distinguished by the presence and absence of NKp44 expression (150, 151). It is thought that ILC1 help control early viral infection by producing IFN-γ (154) and ILC2 and ILC3 can restore help restore airway epithelial integrity and tissue homeostasis after influenza infection (155, 156).

While conventional αβ T cells are the most studied T cell subset, there are many other types of T cells that do not require peptide antigens presented by the MHC molecule for their activation or effector functions. T cells that do not fit into the peptide-MHC paradigm are called unconventional T cells (157). Pigs also harbor a lymphocyte population that express T-cell associated receptors and which functionally resemble NK cells. This population described as $CD3^{+}NKp46^{+}$ cells was able to produce granules, interferon gamma, and expressed NKp30, NKp44 and NKG2D transcripts at a similar level as NK cells. Furthermore, it has been reported that $CD3^{+}NKp46^{+}$ cells are involved in the early phases of influenza infections in pigs where they appear to display similar cytolytic properties to NK cells (158). A rare population of $CD3^{+}NKp46^{+}$ has been reported in humans. However, instead of being considered a subtype of lymphocytes on their own, it is believed that these cells represent cytotoxic T cells that have undergone re-programming of to become more NK-like, in part through the upregulation of NK markers (146, 159).

γδ T cells, which are also considered unconventional T cells, recognize a variety of antigens in a TCR-dependent and independent way. Like other innate-like T cell subsets, they respond rapidly to activation from infection or inflammation (160). These cells are one of the first

responders to an infection and are considered a bridge between the innate and adaptive immune systems. Moreover, they play an important role in host defense, immune surveillance, and homeostasis (161). While γδ T are present in most tissues, it is believed that circulating or peripheral γδ T cells can contribute to the lung resident γδ T cell pool. During a viral infection, such as influenza, γδ T cells become activated and infiltrate into the lungs as early as 1 day post infection (162). Activated γδ T cells produce perforin, granzyme B, tumor necrosis factor-related apoptosis inducing ligand (TRAIL), and interleukin 17A (IL-17A), and upregulate the Fas-FasL pathway, all of which contribute to early innate immune responses during an influenza infection (161, 162). In addition, γδ T cells are capable of lysing influenza infected cells by cell-mediated cytotoxicity. This process relies on γδ T cell activation via the NKG2D receptor and the release of granules to eliminate virus infected cells (161). In pigs, γδ T cells constitute a relatively large proportion of total T cells compared to humans and mice. The prevalence of these cells varies according to different tissues and the age of the animal. Whereas γδ T cells can represent up to 50% of all peripheral T cells in a young pig, they represent only 1-5% of peripheral T cells in humans (161, 163). Another important species-difference is that porcine γδ T cells can be divided into two distinct populations by their expression of CD2 and WC1 markers. In contrast, mice and humans do not express $CD2^{-}WC1^{+}$ γδ T cells (163).

CD8αα T cells are another unconventional innate-like T cell subset found in pigs. These cells are characterized by the expression of CD8α homodimers (164). Although some CD8αα T cells present CD4 and/or CD8β on their surface, the majority express CD8α alone. Interestingly, the CD8αα homodimer cannot function as a TCR co-receptor. Thus these cells are not supported to undergo positive thymic selection by MHC-I thymocytes (165). CD8αα T cells are also distinct from conventional cytotoxic T cells in that they do not undergo clonal expansion or exhaustion

(152). Their function lies in early effector cells during immune challenge, being able to produce IFN-**γ** within hours of stimulation (166). In fact, they express an effector profile with high expression of T-bet, low FOXO1 and hallmarks of activated conventional T cells such as high levels of Helios, a transcription factor induced upon strong TCR stimulation (166). CD8αα T also express NK markers such as NK1.1 and can produce cytolytic granzyme B (152). Thymic CD8αα T cells in pigs express similar markers to humans and are enriched for activation, memory, and tissue-resident markers such as MHC-II, CD44, CXCR3, IL-2R, CXCR3 and Hobit (79).

Other unconventional T cells include NKT cells and mucosal-associated invariant T cells (MAIT). Like γδ T cells, these T cell populations possess a memory phenotype and are poised for rapid effector functions, making them important players in the response to various diseases, including cancer (157). Whereas NKT cells compose 0.1% of T cells in human blood circulation, MAIT cells represent 1-9% and are particularly abundant in the human lung, making up around 4% of all T cells in the pulmonary mucosa (167). They can be directly activated by TCR recognition of vitamin B2 metabolites presented by the MHC-I-like related molecule (MR1)(168). IFN type I (IFN-α or IFN-β) enhances the TCR-mediated activation, however they can also be activated in a TCR-independent manner through the presence of both IL-12 and IL-18 (169, 170). Once activated, MAIT cells are able to produce pro-inflammatory type I and type 17 immune cytokines IFN-γ, TNF**α** and IL-17 and mediate cytolytic function dependent on granzyme B (169). While MAIT recognize bacterial metabolites and are important against bacterial pulmonary infections, they can also be activated during influenza infection, probably due to the virus-induced IFN type I and IL-18 production and have been shown contribute to protection against influenza in the murine model (169, 171-173). MAIT cells are also activated and enriched in other pulmonary viral infections such as human SARS-CoV-2, leading an IL-17 biased type of response

(174). The pig has been proposed as a model to investigate MAIT cell function in disease, but there are no studies on the contributions of MAIT cell to swine influenza immunity (175).

CONCLUSIONS

Animal models have been critical for our current understanding of the pulmonary immune system. There are numerous similarities in the pig and human respiratory systems. However, despite progress in deconvoluting the cellular components of the pig immune compartment, many aspects of this system remain poorly understood due to a lack of pig-specific reagents. Single-cell RNA sequencing is a powerful tool for analyzing complex organs like the lung in an unbiased manner and without the need for marker-based sorting of individual cell subsets for bulk sequencing. Chapter two of this dissertation provides a much-needed single cell atlas of the pulmonary immune compartment of pigs. It also describes transcriptomic changes that occur in response to an influenza infection, with and without oseltamivir treatment, the most commonly prescribed influenza therapy for humans. Our results provide a resource for the development of therapies and vaccines to mitigate influenza infection, disease, and transmission in pigs and humans.

Influenza A virus infections are a major health burden to humans and livestock. Beyond the impact influenza has on swine production, it is necessary to control IAV infection and transmission in pigs in order to avoid viral reassortment that can give rise to new virus strains capable of causing human pandemics. Furthermore, although anti-influenza medication is available for use in humans, there is a growing threat of the emergence of virus-resistant strains that will make these drugs obsolete. Due to difficulties obtaining samples from the lower

respiratory tract of humans, it remains unclear if the popular anti-influenza medication oseltamivir reduces viral-induced lung damage. Chapter three of this dissertation tests the ability of oseltamivir to reduce virus shedding, viral replication, and lung disease in pigs to address important knowledge gaps about the efficacy of this antiviral drug for humans. It also compares oseltamivir to the NKT cell agonist a-GalCer which induces potent immunomodulatory responses in mice that inhibit influenza infections. We assess this agent because it has been considered as a drug to treat influenza-infected humans. Pigs are ideal to test this approach as they are a highly translational influenza model and express NKT cells that are much more similar to human NKT cells than their murine counterparts.

Although the severity of influenza has been associated with an excessive inflammatory response from the host, the broad downregulation of inflammation has not improved patients' clinic outcome. On the other hand, compounds that activate certain pathways or immune cell response have shown promising results in the mouse model. Moreover, there is a need for cost-effective anti-influenza therapies for the livestock industry. This dissertation discusses the effects of the inexpensive immunotherapy compound α-GalCer in the control of influenza progression in pigs.

CHAPTER TWO

INTRODUCTION

The lung is a complex organ composed of the pulmonary endothelium, a layer of squamous endothelial cells lining the entire pulmonary circulation, and a permeable layer of epithelial cells that allows for capillary gas exchange (176). Immune cells dispersed throughout the airway lumen, just beneath the epithelial barrier, surveil the respiratory tract for microorganisms and respond to environmental cues released by the lung structural cells. The respiratory immune repertoire is composed of over 20 types of specialized immune cells (177), some of which aggregate into organized structures that resemble lymph-nodes following infection (178). They also include specialized immune cells that are responsible for restoring epithelial integrity after infection or lung damage, by remodeling and promoting tissue repair. The primary function of the pulmonary immune system is to prevent microbial pathogens from invading the airway tissues. However, it is essential that the immune responses elicited by an infection do not cause inflammatory responses that damage the delicate anatomical structure of the lung tissue to the extent that it compromises gas exchange. As a result, it is important for the pulmonary immune system to provide protection against dangerous pathogens without reacting to harmless commensal microorganisms and environmental antigens present at the epithelial barriers.

Pigs are becoming the large animal of choice to model human diseases, in part because they closely resemble humans in anatomy, physiology, metabolism, and development (88, 179). Pigs are particularly well suited to model the human respiratory diseases since porcine lungs are similar to human lungs for general anatomy, surface area, and structure, even down to the sizes of the bronchioles. Thus, lung procedures such as bronchoscopy, and endotracheal imaging can be

performed on pigs using human instruments (95, 180). Pigs have been used as a model for human anesthesia procedures, respirator intubations, and lung transplantation (181, 182). Additionally, since pigs are subject to genetic editing there is growing interest in producing genome modified swine for xenotransplantation with organs that lack surface glycans that cause acute organ rejection, including for lung transplantation (183). Moreover, genetic editing has been used to create swine models of genetic disorders that affect the lung, such as the pigs with a disruption or mutation in the cystic fibrosis transmembrane conductance regulator (CFTR) anion channel gene that develop airway inflammation, remodeling and mucus accumulation which closely resembles cystic fibrosis in humans (178, 184, 185). Finally, pigs are an excellent model for studying human pulmonary infectious diseases since pigs and humans are infected by many of the same infectious agents and there are many similarities between porcine and human immune systems.

Influenza is a respiratory infection that affects over 9 million humans globally and can be particularly dangerous for young children (2, 21). Like humans, young piglets are more susceptible to severe influenza infections than adult animals. However, influenza viruses can cause significant morbidity in pigs of any age, especially when they result in secondary infections, which is common (186, 187). As a result, influenza causes significant production losses for the pig industry (188). Despite influenza viruses being one of the most widespread and impactful pig pathogens, many aspects about the anti-influenza immune response in pigs remain poorly understood. Addressing this gap in knowledge is important for improving the health of pigs as it is required to produce more effective vaccines and antiviral therapies. It also offers an opportunity to increase our understanding of how the human immune system responds to influenza infections since pigs are considered a highly reliable model of human influenza pathogenicity and immunity. This is because pigs are much more similar to humans than rodent models for proteins involved in pattern

recognition, regulation of interferon-stimulated genes, interferon responses (93, 100). Clinical disease signs and virus transmission are also similar between pigs and humans (88, 93).

ScRNA-seq presents a powerful technology for dissecting the heterogeneity of complex biological systems such as the immune system. This is evidenced by the growing number of scRNA-seq publications that have greatly expanded our knowledge in a wide range of immune-related diseases such as Sars-CoV-19 infection (189) and cancers (190, 191). By profiling the transcriptome of individual cells, this technique overcomes the limitations of the small number of immune reagents available for pigs, which are insufficient to characterize the many different immune cells that constitute the pig's immune repertoire (140).

Here we used scRNA-seq to create a lung immune cell atlas of one-month-old newly weaned pigs. We compared our dataset to publicly available human and mouse lung scRNA-seq datasets with the goal of identifying similarities and differences in immune cell populations and transcriptional profiles. Additionally, we compared lung leukocytes between (i) healthy pigs, (ii) pigs infected with pandemic H1N1 influenza virus (pdmH1N1), and (iii) pdmH1N1 infected pigs treated with the neuraminidase inhibitor oseltamivir, to determine how transcriptional profiles of lung leukocytes are perturbed by influenza infection and antiviral therapy. Our data provide a resource to better understand the pulmonary immune system and antiviral immune responses of pigs. They also elucidate differences in pig, mouse, and human mucosal immunity, which is of interest for understanding the suitability of different animal models for studying human pulmonary immune responses.

MATERIALS AND METHODS

Pigs

Fourteen four-week-old mixed breed pigs seronegative for antibodies against H1N1, H3N2, and B influenza viruses were anesthetized with BAM™ combination drug (Butorphanol, Azaperone, Medetomidine) at a dose rate of 1.0 ml per 75 lbs body weight and intratracheally (i.t.) inoculated with 1 x 10^6 $TCID_{50}$ 2009 pandemic H1N1 A/California/04/2009 (H1N1pdm09) influenza virus, as previously described (Infected group) (78). Seven of these pigs were orally administered 75 mg oseltamivir phosphate (Lupin Pharmaceuticals) twice a day for five days after infection (Inf+Trt group). An additional two control pigs (Healthy group) were mock infected with virus-free Dulbecco's Modified Eagle Medium (DMEM). At 5 days post infection (d.p.i.), necropsies were performed after pigs were sedated with BAM™ and humanely euthanized with a lethal dose of Pentobarbital Sodium IV (150 mg/kg body weight). The experiment was performed in compliance with guidelines from the United States Department of Agriculture and the National Research Council's Guide for the Care and Use of Laboratory Animals. The institutional animal care and use committee (IACUC) at the University of Florida approved the protocol under study number 201708209.

Tissue sampling and cell isolation

Approximately 1 g of tissue collected from the left cranial, middle, and caudal lung lobes were combined and digested with 2.5 mg/mL of Liberase TL (Roche, Indianapolis, IN) in Dulbecco's Modified Eagle Medium (Thermo Fisher, Waltham, MA) at 37°C for 45 minutes, passed through a 100 μm cell strainer (Thermo Fisher, Waltham, MA), and treated with an ammonium chloride-

based red blood cell (RBC) lysis buffer. A Dead Cell Removal Kit (Miltenyi Biotec) was used to remove apoptotic and necrotic cells, following the manufacturer's instructions. The resulting cell suspensions were washed, stained with propidium iodide (PI) for exclusion of dead cells, and FACS sorted for live cells using a Sony SH800 Cell Sorter (Sony Biotechnology, Japan). Sequencing was performed on 2 Healthy, 5 Infected, and 5 Inf+Trt lung samples. Eight samples were from separate individuals and four samples were from pooled cell suspensions of two pigs each (Table 2.1).

Single-cell RNA sequencing

Single cell libraries were prepared using the 10X Genomic Chromium Next GEM Single Cell 3' Reagent Kit (v3.1) according to the manufacturer's instructions. Sequencing was performed on an S4 flow cell of the NovaSeq 6000 sequencer (Illumina) to obtain paired end reads.

Data processing and clustering analysis

Cell Ranger (v4.0) was used to process raw sequence data, demultiplex raw base call files into FASTQ files, align reads to the Sscrofa 11.1 reference genome, and to generate count matrices. Clustering analyses were performed in R (v4.0.2) using the Seurat package (v4.1.0) (Stuart et al 2019). Pre-analysis quality control was performed by removing genes expressed in <3 cells, excluding cells with aberrantly high (>5000) or low (<550) gene counts and high mitochondrial gene expression (>9%), and regressing out cell cycle effects. Data were log-normalized with the function *NormalizeData*, after which the 2,000 most variable genes in each dataset were identified using the *FindVariableFeatures* function. Datasets were integrated with *FindIntegrationAnchor*

followed by *IntegrateData* and *ScaleData* functions. A principal component analysis was conducted on the variable features using the function *RunPCA*. The most variable principal components were selected based on the elbow plot variation and then used to determine the k-nearest neighbors of each cell and construct a shared nearest neighbor graph using the *FindNeighbors* function. The *FindClusters* function using the Louvain algorithm was implemented to cluster cells and a further non-linear dimensional reduction Uniform Manifold Approximation and Projection (UMAP) was performed to place similar cells together in a low-dimensional space. The *BuildClusterTree* function from Seurat was used to generate a hierarchical clustering with default arguments followed by ggtree (v3.2.1) package for tree visualization. Differentially expressed genes (DEGs) were identified within each cluster using the function *FindAllMarkers* with a minimum Log2 fold change threshold of +0.25 using a Wilcoxon Rank-Sum test. Pairwise comparisons between specific clusters were calculated using the function *FindMarkers* at min.pct = 0.25 and logfc.threshold = 0.25. DEGs were visualized using the EnhancedVolcano package (192).

Trajectory analysis

T cell and NK cell clusters (clusters 1:8) subsetted from the main Seurat object were subjected to a pseudotemporal analysis using the R packages Monocle3 (v1.2.9) and Slingshot (v2.4.0). For Monocle3, a region with lung resident naïve T cells (*CCR4*$^{+}$, *CCR7*$^{-}$, *IL7R*$^{+}$, *SELL*$^{+}$, *S1PR1*$^{+}$, *LEF1*$^{+}$) was designated as the root node and cells were ordered onto a pseudotime trajectory according to their differentiation program. The *learn_graph* and *order_cells* functions were run to respectively learn the overall trajectory using the reversed graph embedding algorithm and to place each cell at its proper position through pseudotime. After construction of the trajectory, *graph_test*

function with the Moran I test was used to identify genes whose expressed varied over pseudotime (q_value<0.05). Genes with similar expression patterns were grouped into modules using the *find_gene_modules* function. For the Slingshot analysis, the *as.SingleCellExperiment* function was used to convert the object, after which the function *slingshot* was performed on clusters x-y in Seurat. Finally, a PCA reduction was used to determine dimensionality (*reduced-Dims*) and construct unbiased lineages and the resulting trajectory analysis was graphed using UMAP.

Dataset integration

We used Seurat (v4.1.0) to integrate the lymph node and lung cell data and to perform cross-species comparisons with published datasets of human lung cells (EGAS00001004344 (177)) and mouse lung leukocytes (GSE107947 (193); GSE186976 (194)). The Ensembl genome browser (Ensembl Genes 105) was used to convert human (GRCh38) and mouse (GRCm39) gene names to the corresponding pig names prior to integration (https://www.ensembl.org/biomart/martview/). Only genes with one-to-one orthologs were included in the analyses. Low quality genes and cells were removed from each dataset as described above. Each dataset was independently normalized before identifying the most variable features. A standard integration workflow was then followed. Briefly, the *SelectIntegrationFeatures* function was applied to genes that were consistently variable across datasets. Next, the *FindIntegrationAnchors* function identified a set of anchors (pairs of cells from each dataset that are contained within each other's neighborhoods) between datasets using the top 30 dimensions from the canonical correlation analysis to specify the neighbor search space. Next, an integrated dataset was created by running the *IntegrateData* function. Afterwards, cell cycle effects were regressed out and the clustering analysis workflow was performed using *RunPCA*, *FindNeighbours*, *FindClusters*, and *RunUMAP*, as described

above. The *FindConservedMarkers* function (min.pct = 0.1, only.pos = T) was used to identify DEGs that are conserved across datasets. Next, an analysis was performed to identify species-specific DEGs in select clusters. First, an additional column was added to the Seurat object listing each cluster according to its species origin. Next, the corresponding clusters were analyzed for DEGs using the *FindMarkers* function (min.pct = 0.25, logfc.threshold = 0.25), after which we removed genes that were differentially expressed due to dataset-specific effects and genes that were detected in only one species.

Differential expressed genes (DEGs), function annotation and cell-cell communication analysis

We performed DEG analysis using the *FindMarkers* function in Seurat R package considering $p < 0.05$. Healthy ($n = 2$) and influenza treatments ($n = 5$) datasets were input as ident.1 and ident.2 respectively to obtain DEGs from all cell populations, ranked by average log fold change and false discovery rate (FDR). Enrichment analysis for the functions of the DEGs was conducted using the clusterProfiler (v.4.0) (195) package. We performed the Kyoto Encyclopedia of Genes and Genomes (KEGG) pathway and Gene Ontology (GO) analysis for allocation to relevant GO terms including GO-BP (biological process), GO-CC (cellular component), and GO-MF (molecular function). Gene symbols of differently expressed genes were converted to entrez gene ID according to the org.Ss.eg.db package.

For the inference and analysis of intracellular communication, we used the CellChat (v.1.5) package. We ran the package on an integrated scRNA-seq dataset containing healthy and influenza-infected pigs and mice lung leukocytes (GSE107947 (193); GSE186976 (194)). There was a total of 9,600 cells in the combined dataset, 2,400 from healthy controls and 2,400 from

infected animals of each species. Integration was conducted as detailed previously. Interactions of types Secreted Signaling, ECM-Receptor Signaling, and Cell-Cell Contact were inferred and quantified with the *compareInteractions* through a signaling molecule interaction database using a manifold learning approach and Hill-function-based mass action models for differential expression analysis and statistical test on cell groups (196). Cell-cell communication network was calculated with *aggregateNet* function. Cell pathway ranking was calculated with *rankNet*. The comparison of major cell sources and targets of cell signaling was performed with *net_Analysis_signaling_Role_scatter*. Outgoing and incoming signals of each cell for a certain pathway were achieved with *netVisual_aggregate* and visualized with *netVisual_circle* and *netVisual_heatmap*. Enrichment of ligand-receptor pairs was obtained with *extractEnrichedLR* and visualized with *netVisual_bubble*. Alluvial plots were obtained by using *selectK*, *identifyCommunicationPatterns* and *netAnalysis_river*.

RESULTS

Cellular composition of porcine lung leukocytes

Single-cell RNA-sequencing was performed on the lungs of two healthy six-week-old mixed breed pigs (Figure 2.1A). After removing cells with unusual gene counts and high mitochondrial gene expression, the combined dataset contained 24,560 cells with 4,225 mean reads and 1,310 genes per cell. An unsupervised clustering analysis was performed using Seurat (v4.1.0) after which canonical cell cycle markers were used to regress out cell cycle effects before dimensionality reduction. Twenty-three clusters were obtained (clusters 1-23) (Figure 2.1B), which were annotated according to previously established lineage marker genes (Figure 2.1C & D). Most cells fell within clusters 1-8, which consisted of closely grouped T cell and innate lymphoid cells (ILC)/NK cell populations. B cells respectively separated into a major cluster (cluster 10) that expressed naïve B cell markers (*CCR7*, *CXCR4*, *CXCR5*) and a minor cluster (cluster 11) that expressed antibody secreting (*JCHAIN, PRDM1*) and cell cycling (*DUT*, *PCLAF*) markers.

Among myeloid lineage cells, monocytes, macrophages, and dendritic cell clusters grouped together due in part to their common enrichment of **SIRPA* (CD172α), *HLA-DRA*, *SLA-DQB1*, *CD9*, *AIF1* and *CST3* genes. Clusters 16-18 expressed monocytes genes (*CD14*, **FCGR3A*, *CCR2*, *CX3CR1* and **SIGLEC5*) and were respectively classified as intermediate monocytes (*HLA-DRA*^{intermediate}, *CD14*, **FCGR3A*, *TNF* and *IL1B*), classical monocytes (*HLA-DRA*^{low}, *CD14*^{high}, *ITGAM*, *SELL*, *TNF* and *IL1B*) and non-classic patrolling monocytes (*CX3CR1*^{high}, *CCR2*^{negative}, *CD14*, **FCGR3A*, *KIT*). While all monocytes expressed the degranulation-related genes *GNLY* and *GZMH*, only intermediate and classical monocytes

expressed the inflammatory-related genes *CCL14*, *SERPINB1,* and *F13A1*. Clusters 19 and 20 expressed markers of alveolar macrophages (*PPARG*, *MSR1*, *MRC1*, *ARG1, APOE,* and *CD68*) (Supplementary Figure 2.1A - C). Macrophages in cluster 19 were enriched for tolerogenic genes such as *MERTK*, *IL10,* and *IL4R,* which mediate inhibition of inflammation and allergic responses. Signaling via IL-4 receptors activates macrophages differently to classical inflammatory signaling pathways and stimulates the expression of *STAT6* and STAT-6-response genes such as *ARG1 (197)*. Although *ARG1* was expressed in cluster 19 macrophages, we did not detect *STAT6*. Additionally, cluster 19 macrophages also expressed several genes associated with inflammation and antiviral responses. The *STAT1* signal was prominent in cluster 19 macrophages along with the expression of virus receptor *SIGLEC1*, interferon induced genes *ISG15*, *MX1*, *MX2*, *CXCL10*, and the inflammation related gene *SRSF3*. Macrophages in cluster 20 also presented genes associated with immune tolerance and inflammation. However, this subset was more enriched for *STAT6*, *ARG1*, **ADGRE1,* and *APOE* compared to cluster 19 macrophages. Interestingly, murine $CD169^{+}$ (*SIGLEC1*) macrophages, a population that does not fit the M1 and M2 paradigm, usually express F4/80 encoded by the gene **ADGRE1* (198). Even so, in our dataset, we found that pig macrophages not only express **ADGRE1*, but unlike mice, they are not enriched for *SIGLEC1*. Cluster 20 also expressed classical alveolar macrophage markers, such as *MSR1*, *MRC1* and *LGALS3 (*Supplemental Figure 2.1B*)*. However, they lacked *MARCO*, a class A scavenger receptor expressed in mature alveolar macrophages in mice and humans (123, 199, 200).

We also investigated the expression of non-classical antigen presenting molecules that present antigens to unconventional T cell subtypes (157). The CD1 family contains non-polymorphic molecules which present lipid-containing antigen to unconventional subsets of T cells (157). This family of molecules remains poorly characterized because mice, the most popular

mammalian animal model, only present CD1d. In contrast, humans express five CD1 isoforms (CD1a-e) and pigs express four (CD1a, CD1b, CD1d, and CD1e) (201). In the pig lung dataset, we were able to detect expression of genes encoding CD1a, CD1d and CD1e. All monocytes and macrophages expressed *CD1E*, which assists in loading lipid antigen into the nonpolymorphic MHC-I like molecule CD1b. Alveolar macrophages had the highest expression of *CD1E*, but differently from other macrophages and monocytes, they did not express **CD1D*. **CD1A* expression was restricted to intermediate and non-classical monocytes.

Dendritic cells separated into three clusters that correspond to conventional (clusters 13 and 14) and plasmacytoid (cluster 15) subsets. Cluster 13 was associated with the expression of makers associated with conventional dendritic cell type 2 cells in mice and was therefore designated cDC2. These markers include **SIRPA*, and *TLR4*, as well as high expression of MHC-II and genes involved in cell trafficking (*XCR1*, *CADM1*, *CXCR10*), interferon response (*IRF7*, *AHR*), and transcriptional regulation *ID2*, and *ITGAM*. cDC2 cells also expressed **CD1A*, **CD1D* and *CD1E*. This contrasts with other antigen-presenting cells such as B cells, which strongly express **CD1A*, some **CD1D,* and no *CD1E* (Supplementary Figure 2.1D). Cluster 14 presented markers of human conventional dendritic cell type 1 (*CXCR4* and *BATF3*) and was therefore designated (cDC1) (202). It has been reported that pig cDC1 strongly express *CADM1* and may also express *CD8A* or *XCR1* (203). However, in our dataset, lung cDC1 did not express these genes. Nevertheless, they were enriched for genes associated with cell migration (*CCR7*) and tolerance induction (*IDO1*, *IL4I1*) (204, 205), indicating that cDC1s resemble human cDC1s. As previously reported, both conventional DC groups expressed *LY75* (CD205). However, unlike in blood and similar to other pig lymphoid tissues, not all cDCs were $LY75^{+}$ (203, 206). Plasmacytoid DCs (Cluster 15) upregulated *TNF* and *TNFRSF21* while also presenting *CD36*, *CD8A*, *CD8B* and

IRF8. Three neutrophil subsets were identified (clusters 21-23). Cluster 21 and 23 were enriched for various ribosomal proteins (*RPL3*, *RPL5*, *RPL34*, *RPS3A*, *RPS8*, *RPS15*) nitric oxide (*NOS2*), and granulins (*GNLY*, *GZMH*, *GZMA.1*), which may indicate they were neutrophils undergoing extracellular trap formation (207). In contrast, these genes were barely detectable in cluster 22 neutrophils which instead expressed high levels of common neutrophil markers such as *IL18* and *CXCL8*, the neutrophil collagenases *MMP8* and *MMP9*, lactotransferrin *LTF*, the adhesion molecule *CD24,* and *CD14*. Interestingly, both clusters 21 and 23 had some cells expressing the lymphocyte markers *CD3E*, *CD2,* and *GATA3* (Supplementary Figure 2.1E). A small population of neutrophils expressing TCRαβ and CD3/CD28 has been reported in healthy humans and certain mouse strains (208, 209). These TCR-related expression may protect neutrophils from apoptosis by enhancing the expression of the anti-apoptotic protein Bcl-xL (209). Interestingly, cluster 21 neutrophils had the highest percentage of cells expressing IL-8 (*CXCL8*). Finally, we detected a population of mast cell (cluster 12) that expressed high levels of mast cell markers *MS4A2*, *LTC4S*, *KIT,* and *FCER1A*. *MS4A2* and *LTC4S* are also found in human lung mast cells (190, 210), while *KIT* and *FCER1A* are known markers of both human and mouse mast cells (106, 211, 212) . *GATA2*, which has been identified to promote upregulation of genes that induce mast cells proliferation and survival in mice (211), was also enriched in cluster 12. Mast cells were not identified in previous publications that performed scRNA and single nucleus sequencing of mouse lung cells. However, they were present in human lung datasets (190, 210, 213). Mast cells were not described in previously published pig lung or PBMC scRNA-seq datasets (214, 215).

Characterization of T cells and ILC

Next, we performed a detailed analysis of the T cell and NK cell/ILC compartment. Clusters 1-8 were reclustered at a resolution of 0.7 which generated twelve clusters (Figure 2.2A). The clusters were then classified according to canonical markers that distinguish T cell and ILC subsets in mice and/or humans (Figure 2.2B). A high proportion of T cells were from the γδ lineage since pigs are a γδ T cell high species (163). Consistent with a previous reports that characterized pig γδ T cells, we found two major subsets of these cells; a large *$WC1^{+}GATA3^{hi}CD2^{-}$ ($CD2^{-}$) population, which is unique to γδ T cell high species such as pigs, sheep and bovines, and a smaller population of *$WC1^{lo}GATA3^{lo}CD2^{+}$ ($CD2^{+}$) cells (163, 216, 217). The $CD2^{-}$ and $CD2^{+}$ populations were both enriched for *RHEX*, *GATA3,* and *SOX13*. The porcine $CD2^{+}$ population is preferably found in lymphoid organs and when activated is capable of simultaneously secreting IFN-γ and TNFα (218). In our dataset both *TNF* and *IFNG* expression were barely detectable in this population (Figure 2.2B), indicating that they may not have been in a state of activation. We also observed that the $CD2^{+}$ subset was enriched for genes associated with cell-mediated cytotoxicity and phagocytosis (*CD8A*, *GZMH*, *GZMA.1*, *KLRK1*, **FCGR3A*). Furthermore, consistent with our previous analysis of pig thymocytes (79), $CD2^{+}$ γδ T cells were enriched for genes associated with TCR signaling (*LCK*, *IKZF2* and **PRKCH*). Both *ID2* and *ID3* regulate the levels of E protein activity and thus the γδ T survival and development (219) . *ID2* was not expressed in the $CD2^{-}$ cluster, whereas *ID3* was strongly expressed by $CD2^{+}$ γδ T cells. $CD2^{+}$ and $CD2^{-}$ γδ T cells expressed similar levels of the costimulatory receptor *JAML*. This contrasts with our previous observation that only the $CD2^{-}$ population of thymic γδ T cells expresses this costimulatory receptor (79). Nevertheless, we did detect a minor subset of $CD2^{-}$ γδ T cells (cluster 10) expressing low levels of *GATA3* that was highly enriched for *JAML* (Supplementary Figure 2.2A). These cells

also expressed low levels of **WC1*, which act as hybrid pattern recognition receptors and γδ TCR coreceptors on bovine $CD2^-$ γδ T cells (163, 220, 221). Cluster 10 γδ T cells were enriched for other costimulatory molecules such as *IL7R*, *IL2RA,* and *TMIGD2* and expressed high levels of the antiviral genes *IFITM1* and *CAMK2N1*, which are also expressed by human γδ T cells and MAIT cells. We also detected *RORC* in cluster 10 (Supplementary Figure 2.2B), which is required for lineage commitment of a subset of IL-17 producing γδ T cells in mice known as Tγδ17 (222, 223). However, we did not detect expression of IL-17 or IL-23 in cluster 10 γδ T cells, which are cytokines expressed by activated Tγδ17 (224). Finally, a subpopulation of cluster 10 cells had an expression pattern consistent with type-3 innate lymphoid cells (ILC3) (151, 225), including that they lacked $CD3E^-$ and $*TRGC1^-$ and expressed *AHR*, *RORC*, *KIT, ID2* and *KLRB1* (Supplementary Figure 2.2B). This indicates that like in humans, pigs do not have a substantial frequency of ILC3 in the lung.

We identified six distinct subtypes of αβ T cells. Cluster 3 was composed of $CD8A^+$ T cells that were transcriptionally similar to the adjacent population of NK cells, their common expression NK cell-associated genes (*GZMA.1*, **GZMM*, *GZMH*, *KLRB1*, *KLRG1*, *NKG7, TBX21*, *ZEB2*). We therefore designated this cluster as NK-like CD8 T cells. Cluster 5 was comprised of a cytotoxic T cell subset that expressed a high *CD8A* to *CD8B* ratio. These cells were enriched for the granzyme gene *GZMK*, which was rare in other cell subtypes, as well as *CD45*, the NK associated genes **FCGR3A* and *NKG7*, the chemokine *CXCR6*, and the exhaustion marker *LAG3*. Among the four remaining T cell clusters (clusters 6-9), cluster 6 was enriched for chemokine receptors associated with tissue resident T cells ($CCR4^+$, $CXCR3^+$), while clusters 7, 8, and 9, were enriched for *CCR7*, which is a chemokine receptor expressed by blood-derived peripheral T cells (226, 227) (Figure 2.2B). Tissue resident T cells were enriched for *CD44* and *IL7R* genes. They

also co-expressed *CD4* and *CD8A,* which is indicative of an effector memory phenotype in pigs (228). The majority of $CD4^+CD8^+$ were in tissue resident T cell subset, and tissue resident T and Peripheral CD4 T subsets had similar percentage of $CD4^+$ cells (Table 2.2). Peripheral T cells had a naïve phenotype, including high *LEF1*, *TCF7,* and *SELL* expression and low *IL2RA* expression. A small number of Cluster 6 cells expressed the T regulatory cell (Treg) markers *FOXP3* and *CTLA4*. These cells were of a much lower frequency than has been observed in pig thymus and PBMC scRNA-seq datasets (79, 229). Cluster 9 was comprised of $CD4^-$ T cells expressing a high ratio of *CD8A* to *CD8B* (8:1). These cells were enriched for transcription factor *ZNF683* (Hobit), the T cell memory marker *CCL5* that identifies $CD8^+$ TEM cells (230), and the NK cell signature genes *NKG7*, *KLRK1,* and **KLRD1* (231). This transcriptional profile is consistent with previously described populations of $Hobit^+CD8\alpha\alpha$ T cells described in previous pig thymus and PBMC datasets. However, cluster 9 T cells were also enriched for **PPTG1* and inflammatory/degranulation markers *NPY* and *MARCKS,* which were barely detected in their thymic and PBMC counterparts, indicating a functional difference.

Among the $CD3^-$ subsets, we observed three clusters of NK cells (clusters 1, 2, and 4). Cluster 1 NK cells were enriched the transcription factors associated with terminal NK cell *TBX21* (T-bet) and *ZEB2*, the inhibitory receptor *ADGRG1*, leukocyte-adhesion molecules *ITGAM* (CD11b) and *ITGAL* (CD11a), and *IFNG*. Similar to human circulating NK cells, this subset expressed the egress and circulation markers *CX3CR1*, *CXR2,* and *S1PR5* (225). The largest of the NK clusters, cluster 2, was enriched for perforin and a variety of granzyme genes, including *PRF1*, *GNLY,* and *GZMH*. Like cluster 1 NK cells, this subset also expressed effector function and circulation markers. However, cluster 2 expressed higher levels of ribosomal protein associated genes and **FCGR3A* compared to cluster 1 NK cells. Cluster 4 NK cells had much higher levels

of levels of *GZMA.1*, *EOMES*, *XCL1*, *KLRB1,* and *ISG15* expression compared to the other NK cell clusters. Similar to human lung resident NK cells, this cluster was enriched for lung homing (*CCR5*, *CXCR3*, *SELL*), latency (*LEF1*, *TCF7*), and tissue resident signature markers (*RGS1*, *CXCR6*, *CRTAM*). Unlike human NK cells, all pig NK cells expressed **FCGR3A* which encodes CD16. Interestingly, a small number of cells in cluster 4 presented *SLC4A10* and high levels of *KLRB1* which are markers of mucosal associated invariant T (MAIT) cells. However, we did not detect other markers of MAIT cells (*CD3E*, *RORC*, *IL23R*, *IL26*, *ZBTB16*) (Supplementary Figure 2.2C). This suggests that makers of human MAIT cells, including *SLC4A10* (232), may not distinguish MAIT cells in pigs.

Trajectory analysis of lung T and NK cells

To characterize the transcriptional relatedness of T and NK cell subsets, we subjected their clusters to a trajectory analysis (Figure 2.2C). Since our data is a heterogeneous grouping of cell types and states, we used two R packages, Slingshot and Monocle3, that are able to account for multiple branching lineages of differentiation (233, 234). Slingshot uses a fully unsupervised non-linear tree-shaped inference method to predict developmental chronologies, whereas Monocle3 uses a tree-based Louvain detection algorithm and requires the designation of a root node within a cluster. We assigned the Monocle trajectory root in cluster 6 which harbors cells expressing naïve and lung homing T cell markers (Supplementary Figures 2.2D & E). The differentiation trajectories were generally similar between packages, including that Slingshot predicted cluster 6 to be the root cluster and that naïve lung-resident T cells segregated into three main branches each containing transcriptionally similar cell clusters (Supplementary Figure 2.2F). The first branch passed through peripheral $CD4^+$ and $CD8^+$ T cells as well as CD8αα T cells due in part to their

common expression of *CCR7* and *LEF1*. A second branch connected resident memory T cells, cytotoxic effector T cells, and NK cells due to their common expression of cytolytic genes. A third trajectory branched through γδ T cells, passing from the $CD2^+$ subset onto in the $CD2^-$ subset. A hierarchical clustering tree was constructed for the T and NK cell clusters using average cell expression from each identity class. Branch organization was based on a distance matrix for the gene expression space and visualized with ggtree package (Figure 2.2D). In general, this analysis arranged cells into the same three branches produced by the trajectory analyses. However, tissue resident NK cells (cluster 4) and $CD2^-$ γδ T were closer to αβ T cells than to other NK cell subsets and $CD2^+$ γδ T cells, whereas in the pseudotime analysis γδ T cells followed a trajectory line. Hierarchical clustering also related $CD2^-$ γδ T to CD8αα T cells and resident T cells, probably in part for their lung-homing CCR4 expression. This agrees with previous reports that $CD2^-$ γδ T cells become tissue-resident cells with specialized effector functions (218, 220, 235).

Genes that varied according to the differentiation trajectory were clustered into 5 modules using Monocle3 (Figure 2.2E & F). Module 1 segregated with γδ T cells and CD8αα T cells and included the transcription factors *RHEX* and *MAF* as well as the IL33 receptor *IL1RL1*. Module 2 segregated with cytotoxic cell types such as NK cell and $CD2^-$ γδ T cells. Genes in this module included the transcription factors Hobit (*ZNF683*) and *EOMES*, which are important in the formation and maintenance of the memory CD8 T cell phenotype (236), as well as receptors for IgE (*FCER1G*) and killer lectin (*KLRB1*). Module 3 was enriched for the MHC-II genes *HLA-DRA* and *SLA-DRB1I,* and the semaphorin receptor *PLXNC1*, which regulates cell motility and migration, and the immune response (237). Module 3 was upregulated in αβ T cells compared to NK cells and γδ T cells. Module 4 was enriched mainly in clusters five and six. It included genes associated with T cell activation such as *TNF*, *CCR5* and *CD40LG*, as well as *CXCR6*, a receptor

for the cytokine CCL16 that is part of a signaling pathway that regulates T lymphocyte migration to various peripheral tissues, including the lung (238, 239). Module 5 varied with memory and effector T cells and tissue resident NK cells and included several antiviral genes (*IFI6*, *ISG15*, *MX1*) as well as the transcription factors *STAT1* and *STAT2* that are key mediators of type I and type III interferon signaling.

Cross-species comparison of pig, mouse, and human lung leukocytes

To compare the transcriptional landscape of pig, mouse, and human lung leukocytes, we integrated our pig lung dataset with published lung cell datasets from three healthy humans (46 year old male, 75 year old male, and a 51 year old female) (177) and six healthy mice (one 5.5 week old C57BL/6J female and five 10 week old BALB/c females) (193, 194). Human and mouse gene names were converted into the corresponding pig gene names to generate a single unified gene nomenclature. Low quality genes and cells were removed from each dataset as described above. To reduce batch effects, datasets were randomly downsized so that each species contained a similar number of cells. The final dataset contained 2,424 pig cells, 2,382 human cells and 2,411 mouse cells. Pig, human, and mouse cells had a mean depth read of 4,002, 4,513, and 4,041 reads per cell, respectively. Batch-specific distribution for gene count, transcript count, and mitochondrial read fraction (Supplementary Figure 2.3A-C) indicate that the pig dataset has adequate quality compared to the other species datasets.

An unsupervised graph-based clustering analysis using the Louvain algorithm in Seurat resolved each dataset into 12 clusters (Figure 2.3A). We found significant conservation as well as species-specific variation in cell types. As a proportion of total cells, the human dataset had a significantly higher proportion of myeloid cell type clusters (52%) compared to the pig (11%) and

mouse (22%) datasets (Table 2.3). This may be due to differences in tissue dissociation protocols among studies, which varied by tissue digestion media, mechanical preparation technique, and cell enrichment methods (177). Nevertheless, we were able to identify four major myeloid cell types that were conserved across species, namely, neutrophils, dendritic cells, monocytes, and macrophages.

We compared lymphoid cell clusters across species, which included αβ T cells, γδ T cells, NK cells, B cells, and type-2 innate lymphoid cells (ILC2). Pig and human clusters were present in similar proportions with the exception that pigs had a higher proportion of $CD2^-$ γδ T cells and a lower proportion of ILC2s compared to humans (Figure 2.3B). $CD2^-$ γδ T cells are abundant in pigs and other *Laurasiatheria* species and expresses many of the same transcription factors as IL17-producing γδ T cells in mice (*SOX13*, *GATA3*, *ID3* and *MAF*) (79, 160). Humans had similar levels of peripheral T cells as pigs but ~ 2.5 times more tissue resident T cells. Mouse lymphocytes were composed of a much higher proportion of B cells and significantly fewer NK cells compared to both pigs and humans, which is consistent with previous cross-species scRNA-seq analyses that compared lungs of these species (210, 240). As a proportion of lymphocytes, mice had a much higher fraction of peripheral T cells (25%) than pigs (7%) and humans (11%). Mice were similar to humans and different to pigs in that they had low level of $CD2^-$ type γδ T lymphocytes and a significant population of ILC2 cells, which were barely detected in pigs. Although the mouse cluster that overlapped with human ILC2 expressed many of the same markers, several important differences in lineage-defining genes point to the acquisition of species-specific adaptations (Supplementary Figure 2.3D).

Next, we compared transcription factor expression levels among pig, human, and mouse leukocyte subsets according to the top five most expressed transcription factors in each pig cell

cluster (Figure 2.3C). Overall, most transcription factors expressed by individual pig clusters were at least partially expressed by their human and mouse counterparts. Genes which displayed similar expression patterns across all three species included *MEF2C*, *CEBPB*, *HMGB2*, *SPI1*, and *FOS*. Transcription factors that were more highly expressed in pigs compared to mice and humans included genes that were expressed by several pig clusters (*IKZF2*, *AHR*, *TCF7*), genes that were specifically enriched in γδ T cells (*SOX13*, *GATA3* and *YBX3*), genes that were enriched in $CD2^+$ γδ T cells and NK cells (*IKZF3*, *ZNF683*), *ID3* that was enriched in pig B cells and γδ T cells, and *STAT1* that was enriched in pig neutrophils, monocytes, dendritic cells, and macrophages. Transcription factors that were similarly expressed in pig and human clusters with lower expression in mouse clusters included *ID2*, which was enriched in pig and human T cells and NK cells, as well as *GATA2* and *MITF*, which were more highly expressed by pig and human mast cells, basophils, and ILC2s than the corresponding mouse cells. Transcription factors that were similarly expressed between pigs and mice compared to humans included *ATF3*, a negative regulator of TLR signaling that was upregulated in myeloid lineage cell clusters, *SP110*, a nuclear body protein which was expressed in most pig and mouse clusters and barely detected in human leukocytes, and *RASSF4,* a tumor suppressor that was expressed in a high proportion of pig and mouse dendritic cells, monocytes and alveolar macrophages and mostly absent from the corresponding human clusters. Collectively, these results demonstrate that lung leukocyte subsets are proportionally more similar between pigs and humans than between mice and humans.

Transcriptional changes induced by influenza infection

We compared lung leukocytes from our healthy pigs (Healthy; 22,259 cells, 1,401 genes, 3,780 transcripts) to pigs infected with pdmH1N1 2009 influenza virus (Infected; 26,907 cells,

1,695 genes, 4,750 transcripts) as well as pdmH1N1 infected pigs treated with a five-day course of oseltamivir phosphate (Inf+Trt; 35,291 cells, 1,583 genes, 4,446 transcripts) (Supplementary Figure 2.4A & B). We integrated the data using Seurat as previously described and analyzed treatment groups for differentially expressed genes, KEGG pathways, and gene ontology (GO) terms. Overall, 942 genes were differentially expressed between Healthy and Infected pigs, while only 67 genes were differentially expressed between the Infected and Inf+Trt groups (Figure 2.4A & Supplementary Figure 2.4C). Influenza infection upregulated KEGG pathways associated with Influenza A immunity, viral infection immunity, and IgA production, while downregulating pathways associated with cellular translation and signal transduction processes, including ribosome, rap1, and sphingolipid signaling, and drug metabolism (Figure 2.4B). The GO term analysis showed enrichment of genes involved in regulation of viral genome replication and cellular response to type I interferon signaling (Figure 2.4C). This includes the interferon induced gene *IFI6*, also associated with human influenza infection (241), *MX1* and *MX2*, which block viral transcription and replication, *HERC5* and *HERC6*, which reduce influenza virus replication through the conjugation of *ISG15* to viral proteins, and the antiviral response regulator *STAT1*.

In order to compare cell type frequencies across treatments, lymphoid and myeloid cell subpopulations were annotated according to the Healthy treatment group (Supplementary Figure 2.4D) and afterwards compared to Infected and Inf+Trt pigs (Figure 2.4D). Compared to the Healthy pigs, both infected groups had a higher frequency of B cells expressing inflammatory genes, including *CXCL8*, **CXCR2* (which encodes the receptor for CXCL8), *MARCKS*, **CCL15*, *IFIT1, ISG15,* and *FCER1G*, which encodes the IgE receptor (Supplementary Figure 2.4E). A similar population of B cells expressing inflammatory genes has been identified in mouse (242). Compared to Healthy pigs, Infected and Inf+Trt pigs had a higher proportion of cytotoxic T cells

(cluster 3), peripheral T cells (cluster 6), and inflammatory B cells (cluster 10) (Supplementary Figure 2.4F). Healthy pigs presented a higher frequency of cycling lymphocytes and NK cells when compared to Infected pigs. Among myeloid cell types there was no statistical difference between in the proportion of cells from Healthy and Infected pigs, however the Healthy group tended to have higher frequencies of cDC1 and Neutrophils $CD3^{+}$ (cluster 14) (Figure 2.4D). Overall, the proportions of both lymphoid and myeloid cell types were similar between Infected and Inf+Trt pigs. However, Inf+Trt pigs did tend to have higher levels of $CD3E^{+}$ neutrophils (cluster 12) and lower levels of monocytes compared to Infected pigs. Next, we compared DEGs within cell types. Between Healthy and Infected pigs, the most transcriptionally variable lymphocyte populations were B cells (1,243 DEGs), followed by cytotoxic T cells (1,169 DEGs), $CD2^{+}$ γδ T cells (1,143 DEGs), peripheral T cells (983 DEGs), and NK cells (892 DEGs). Among the myeloid cell populations, mast cells (2,087 DEGs), monocytes (1,731 DEGs) and pDCs (1,557 DEGs) were the most transcriptionally distinct between Healthy and Infected pigs (Figure 2.4E-I, Table 2.4 and Supplementary Figure 2.4H- L).

Cytotoxic T cells from infected pigs were enriched for genes encoding antiviral and inflammatory responses (*IFIT1*, *IFI6*, *MX1*, *HERC5*, *HERC6*, *CXCL8*, *STAT1*, *GZMA*, *CCL4*), ATP-dependent RNA helicases required for altering RNA secondary structure (*DDX5*, *DDX3X*), and cell proliferation and maturation molecules *(FOS*, *CD69*) (Figure 2.4E). Peripheral T cells from infected pigs were enriched for the T cell costimulatory molecule gene *CD28*, and several interferon-response and interferon-regulatory factor genes, such as *BCLAF1*, *IFI6*, *IFIT1* and *ISG15* (Supplementary Figure 2.4H). They also upregulated *IKZF1* (Ikaros), a transcription factor that plays a crucial role in the differentiation and effector functions of T and B cells (243, 244),

and *ZFP36* an anti-inflammatory modulator that restrains T cell responses during acute viral infection in order to suppress inflammation-related tissue damage (245).

Compared to Healthy pigs, both $CD2^+$ and $CD2^-$ γδ T cells from Infected pigs were enriched for genes involved in the type I interferon response (*IFIT1*, *IFI6*, *MX1*, *ISG15* and *STAT1*) (Figure 2.4F & G). Furthermore, both subtypes upregulated the cyclooxygenases *COX1* and *COX3*, *CD69*, and *CD84,* which is a member of the SLAM family that regulates T cell function (246). $CD2^+$ but not $CD2^-$ γδ T cells downregulated *SELL* (CD62L) after infection (Supplementary Figure 2.4G). Only $CD2^+$ γδ T cells upregulated *GZMA.1, RORA,* and *CD8A* in Infected compared to Healthy pigs. Overall, influenza infection caused $CD2^+$ γδ T cells to present a cytotoxic and pro-inflammatory gene expression profile characterized by the enrichment of granzyme genes (*GNLY*, *GZMH*), NK receptors (*KLRB1*, *NKG7*), the transcription factors *TBX21* and *ZNF683* (Hobit), and pro-inflammatory cytokine receptor *IL6R*. They also upregulated genes within the NF-kappaB (*TLR2*, *TLR4*, *TLR6*, *MYD88*, *TRAF6*, *NFKBIA*) and RIG-I (*PHB2*, *DHX58*, *GPATCH3*) signaling pathways. Compared to CD^-, $CD2^+$ γδ T cells upregulated the transcription factors *GATA3*, a master regulator of the differentiation of Th2 cells, and *YBX3*, which is involved in a number of cell processes including differentiation and stress (247). They also upregulated a variety of T cell markers (*CD3E*, *IL7R*, *CD69*, *SELL*) and receptors for pro-inflammation cytokines (*IL1R1*, *IL6R*). A KEGG pathway analysis of DEGs between $CD2^+$ and $CD2^-$ γδ T cells from Infected versus Healthy pigs indicate that the $CD2^+$ subset is primed to induce a cytotoxic response with granzyme production while the $CD2^-$ subset has a more negative regulation of immune response.

NK cells in Infected pigs upregulated *COX1* and *COX2*, genes associated with the interferon response (*STAT1*, *IFIT1*, *ISG15, GVIN1, HERC6*), *ITGA4* (integrin alpha 4), which is a subunit of the VLA-4 receptor required for NK adherence and migration through the blood and

extracellular matrix (248), and the chemokine *CCL4* that binds to CCR5 and plays a role in T cell recruitment (Figure 2.4H).

Compared to Healthy pigs, Infected pig B cells upregulated the activation/maturation markers *PAX5*, *JCHAIN*, and *CD83,* as well as *CCR7*, a chemokine that facilitates lymph node homing (Figure 2.4I). Both Infected and Inf+Trt B cells expressed more *CD69* than Healthy pigs, which is a marker of memory B cells in the lung (249, 250). However, markers of lung homing, such as *CXCR3*, *S1PR1*, *ITGAE* (CD103), and the memory B cell markers *CD27*, *CD38*, *ITGB1*, and *ITGA4* were similar among all three treatment groups. A GO analysis indicated that the type I interferon response was upregulated in B cells after influenza infection. Type I interferon signaling is reported to promote B cell survival and activation by inducing B lymphocyte stimulator expression and lowering the B cell receptor (BCR) signaling threshold (251, 252). Collectively, these data suggest that at five days post infection, B cells are responding to IFN α/β secretion and exhibiting signs of activation, migration, and memory.

Among the myeloid cell subpopulations, we found that, compared to Healthy pigs, Infected pig monocytes (cluster 16) and macrophages (cluster 17) upregulated *CD163* and *MARCKS,* as well as *CTSB* that plays an important role in intracellular proteolysis and autophagy (253). Both clusters 16 and 17 also upregulated complement system genes (*CFP*, *CFD*, *C1QA*, *C1QB*, *C1QC*). Macrophages upregulated both the alveolar macrophage chemotactic factor 2 (*AMCF-II*) and the myeloid master regulator *SPI1* (PU.1). In contrast, monocytes downregulated *SPI1*. An interrogation of KEGG pathways showed that influenza infection caused macrophages to downregulate pathways involved in suppressing influenza A viruses, viral protein interaction with cytokine, and monocyte chemotaxis, while activating non-small cell lung cancer and Ras signaling pathways. On the other hand, influenza infection caused monocytes to activate complement and

coagulation cascades and to upregulate receptors for antibodies. Additionally, they downregulated glycolysis and anti-COVID-19 response pathways.

Effect of influenza infection on cell-cell lung leukocyte communication

Next, we used CellChat (v.1.5), a tool for analysis and visualization of cell-cell interactions, to identify potential intercellular communication networks between cell types in healthy versus infected pig lungs. For comparison, the same analysis was applied to a published scRNA-seq analysis of lung leukocytes from healthy and influenza infected mice (254). Mouse samples were composed of: i) five females BALB/c mice infected with A/Fort Monmouth/1/1947/Mouse-Adapted H1N1 and lungs collected seven days post-infection, and ii) one C57BL/6J female infected with A/Puerto Rico/8/1934 H1N1 and lung collected two days post infection (193, 194). To reduce batch effects, the CellChat objects were created from an integrated Seurat dataset containing equal numbers of pig and mouse cells (Supplementary Figure 2.5A). Influenza infection resulted in an increase in the number and strength of predicted receptor-ligand interactions in both species compared to their healthy counterparts (Figure 2.5A & B). However, the number and strength of these interactions were greater in pigs compared to mice. In both infected pigs and mice, most of the interactions were categorized as Secreted Signaling (31% in pig vs 37% in mice) or ECM-Receptor signaling (60% in pig vs 40% in mice), while Cell-Cell contact represented a small proportion of the interactions, especially in pigs (9% in pig vs 23% in mice) (Table 2.5). Influenza enhanced 37 and 16 ligand-receptor pathways in pigs and mice, respectively (Supplementary Figure 2.5B). CellChat ligand-receptor interactions that were impacted by influenza infection in both species, included (i) TNFα, (ii) chemokine ligand-receptor pairs (CXCL), (iii) CD39, and (iv) intracellular adhesion molecule 1 (ICAM-1). Next, we

determined which cell types were the dominant communication hubs in each species (Figures 2.5C & D). In pigs, mast cells, macrophages, and monocytes were the dominant sources of outgoing signals while macrophages, monocytes, NK cells, and NK-like CD8 T cells were the strongest receivers (Figure 2.5C). In mice, influenza increased the communication signals from macrophages to macrophages and from macrophages to monocytes (Figure 2.5D). Resident T cells was the cell type which receive the most incoming signals.

Due to their prominence in both pig and mouse influenza communication networks, we performed a more detailed analysis of macrophages, monocytes, tissue resident T cells, NK cells, and NK-like CD8T cells. The total number of receptor-ligand pairs identified for each cell type is displayed in Table 2.6.

A detailed cell-cell interaction network of both species identified a number of ligand-receptor interactions that were similarly expressed in influenza infected pigs and mice (Figures 2.6 & 2.7). This included (i) macrophage migration inhibitory factor (MIF) signaling pathways (CD74+CXCR4, CD74+CXCR2) from B cells, αβ T cells, and γδ T cells to all other cell types, (ii) APP-CD74 signaling from macrophages, monocytes, and mast cells to all B, macrophages, mast, and DCs, (iii) MHCII-CD4 interactions from B cells and macrophages to peripheral T cells, (iv) CXCL10-CXCR3 from macrophages, monocytes and DCs to resident T cells, (v) CCL5-CCR5 from NK, macrophages and DCs to macrophages and resident T cells, and (vi) TNF-TNFRSF1B from macrophages to most other cell types. Notable differences in cell-cell interactions between species include (i) ICAM1-ITGAM/ITGAL from monocytes to all lymphoid cells, (ii) CXCL2-CXCR1 from monocytes to monocytes and neutrophils, and (iii) IL-16-CD4 from macrophages, monocytes and αβ T cells to peripheral T cells in pigs.

Next, we interrogated how lung leukocytes from infected pigs interact with each other according to the outgoing and incoming communication networks they share. The result of this analysis is a collection of so-called communication patterns that connect cell types with signaling pathways either from the standpoint of outgoing signaling when treating cells as senders or incoming signaling that treats cells as receivers (196). Three outgoing signaling patterns were detected (Figure 2.8A, Supplementary Figure 2.5C). The first pattern (pattern 1-outgoing) originated from macrophages, monocytes, and dendritic cells and indicate that these cells synergize to modulate T cell activation (MHC-II, CD80, CD86, GRN) and leukocyte recruitment and adhesion (ICAM, PECAM1, CXCL). The second pattern (pattern 2-outgoing) originated from mast cells alone and sent signals associated with cell adhesion and migration, and tissue remodeling (MK, ANGPTL, AMK, laminin, collagen). The third pattern (pattern 3-outgoing) emanated from all lymphoid cell types (NK cells, B cells, αβ T cells and γδ T cells) and neutrophils. This pattern was dominated by B cell and T cell co-stimulatory signals (CD6, CD22, CD40, CD45, CD48, LIGHT) and cytokines/chemokines (CCL, XCR, TGFβ, TNF, CSF, IL16). Five incoming patterns were identified (Figure 2.8B). The first (pattern 1-incoming) targeted NK cells, NK-like CD8 T cells, and neutrophils via expression of various ligand-receptor interactions, including ICAM, complement, Thy1, and GRN. Pattern 2-incoming ligand-receptors targeted macrophages via CD45, CCL, CSF, LIGHT, CD39, as well as Chemerin, which suppresses the M2 polarization of macrophages (255, 256). The third pattern (pattern 3-incoming) targeted mast cells through VCAM and VEGF signaling pathways. Pattern 4-incoming targeted peripheral, resident, and γδ T cell subsets predominantly through T cell co-stimulatory signals (MHC-II, CD80, CD86). The final pattern (pattern-5 incoming) targeted dendritic cells via the chemokine receptor XCR, non-conventional WNT signaling, and the adhesion molecule CADM receptor-ligand interactions.

A similar communication analysis was performed for the influenza infected mice dataset (Figures 2.8C & D, Supplementary Figure 2.5D). This identified three outgoing signaling patterns that targeted the same cell types targeted by the three outgoing signaling patterns identified in infected pigs. There was also considerable overlap between pig and mouse receptor-ligands in patterns one and three. In contrast to the outgoing patterns, there was little overlap between mouse and pig incoming patterns with many of the receptor-ligand interactions connected to different networks of cells.

To assess the impact of influenza infection on overall signaling patterns, we plotted the signaling strength of receptor-ligand pathways across different cell types for the Healthy and Infected pig groups (Figure 2.8E & F). Several signaling pathways were expressed only in Infected pigs, including pathway important for tissue remodeling (laminin, collagen, SEMA7, FN1, VEGF), cell growth and differentiation (MK), cell migration (VCAM, THBS, XCR, CDH5), and tumor cell apoptosis (CADM1). We also observed that macrophages and mast cells were particularly affected by infection with the induction of several signaling pathways that undetected in Healthy pigs, such as chemerin, complement, PROS and VCAM. Other interesting effects of infection were the increase in granzyme (GRN) signaling by NK cells, the increase in CD45, TGFβ and TNFα by macrophages, and MHC-II by peripheral T cells.

When the same analysis was performed for mice, we observed influenza induced pathways related to cell migration and motility (HGF, CDH), pro-inflammation (chemerin), and programmed cell-death (PD-L1, PDL2) across different cell types. We have also observed the TGFβ signaling pathway was weaker in infected mice compared to healthy ones. Macrophages and resident T cells were particularly affected by infection in mice. Macrophages induced several pathways including cytokine production (CCL), CD39, LIGHT, a tumor necrosis superfamily

pathway, and SEMA7. Resident T cells induced T cell activation (LCK), cell adhesion (PARs) and LIGHT during infection.

Overall, these results indicated that mast cells, macrophages and monocytes represented cell-cell interaction hubs during influenza infections in pigs, with multiple chemokine and cytokine incoming and outgoing signals. Moreover, a number of these cell-cell interactions and cytokine networks were conserved in mice despite substantial differences in technical and biological parameters, including species, virus strain, time of sample collection, and sequencing saturation.

DISCUSSION

Pigs are an important agricultural species that are susceptible to numerous respiratory pathogens, including some that infect humans. Swine are also emerging as a valuable translational model to bridge mouse and non-human primate models (228). Given that the porcine respiratory system shares many physiological and anatomical similarities with humans, they are particularly useful for studying human respiratory diseases. This includes pulmonary infections and inflammatory disorders, as well as genetic conditions that affect the lung, such as cystic fibrosis (184, 257). Also, recent technical advances in genetic editing and cloning have spurred interest in using pig lungs for xenotransplantation into humans (182, 258). Nevertheless, there remain important gaps in our understanding of the cell types and cellular pathways that constitute the pig lung cell composition, including the pulmonary immune cells (140, 259). These gaps are beginning to be addressed by an increasing number of scRNA-seq studies that have allowed unprecedented analysis of pig tissues (79, 214, 229). This includes three scRNA-seq analyses of pig lungs (210, 260).

The current work used scRNA-seq to perform a high-resolution transcriptomic analysis of the pulmonary immune cell types in healthy and influenza-infected six-week-old pigs, which developmentally corresponds to children under five years of age (261). These data were compared with published scRNA-seq datasets of mouse and human lung tissue.

Our study identified 28 cell subsets, 13 of myeloid-origin and 15 of lymphoid origin, with distinct transcriptional profiles. This includes several innate-like lymphocyte subsets, CD8αα T cells, NK-like CD8 T cells, lung-resident NK cells, and γδ T cells, which contribute to the early stages of antiviral immune responses (162).

We detected three transcriptionally distinct γδ T cell populations. The largest of these corresponds to a previously described pig *$WC1^{+}GATA3^{hi}$CD2^{-} population. Transcriptionally, CD2^{-} γδ T cells are enriched for γδ T cell signature genes (*ID3*, *SOX13)* and the TCR co-receptors *ZAP70*, *CD3E*, and **WC1*, which agrees with previous reports (214, 262). In comparison to scRNA-seq profiling in other pig tissues, we observed that lung CD2^{-} γδ T cells made up a much higher proportion of γδ T cells in the lung than the intestinal mucosa, which supports the finding that the lung has a bias for CD2^{-} γδ T cells (163). Our study also agrees with previous reports that despite high expression of *GATA3*, which is a transcription factor that enhances *IL4* gene regulation, CD2^{-} γδ T do not express *IL4* (262). Additionally, most lung CD2^{-} γδ T cells were *SELL* (CD62L)^{hi} whereas ileac CD2^{-} γδ T cells were mostly *SELL*^{lo}. Although human and cattle γδ T cells can be divided into central and effector memory subsets based on CD62L expression, we found no evidence that pig lung CD2^{-} γδ T cells were memory γδ T cells since they lacked other memory markers. Additionally, the fact that pig lung CD2^{-} γδ T cells integrated with human lung γδ T cells, while pig blood CD2^{-} γδ T cells had the highest mapping score with human ILCs (214), is further evidence that pig lung CD2^{-} γδ T cells have a distinct phenotype from those found in the blood. On the other hand, lung CD2^{+} γδ T cells had similar transcriptomic profile to those found in blood and ileum. The CD2^{+} γδ T cell subset appeared to be specialized to perform cytolytic effector functions since this cluster was enriched for the pro-inflammatory transcription factors *TBX21* and *EOMES,* inflammatory cytokines *TNFA* and *IFNG*, and granzymes *GZMH* and *GNLY*. This transcriptional profile agrees with CD2^{+} γδ T cells profiled in pig blood and ileum by scRNA-seq. However, tissue-specific differences also exist. For instance, lung CD2^{+} γδ T cells were enriched for *FCER1G, ITGB1,* and the chemokine *XCL1* which were not detected in ileum CD2^{+} γδ T cells. These site-specific differences in lineage defining genes point towards the

acquisition of site-specific adaptations of γδ T cell subsets, perhaps for different pathogens. Finally, our data indicate that γδ T cells differentiate into $CD2^+$ and $CD2^-$ subsets before they populate the lung tissue as they clustered separately in UMAP space with no transitioning cells between clusters. This contradicts previous reports which suggested that the $CD2^-$ population represent naive γδ T cells that differentiate to $CD2^+$ γδ T cells once activated (259, 263). Moreover, it agrees with publications that $CD2^-$ and $CD2^+$ γδ T are a developmentally distinct γδ T cell subsets that complete their differentiation in the thymus (163, 220, 262).

Our pseudotime analysis and hierarchical clustering tree showed that NK cells are transcriptionally related to $CD2^+$ γδ T cells, tissue effector memory, and NK-like CD8 T cells. The latter is a cell type that resembles an innate $CD8^+$ T cell population, referred to as cytotoxic CD8 T cells, previously identified from a pig thymus dataset (79). These cells have a memory T cell phenotype and express several genes associated with cytotoxic functions. Another notable lineage connected tissue resident αβ T cells with $CD2^-$ γδ T cells, and CD8αα T cells. The latter is a minor T cell subset that has been identified in pig thymus, blood, and ileum that is enriched for *ZNF683, CD44, *IL2RB, CCL5, KLRK1, *KLRD1*, and *XCL1*. These cells resemble a population of mouse cells found in the intestinal epithelial layer that is thought to play a regulatory role in inhibiting intestinal inflammation (264, 265). Homodimer CD8α has also been found to play a role in controlling herpes virus infection in the human skin (266).

Our cross-species analysis indicates that the immune cell composition of pig lungs is more similar to humans than to mice, particularly as regards their relatively low proportion of B cells and peripheral T cells and high concentration of NK cells. Our results are consistent with a previous comparison of pulmonary scRNA-seq datasets among these species (210). Pigs were unique for their high proportion of γδ T cells which presents a significant divergence from mice

and humans with potentially important implications for how these different species respond to respiratory infections. γδ T cells express receptors for multiple cytokines secreted by innate immune cells after microbial exposure and respond by secreting large amounts of proinflammatory of cytokines within hours after activation. Thus, having high concentrations of these cells in the respiratory tract may improve pathogen clearance. On the other hand, it is also possible that they may exacerbate lung disease under certain circumstances since accumulation of inflammatory cells in the airway tissue is an important contributor to pulmonary lesion (267-269). Our comparison of transcription factor profiles within clusters found a high degree of conservation among species, indicating that transcription factor binding specificities are highly conserved within cell types for pigs, mice, and humans. One exception was in the mast/ILC2 cluster in which human and pigs were enriched for *ID2*, a transcriptional regulator required for innate lymphoid cell fate determination, and *GATA2* and *MITF* which are transcription factors required for mast-cell mediated responses (211). The corresponding mouse cluster was enriched for *MEF2A*, *ATF3* and *ID3*, that respectively regulates apoptosis, inflammation and survival, TLR4-driven inflammation, and the development of regulatory ILCs (270-272).

Our study analyzed perturbations in cell types and transcriptional networks caused by influenza virus infection and oseltamivir treatment and compared these results to published datasets from healthy and influenza infected mice. Influenza infection caused the upregulation of antiviral and interferon immune signatures across all cell types. Furthermore, we observed an increase in the proportion of cytotoxic T cells, peripheral T cells and B cells, while the proportion of NK cells and cycling cells decreased. This agrees with previous mouse studies which found that at a similar time after a sublethal influenza infection there was an increase in lymphocyte B and T migration, and a concomitant reduction in NK cells (273-275). In contrast, leukopenia, or decrease

count on lymphocytes, is typically seen as marker of severe and/or lethal influenza in mice and humans (275, 276).

Oseltamivir treatment caused very few changes in gene expression compared to influenza infected pigs that remained untreated, which indicates that administering this therapy did not significantly impact the anti-influenza virus response. Nevertheless, we did observe decrease in *STAT1*, several interferon-related genes (*IRF7*, *ISG15*, *IFI6*, *IFIT2*, *IFITM3*) and *CCL4*, that indicate a general reduction in viral-replication control response. Moreover, the CCL4 receptor, CCR5, promotes the recruitment of adaptive and innate immune cells into the site of infection, which is critical to viral clearance, but can also aggravate inflammation and pulmonary damage (277, 278).

When DEGs were examined in individual cell types we found that B cells, followed by cytotoxic T cells, and $CD2^+$ T cells were the lymphoid cells the most impacted by influenza infection. B cells upregulated several key transcription regulators (*EBF1*, *TCF4*, *PAX5*, *MYC*) and genes in response to type I interferon (*IRF7*, *IRF8*), indicating these cells are proliferating and differentiating towards a mature B cell state and may be undergoing somatic hypermutation and class-switch recombination. A similar B cell phenotype is found in germinal centers and plasma cells, and it is likely such B cells are important in the production of high affinity antibodies and overall adaptive response to influenza (279). Influenza infection cause $CD2^+$ γδ T cells to upregulate proinflammatory genes known to be important for suppressing virus replication. Some of these genes were also upregulated by influenza in $CD2^-$ γδ T cells. However, $CD2^-$ γδ T cells subset expressed lower levels of cytotoxicity genes *GNLY*, *GZMA.1*, *KLRK1* than $CD2^+$ T cells. This suggests that while the two γδ T cell subset play similar functions during viral respiratory infections in pigs, $CD2^+$ γδ T cells appear to function as mediators of cytotoxicity and

inflammation during the early stage of disease. NK cells presented a transcriptional profile that is consistent with a human population of NK cells that arise after influenza infection, which upregulate *STAT1* and *CCL4* (280). NK cells are also known to produce large quantities of IFN-γ following influenza infection (281). However, we did not detect a difference in *IFNG* expression between infected and healthy pigs. This may have been because cells isolated for scRNA-seq were collected five days post infection, which is past the peak of IFN-γ production.

Our comparison of communication networks found that influenza infection had a more profound effect on the number and strength of cell-cell interactions in pigs compared to mice. This is surprising as influenza infections cause much more severe disease in most inbred strains of mice compared to pigs as they carry a dysfunctional copy of the Mx1 antiviral gene (282). Some receptor ligand interactions were conserved between species, such as the TNF and MHC-II/CD4 signaling between macrophages and peripheral T cell, and FN1-CD44 signaling between monocytes and lymphoid cells. However, there were also substantial differences in cell types, receptor-ligand interactions, and incoming and outgoing signaling patterns between species. This likely reflects the differences in mouse and pig antiviral immune defenses that include several non-orthologous antiviral genes with low sequence similarity (93, 283). Analysis of the pig networks suggests that mast cells, macrophages, and monocytes were the dominant sources of outgoing signals while macrophages, monocytes, NK cells, and NK-like CD8 T cells were the strongest receivers. These cells coordinated a complex network of signaling pathways that include T cell co-stimulation, cytokine and chemokine signaling, tissue remodeling, and cell cytoskeletal reorganization. These results indicate that five days after infection, pig lungs are undergoing dynamic changes in tissue architecture, cell recruitment, and cellular activation in response to ongoing virus replication.

In summary, our analysis of the pulmonary microenvironment of healthy and influenza infected pigs revealed the complexity of cell types constituting lung leukocytes as well as the scope of interactions between lymphoid and myeloid cell subtypes to support anti-influenza immune responses. The complexity that our single cell transcriptomics study provides represents a substantial advance from the limited resolution of bulk population studies and other conventional approaches for studying the pulmonary immune system. Our systematic comparison of lung leukocytes between pig and human and between pig and mouse highlights species-specific cell states that should be taken into consideration when using pigs or mice to model human influenza virus infections.

Limitations of the study

Although this study has provided a comprehensive transcriptional analysis of pig lung leukocytes, we only profiled pigs at a single age and did not include non-leukocyte cell populations. Moreover, lung samples were obtained at a single time point after influenza virus infection. In the future, it will be important to expand our dataset to capture the full extent of lung cellularity at different ages and different timepoints after influenza infection. Additionally, we cannot exclude that some of the interspecies differences we observed in cell subsets and intercellular communication networks were due to biological and technical effects, such as differences in physiological age, tissue preparation methods, and sequencing saturation. Hence, validation of our findings is required using additional datasets as they become available.

Table 2.1. Quantity of samples in each treatment group in the pig dataset

Infection/ Treatment	Pooled animals per sample	Samples
mock/mock	1	2
pdmH1N1/mock	1	3
pdmH1N1/mock	2	2
pdmH1N1/OS	1	3
pdmH1N1/OS	2	2
Total		12

Table 2.2. Percentage of CD4+ and CD4+CD8A+ cells per total cluster cells and ratio of CD8A/CD4 and CD8A/CD8B markers in lymphoid cell types

		Percentage (%)		Ratio	
Cluster	Cell type	*CD4*$^{+}$	*CD4*$^{+}$ *CD8A*$^{+}$	*CD8A*/*CD4*	*CD8A*/*CD8B*
3	NK-like CD8 T cells	0	0	735.0	3.4
4	Resident NK Cells	0	0	73.3	31.4
5	TEM cytotoxic T cells	0.9	0.7	38.1	3.2
6	Resident T cells	31.1	11.0	0.6	9.9
7	Peripheral CD4 T cells	38.5	1.7	0.1	3.3
8	Peripheral CD8 T cells	3.8	3.5	8.2	1.3
9	CD8αα T cells	0.5	0.5	28.5	8.1

Table 2.4. Total number and percentage of single cells belonging to the lymphoid or myeloid type of cells

	Lymphoid		Myeloid	
	n	%	*n*	%
Pig	2156	88.94	268	11.06
Human	1142	47.95	1240	52.06
Mouse	1880	77.97	531	22.02

Table 2.5. Quantification of cell-cell communication in each dataset populations

Dataset	Signaling Pathways	ECM-Receptor	Cell-Cell Contact	Total
Pig	119	0	36	155
Pig flu	176	340	51	567
Mouse	166	339	150	655
Mouse flu	195	208	118	521

Table 2.6. Differential expressed genes in influenza compared to healthy pigs and oseltamivir treated compared to influenza-infected pigs for different immune cell populations

Cell population	DEGS Healthy vs Infected	DEGS Infected vs Inf+Trt
NK cells	892	158
NK-like CD8 T	550	52
Cytotoxic T cells	1169	54
T cells	1094	80
Peripheral T cells	983	73
$CD2^{-}$ γδ T cells	735	79
$CD2^{+}$ γδ T cells	1143	261
B cells	1294	111
Ab producing B cells	1020	494
Neutrophils $CD3E^{+}$	802	242
Neutrophils	1296	686
Neutrophils $CD3E^{+}$	828	464
Mast	2087	870
Monocytes	1731	568
Macrophages	1253	515
cDC1	1011	458
cDC2	1309	211
pDC	1557	299

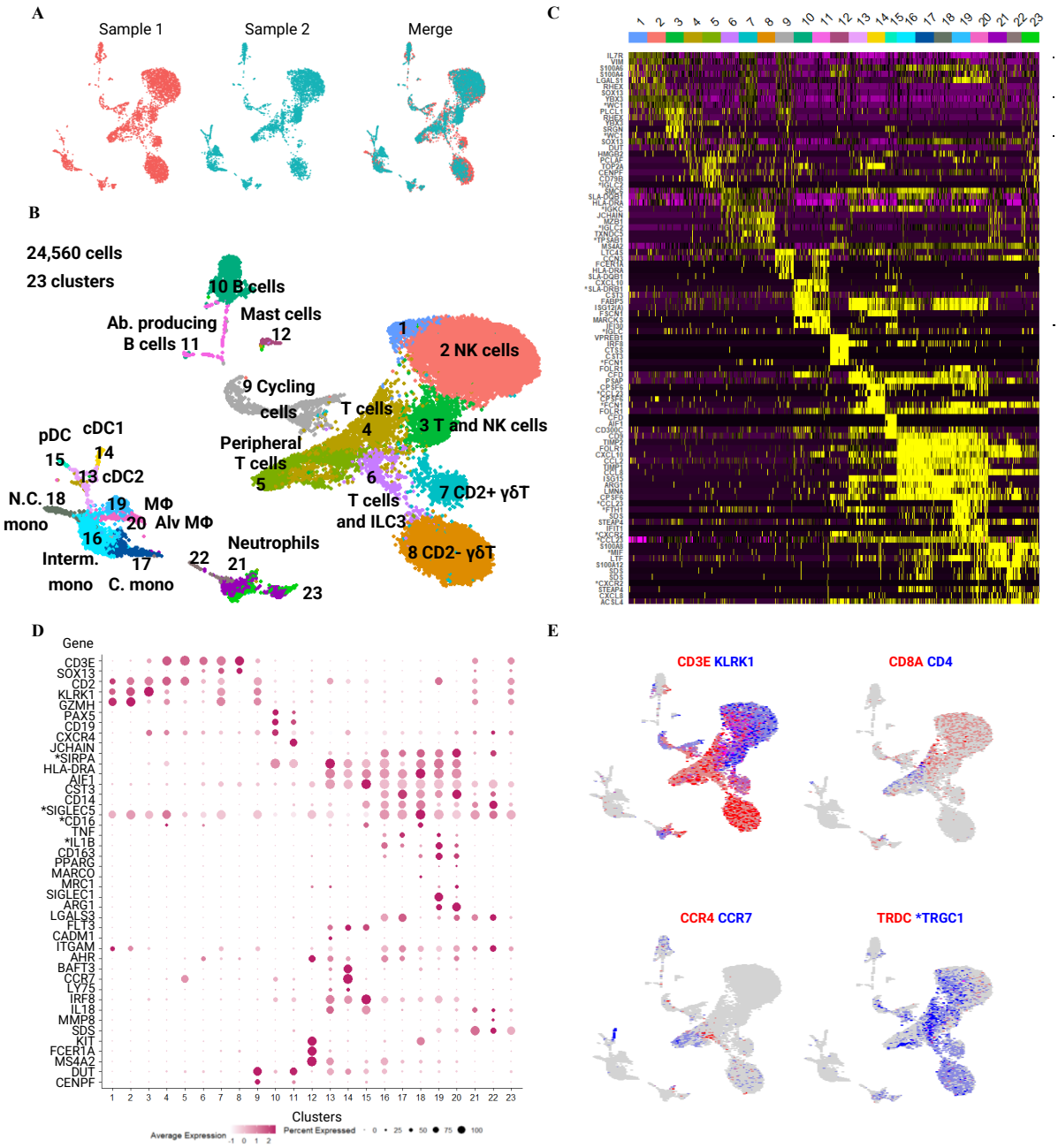
A
Sample 1
Sample 2
Merge
B
24,560 cells
23 clusters
10 B cells
Mast cells
12
Ab. producing
B cells 11
1
2 NK cells
9 Cycling
cells
T cells
4
3 T and NK cells
Peripheral
T cells
5
6
T cells
and ILC3
7 CD2+ γδT
8 CD2- γδT
pDC
15
cDC1
14
13 cDC2
N.C. 18
mono
19
MΦ
20
Alv MΦ
16
Interm.
mono
17
C. mono
Neutrophils
22
21
23
C
D
Gene
CD3E
SOX13
CD2
KLRK1
GZMH
PAX5
CD19
CXCR4
JCHAIN
*SIRPA
HLA-DRA
AIF1
CST3
CD14
*SIGLEC5
*CD16
TNF
*IL1B
CD163
PPARG
MARCO
MRC1
SIGLEC1
ARG1
LGALS3
FLT3
CADM1
ITGAM
AHR
BAFT3
CCR7
LY75
IRF8
IL18
MMP8
SDS
KIT
FCER1A
MS4A2
DUT
CENPF
1 2 3 4 5 6 7 8 9 10 11 12 13 14 15 16 17 18 19 20 21 22 23
Clusters
Average Expression
Percent Expressed
E
CD3E KLRK1
CD8A CD4
CCR4 CCR7
TRDC *TRGC1

Figure 2.1. Single-cell transcriptomic analysis of the cellular composition of the pig lung. (A) Two-dimensional visualization of uniform manifold approximation and projection (UMAP) showing integrative analysis of lung leukocytes from two pigs. **(B)** UMAP visualization of lung leukocyte clusters identified using the graph-based Louvain algorithm at a resolution of 0.6. **(C)** Heatmap displaying the row-scaled mean expression of the top five highest differentially expressed genes factors per cluster. Asterisks indicate non-annotated genes. **(D)** Dot plot showing the Z-scored mean expression of marker genes used to designate each cell cluster into a cell subtype. Color saturation indicates the strength of expression in positive cells, while dot size reflects the percentage of each cell cluster expressing the gene. Asterisks indicate non-annotated genes. **(E)** The same UMAP as shown in (B) representing classical T and NK markers.

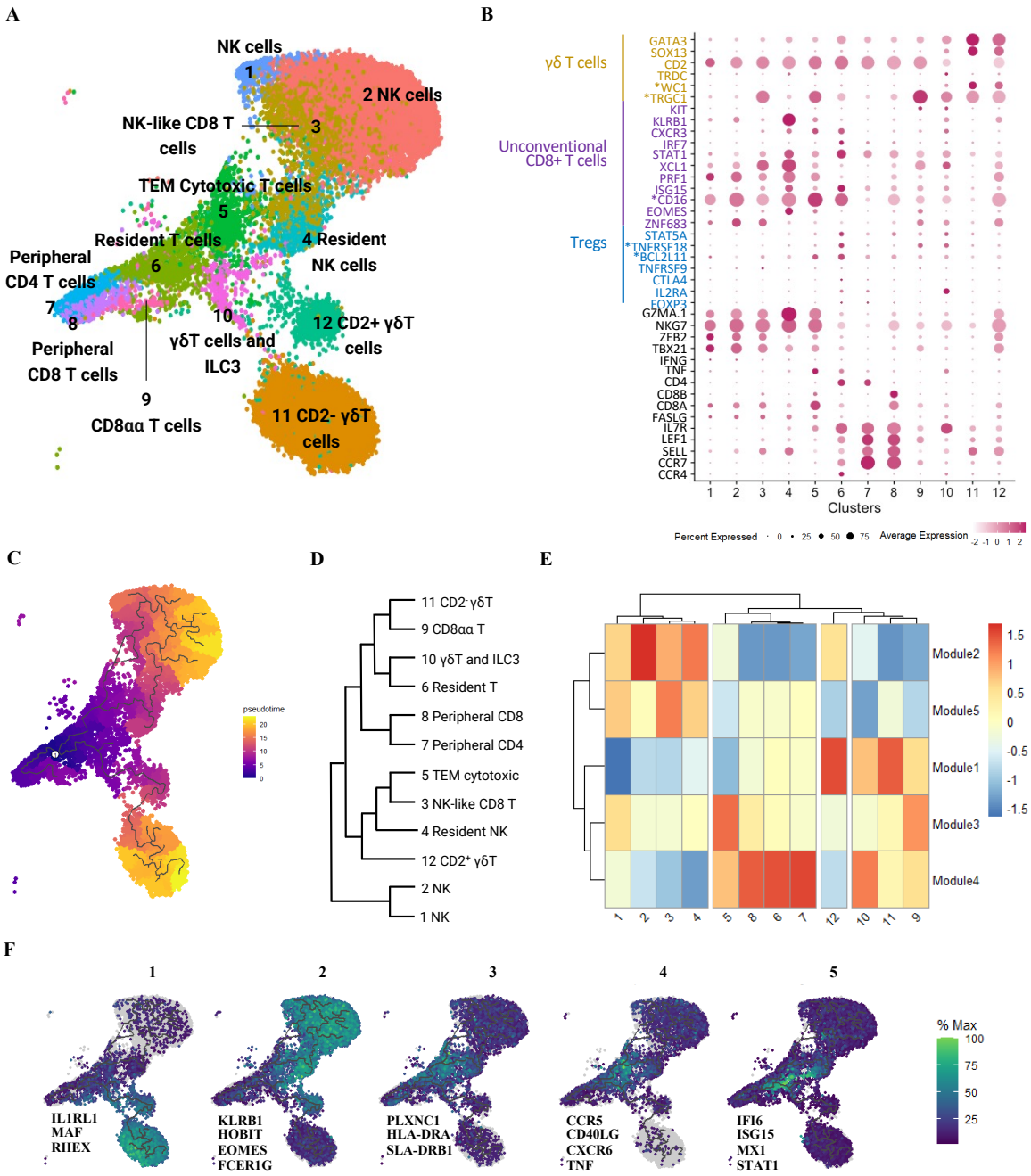
A
NK cells
1
2 NK cells
NK-like CD8 T cells
3
TEM Cytotoxic T cells
5
Resident T cells
4 Resident NK cells
Peripheral CD4 T cells
6
7
8
10
12 CD2+ γδT cells
γδT cells and ILC3
Peripheral CD8 T cells
9
CD8αα T cells
11 CD2- γδT cells
B
γδ T cells
Unconventional CD8+ T cells
Tregs
GATA3
SOX13
CD2
TRDC
*WC1
*TRGC1
KIT
KLRB1
CXCR3
IRF7
STAT1
XCL1
PRF1
ISG15
*CD16
EOMES
ZNF683
STAT5A
*TNFRSF18
*BCL2L11
TNFRSF9
CTLA4
IL2RA
FOXP3
GZMA.1
NKG7
ZEB2
TBX21
IFNG
TNF
CD4
CD8B
CD8A
FASLG
IL7R
LEF1
SELL
CCR7
CCR4
1 2 3 4 5 6 7 8 9 10 11 12
Clusters
Percent Expressed
Average Expression
C
pseudotime
D
11 CD2- γδT
9 CD8αα T
10 γδT and ILC3
6 Resident T
8 Peripheral CD8
7 Peripheral CD4
5 TEM cytotoxic
3 NK-like CD8 T
4 Resident NK
12 CD2+ γδT
2 NK
1 NK
E
Module2
Module5
Module1
Module3
Module4
1.5
1
0.5
0
-0.5
-1
-1.5
F
1
2
3
4
5
IL1RL1
MAF
RHEX
KLRB1
HOBIT
EOMES
FCER1G
PLXNC1
HLA-DRA
SLA-DRB1
CCR5
CD40LG
CXCR6
TNF
IFI6
ISG15
MX1
STAT1
% Max
100
75
50
25

Figure 2.2. Characterization and trajectory analysis of pig lung lymphoid cells. (A) UMAP plot of T lymphocytes, innate lymphoid cell (ILC) and NK cell subsets clustered using the graph-based Louvain algorithm at a resolution of 0.7. **(B)** Dot plot showing the Z-scored mean expression of marker genes used to designate lymphoid clusters into each cell subtype. Color saturation indicates the strength of expression in positive cells, while dot size reflects the percentage of each cell cluster expressing the gene. Asterisks indicate non-annotated genes. **(C)** Pseudotime trajectory created by Monocle3 using lymphoid clusters from (A). **(D)** Hierarchical clustering tree built by Seurat and visualized with the ggtree package using the default options. **(E)** Heatmap of five gene modules whose expression varied across pseudotime between clusters. **(F)** UMAP plots showing the expression profiles of select genes from modules 1-5.

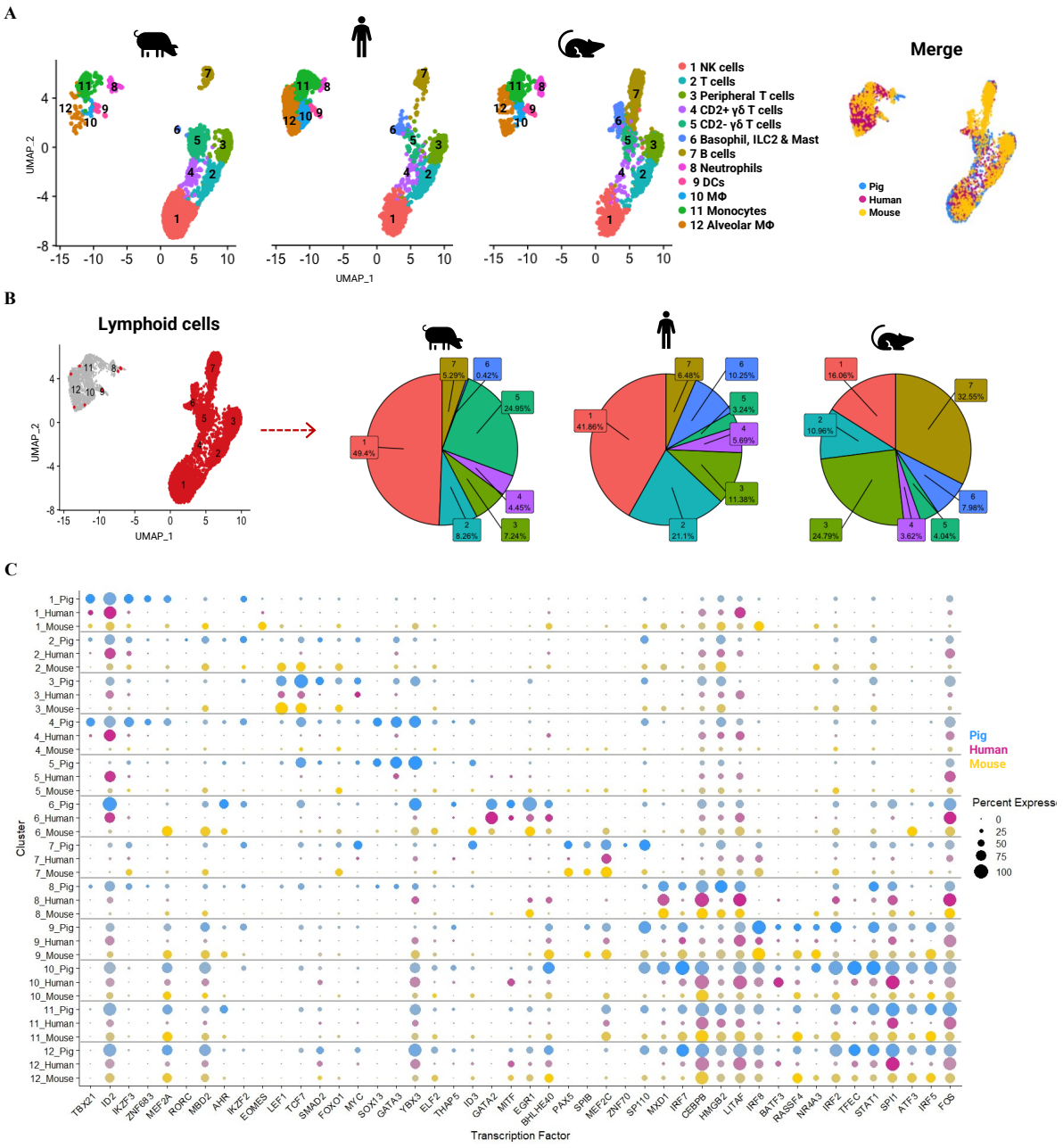
A
1 NK cells
2 T cells
3 Peripheral T cells
4 CD2+ γδ T cells
5 CD2- γδ T cells
6 Basophil, ILC2 & Mast
7 B cells
8 Neutrophils
9 DCs
10 MΦ
11 Monocytes
12 Alveolar MΦ
Merge
Pig
Human
Mouse
UMAP_1
UMAP_2
B
Lymphoid cells
C
Cluster
Transcription Factor
Percent Expressed
Pig
Human
Mouse

Figure 2.3. Integrative analysis of pig, human and mouse lung leukocytes. (A) UMAP displaying an integrative analysis of human, mouse, and pig lung leukocytes using a canonical correlation approach to identify shared genes between datasets. **(B)** The percentage of lymphoid cells present in each species. **(C)** Dot plot displaying the z-scored mean expression of the most highly expressed pig transcription factors for each cell type. Each color corresponds to a distinct species. Color saturation represents the intensity of the gene expression while the dot size denotes the proportion of cell clusters that express the gene.

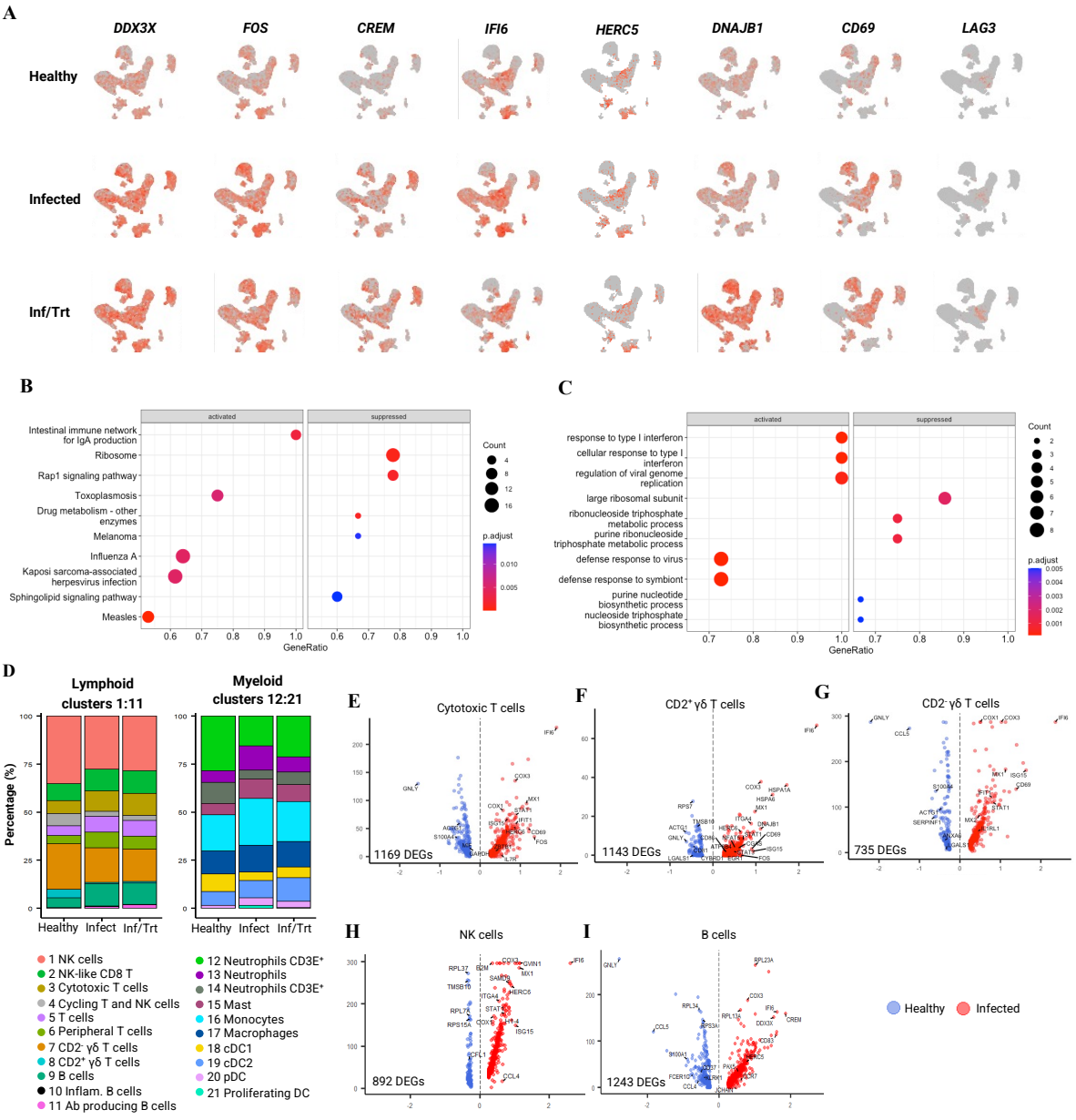
A
DDX3X
FOS
CREM
IFI6
HERC5
DNAJB1
CD69
LAG3
Healthy
Infected
Inf/Trt
B
activated
suppressed
Intestinal immune network for IgA production
Ribosome
Rap1 signaling pathway
Toxoplasmosis
Drug metabolism - other enzymes
Melanoma
Influenza A
Kaposi sarcoma-associated herpesvirus infection
Sphingolipid signaling pathway
Measles
GeneRatio
Count
p.adjust
C
response to type I interferon
cellular response to type I interferon
regulation of viral genome replication
large ribosomal subunit
ribonucleoside triphosphate metabolic process
purine ribonucleoside triphosphate metabolic process
defense response to virus
defense response to symbiont
purine nucleotide biosynthetic process
nucleoside triphosphate biosynthetic process
GeneRatio
D
Lymphoid clusters 1:11
Myeloid clusters 12:21
Percentage (%)
Healthy
Infect
Inf/Trt
1 NK cells
2 NK-like CD8 T
3 Cytotoxic T cells
4 Cycling T and NK cells
5 T cells
6 Peripheral T cells
7 CD2- γδ T cells
8 CD2+ γδ T cells
9 B cells
10 Inflam. B cells
11 Ab producing B cells
12 Neutrophils CD3E+
13 Neutrophils
14 Neutrophils CD3E+
15 Mast
16 Monocytes
17 Macrophages
18 cDC1
19 cDC2
20 pDC
21 Proliferating DC
E
Cytotoxic T cells
1169 DEGs
F
CD2+ γδ T cells
1143 DEGs
G
CD2- γδ T cells
735 DEGs
H
NK cells
892 DEGs
I
B cells
1243 DEGs
Healthy
Infected

Figure 2.4. Transcriptional analysis of changes induced by influenza infection in pigs. (A) UMAP plots displaying the expression patterns of selected genes in healthy, influenza-infected, and influenza-infected oseltamivir-treated pigs. **(B)** Dot plot displaying the ten most enriched KEGG pathways in influenza-infected pigs. **(C)** Dot plot displaying the ten most enriched GO terms in influenza-infected pigs. **(D)** Frequency of lymphocyte and myeloid cell subpopulations in each treatment group. **(E-I)** Volcano plots showing differentially expressed genes between Healthy and Infected pigs, **(E)** cytotoxic T cells, **(F)** $CD2^{+}$ γδ T cells, **(G)** $CD2^{-}$ γδ T cells, **(H)** NK cells, and **(I)** B cells. The x-axis and y-axis represent log2 (fold change) and -log10 (p-value), respectively.

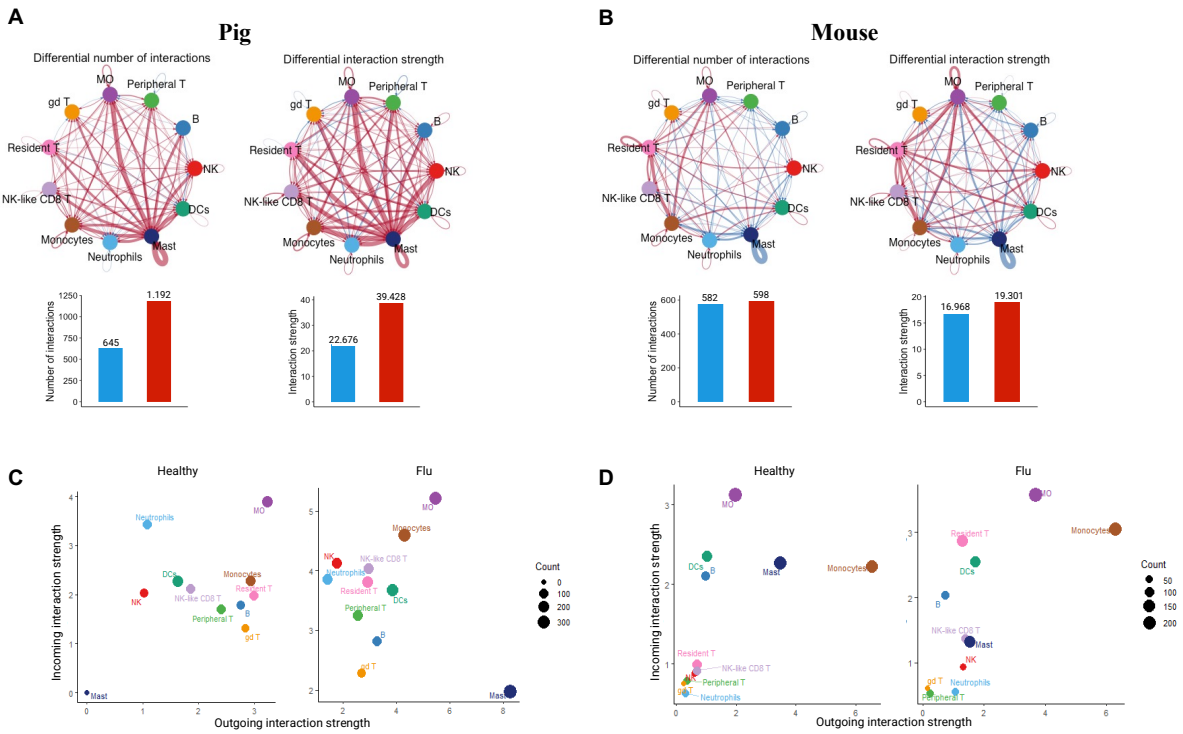

Figure 2.5. Cell-cell communication in healthy and influenza infected animals. (A-B) Circular plots displaying the number and strength of the main cell-cell interactions in healthy (blue) and influenza-infected (red) pigs **(A)** and mice **(B)**. Public datasets containing mouse lung cell samples were used (193, 194). The number and strength of interactions for healthy and infected animals of each species is quantified by bar plots below each circular plot. **(C-D)** Scatter plots showing the major source and targets of cell communication in healthy and influenza infected **(C)** pigs and **(D)** mice. The color indicates immune cell subtypes and dot size is proportional to the number of inferred communication (incoming and outgoing signaling) associated with each cell type.

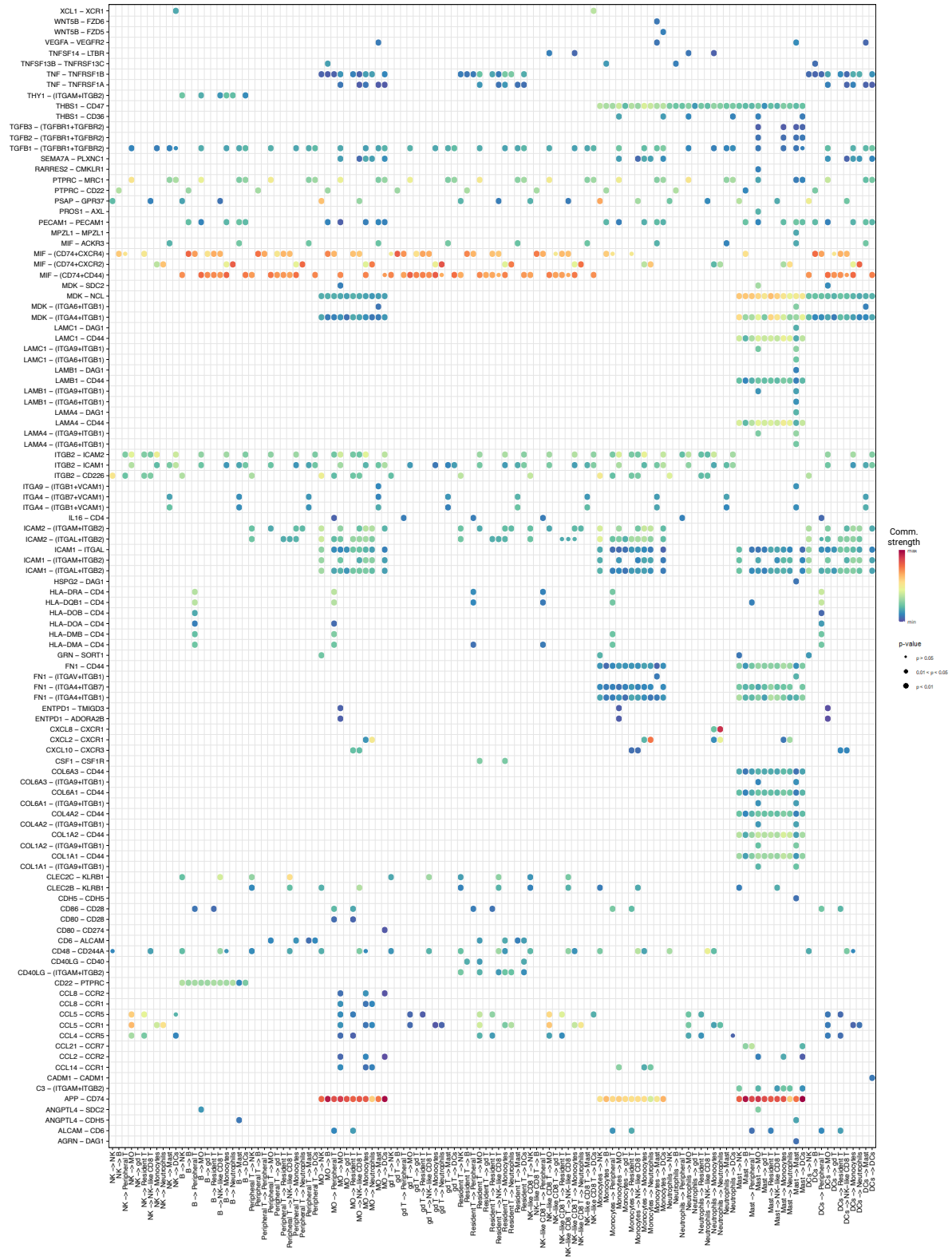
XCL1 – XCR1
WNT5B – FZD6
WNT5B – FZD5
VEGFA – VEGFR2
TNFSF14 – LTBR
TNFSF13B – TNFRSF13C
TNF – TNFRSF1B
TNF – TNFRSF1A
THY1 – (ITGAM+ITGB2)
THBS1 – CD47
THBS1 – CD36
TGFB3 – (TGFBR1+TGFBR2)
TGFB2 – (TGFBR1+TGFBR2)
TGFB1 – (TGFBR1+TGFBR2)
SEMA7A – PLXNC1
RARRES2 – CMKLR1
PTPRC – MRC1
PTPRC – CD22
PSAP – GPR37
PROS1 – AXL
PECAM1 – PECAM1
MPZL1 – MPZL1
MIF – ACKR3
MIF – (CD74+CXCR4)
MIF – (CD74+CXCR2)
MIF – (CD74+CD44)
MDK – SDC2
MDK – NCL
MDK – (ITGA6+ITGB1)
MDK – (ITGA4+ITGB1)
LAMC1 – DAG1
LAMC1 – CD44
LAMC1 – (ITGA9+ITGB1)
LAMC1 – (ITGA6+ITGB1)
LAMB1 – DAG1
LAMB1 – CD44
LAMB1 – (ITGA9+ITGB1)
LAMB1 – (ITGA6+ITGB1)
LAMA4 – DAG1
LAMA4 – CD44
LAMA4 – (ITGA9+ITGB1)
LAMA4 – (ITGA6+ITGB1)
ITGB2 – ICAM2
ITGB2 – ICAM1
ITGB2 – CD226
ITGA9 – (ITGB1+VCAM1)
ITGA4 – (ITGB7+VCAM1)
ITGA4 – (ITGB1+VCAM1)
IL16 – CD4
ICAM2 – (ITGAM+ITGB2)
ICAM2 – (ITGAL+ITGB2)
ICAM1 – ITGAL
ICAM1 – (ITGAM+ITGB2)
ICAM1 – (ITGAL+ITGB2)
HSPG2 – DAG1
HLA–DRA – CD4
HLA–DQB1 – CD4
HLA–DOB – CD4
HLA–DOA – CD4
HLA–DMB – CD4
HLA–DMA – CD4
GRN – SORT1
FN1 – CD44
FN1 – (ITGAV+ITGB1)
FN1 – (ITGA4+ITGB7)
FN1 – (ITGA4+ITGB1)
ENTPD1 – TMIGD3
ENTPD1 – ADORA2B
CXCL8 – CXCR1
CXCL2 – CXCR1
CXCL10 – CXCR3
CSF1 – CSF1R
COL6A3 – CD44
COL6A3 – (ITGA9+ITGB1)
COL6A1 – CD44
COL6A1 – (ITGA9+ITGB1)
COL4A2 – CD44
COL4A2 – (ITGA9+ITGB1)
COL1A2 – CD44
COL1A2 – (ITGA9+ITGB1)
COL1A1 – CD44
COL1A1 – (ITGA9+ITGB1)
CLEC2C – KLRB1
CLEC2B – KLRB1
CDH5 – CDH5
CD86 – CD28
CD80 – CD28
CD80 – CD274
CD6 – ALCAM
CD48 – CD244A
CD40LG – CD40
CD40LG – (ITGAM+ITGB2)
CD22 – PTPRC
CCL8 – CCR2
CCL8 – CCR1
CCL5 – CCR5
CCL5 – CCR1
CCL4 – CCR5
CCL21 – CCR7
CCL2 – CCR2
CCL14 – CCR1
CADM1 – CADM1
C3 – (ITGAM+ITGB2)
APP – CD74
ANGPTL4 – SDC2
ANGPTL4 – CDH5
ALCAM – CD6
AGRN – DAG1
Comm. strength
max
min
p-value
p > 0.05
0.01 < p < 0.05
p < 0.01

Figure 2.6. Ligand and receptor pairs in influenza-infected pig lung leukocytes. Ligand and receptor pairs displayed according to source and target cell subtypes in influenza-infected pigs during cell-cell communication by cell subtype. Dot size represents the significance of the receptor-ligand interaction for each sender and receiver pair.

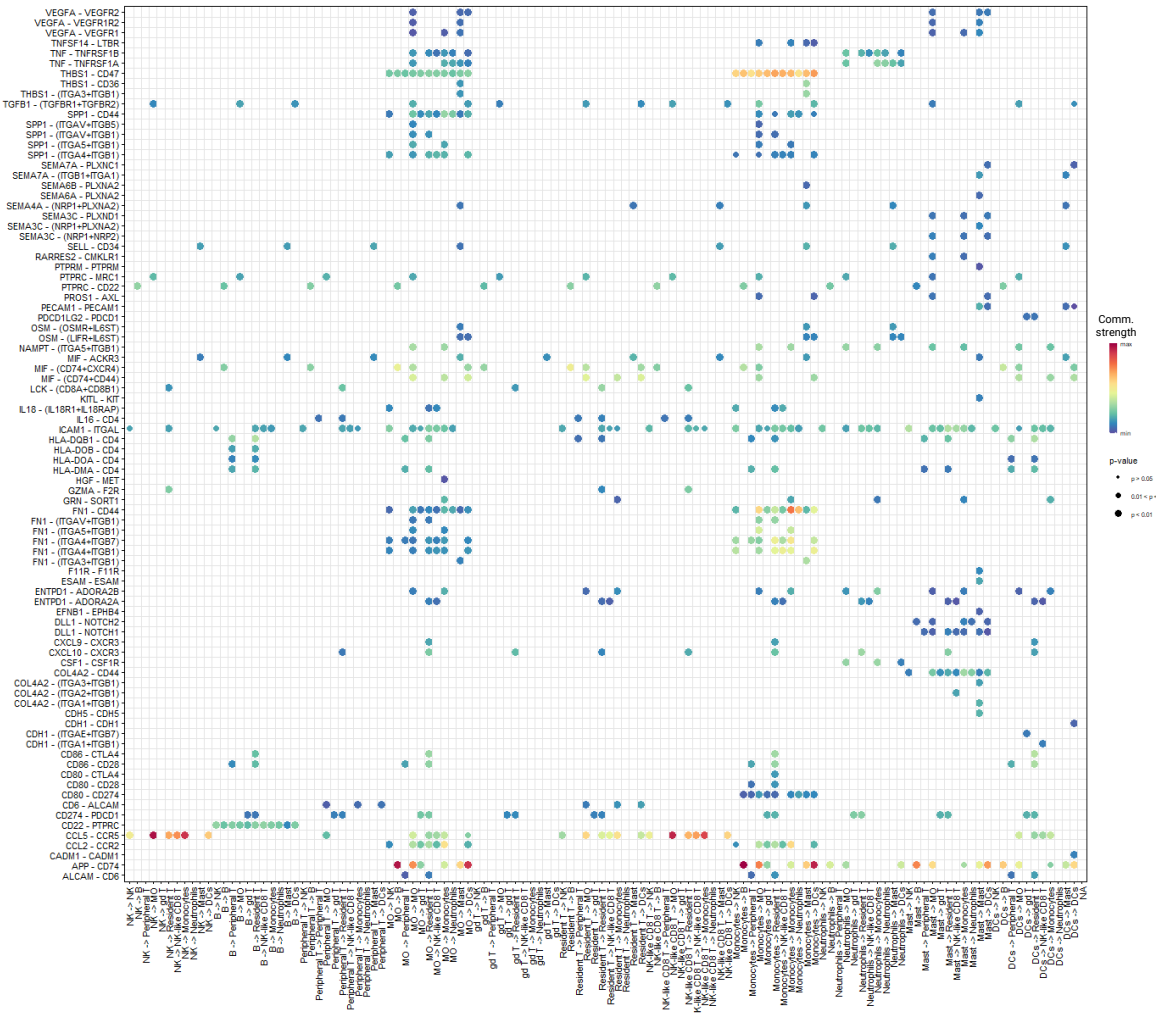

Figure 2.7. Ligand and receptor pairs in influenza-infected mice lung leukocytes. Ligand and receptor pairs displayed according to source and target cell subtypes in influenza-infected mice during cell-cell communication by cell subtype. Dot size represents the significance of the receptor-ligand interaction for each sender and receiver pair. Public datasets containing mouse lung cell samples was used (193, 194).

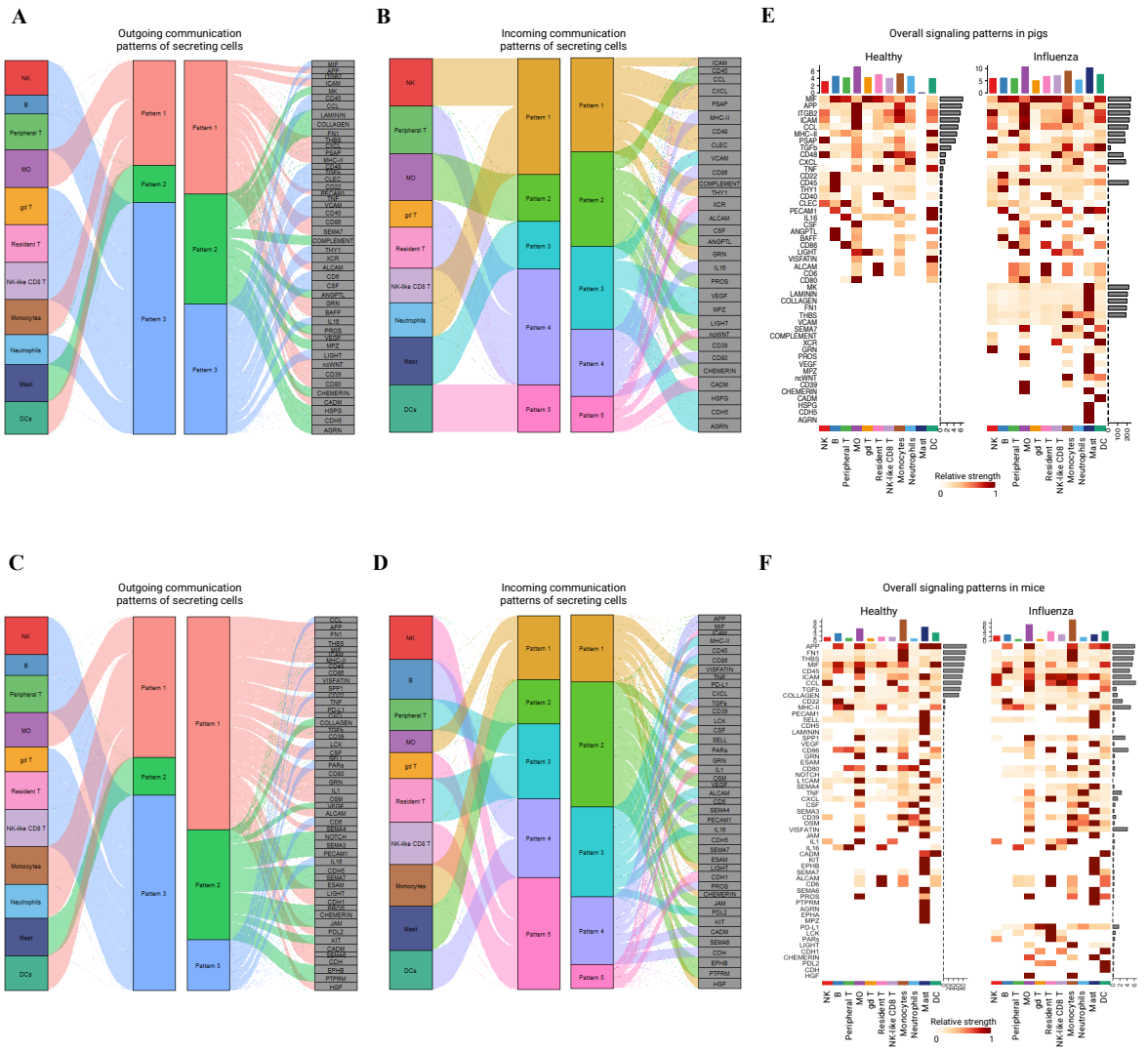

Figure 2.8. Communication pattern analysis between lung leukocytes in influenza-infected pig and mice. (A-B) Outgoing **(A)** and incoming **(B)** communication patterns of cell-cell signaling pathways in leukocytes from infected pigs. **(C-D)** Outgoing **(C)** and incoming **(D)** communication patterns of cell-cell signaling pathways in leukocytes from infected mice. **(E-F)** Heatmaps showing the relative strength of predicted cell communication pathways (outgoing and incoming signaling) for each cell type in healthy and influenza-infected pigs **(E)** and mice **(F)**.

A

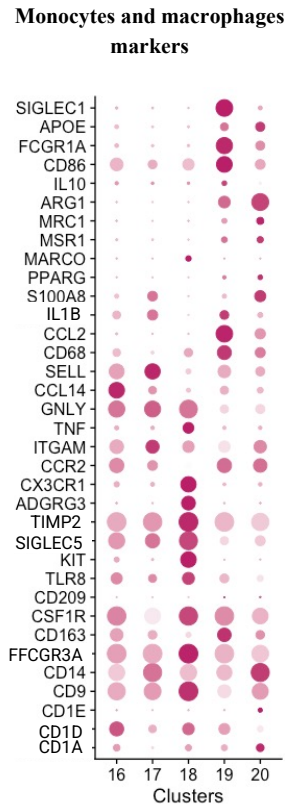

B

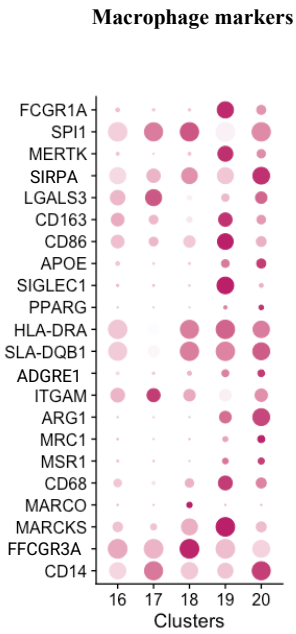

C

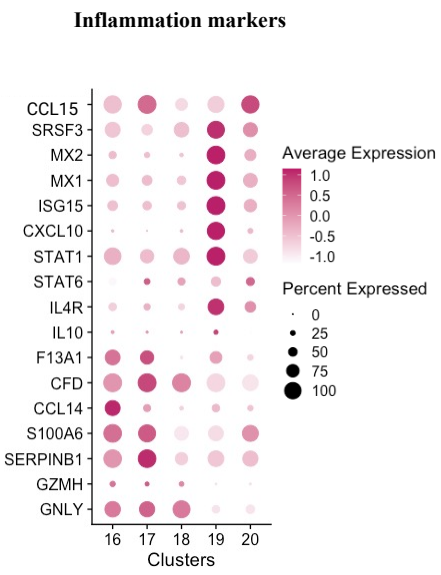

D

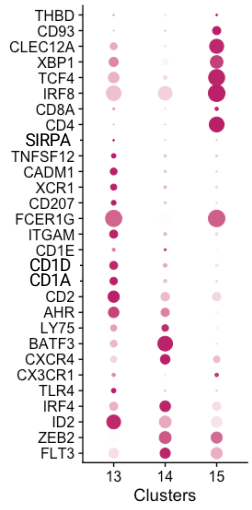

E

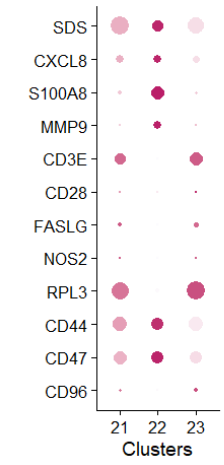

Cluster legend

13 cDC2
14 cDC1
15 pDC
16 Intermediate monocytes
17 Classical monocytes
18 Non-classical monocytes
19 MΦ
20 Alv. MΦ
21 CD3+ neutrophils
22 Neutrophils
23 CD3+ neutrophils

Supplementary Figure 2.1. Dot plot displaying markers used to differentiate **(A)** monocytes and macrophages; **(B)** macrophages; **(C)** monocytes and macrophages with pro-inflammatory markers; **(D)** DC markers; **(E)** neutrophil markers.

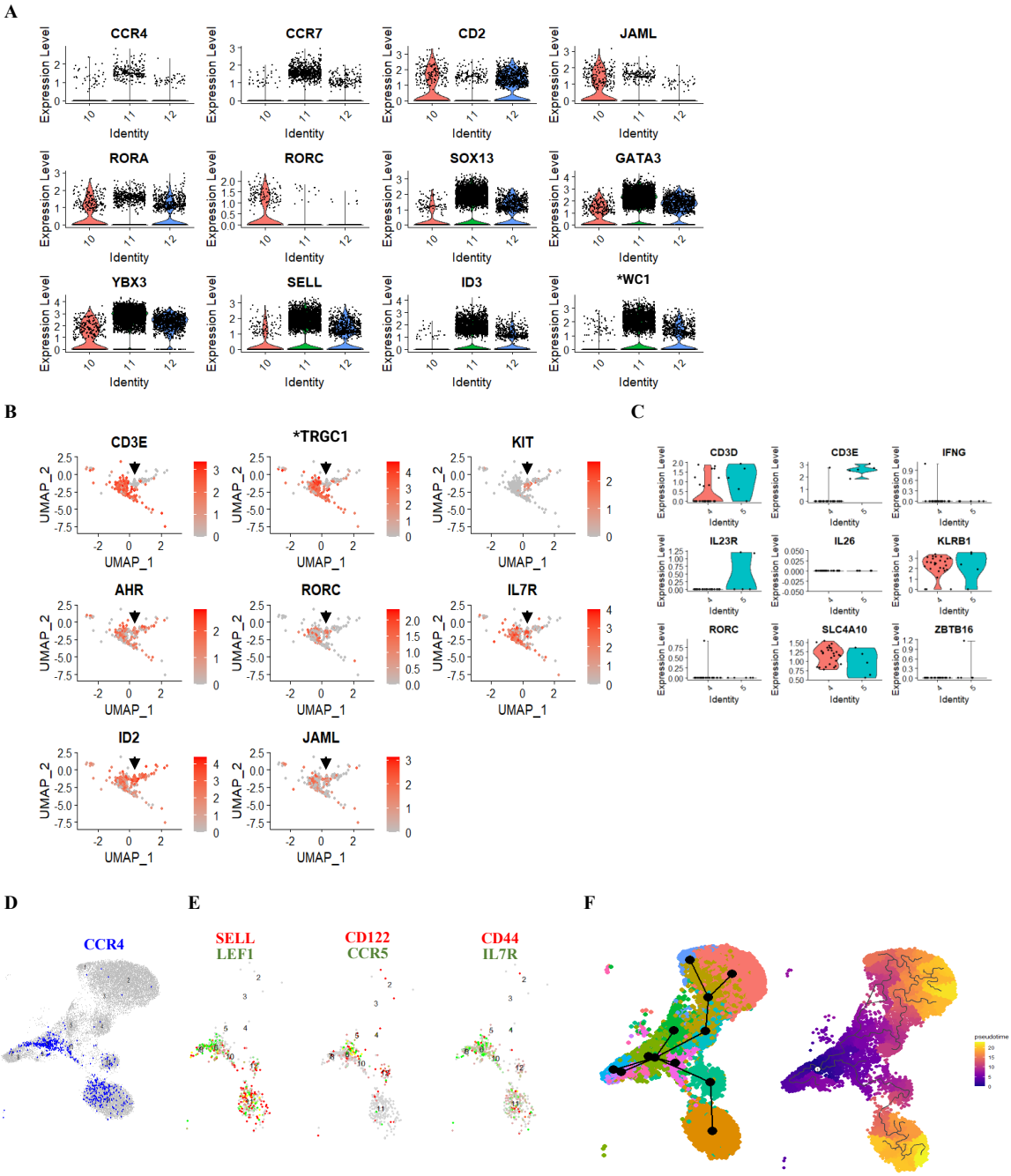
A
CCR4
CCR7
CD2
JAML
RORA
RORC
SOX13
GATA3
YBX3
SELL
ID3
*WC1
Expression Level
Identity
B
CD3E
*TRGC1
KIT
AHR
RORC
IL7R
ID2
JAML
UMAP_1
UMAP_2
C
CD3D
CD3E
IFNG
IL23R
IL26
KLRB1
RORC
SLC4A10
ZBTB16
D
CCR4
E
SELL
LEF1
CD122
CCR5
CD44
IL7R
F
pseudotime

Supplementary Figure 2.2. (A) Violin plots illustrating the expression levels of 12 genes differentially expressed by minor $CD2^-$ (cluster 10), $CD2^-$ (cluster 11), and $CD2^+$ (cluster 12) γδ T cell subsets from Figure 2. Each dot represents one cell. **(B)** UMAP plots of cells in cluster 10 displaying genes used to identify innate-like T cell type 3 (ILC3) in pigs. ILC3 can be identified by the absence of *CD3E* and **TRGC1* and the expression of *KIT*, *AHR*, *RORC*, *IL7R*, *ID2* and *JAML*. **(C)** Violin plots illustrating the expression levels of MAIT cell markers in cell clusters 4 and 5 in pigs. The cells displayed were pre-selected based on the expression of *SLC4A10* > 0. *SLC4A10* is a MAIT cell lineage marker. Each dot represents one cell. **(D)** UMAP visualization of *CCR4*+ cells (blue). **(E)** The same UMAP plot showing classical markers for naïve (*SELL*, *LEF1*) and activated (*CD122*, *CCR5*, *CD44*, *IL7R*) T cells. **(F)** Unsupervised trajectory generated by the Slingshot (left) and Monocle3 (right) packages.

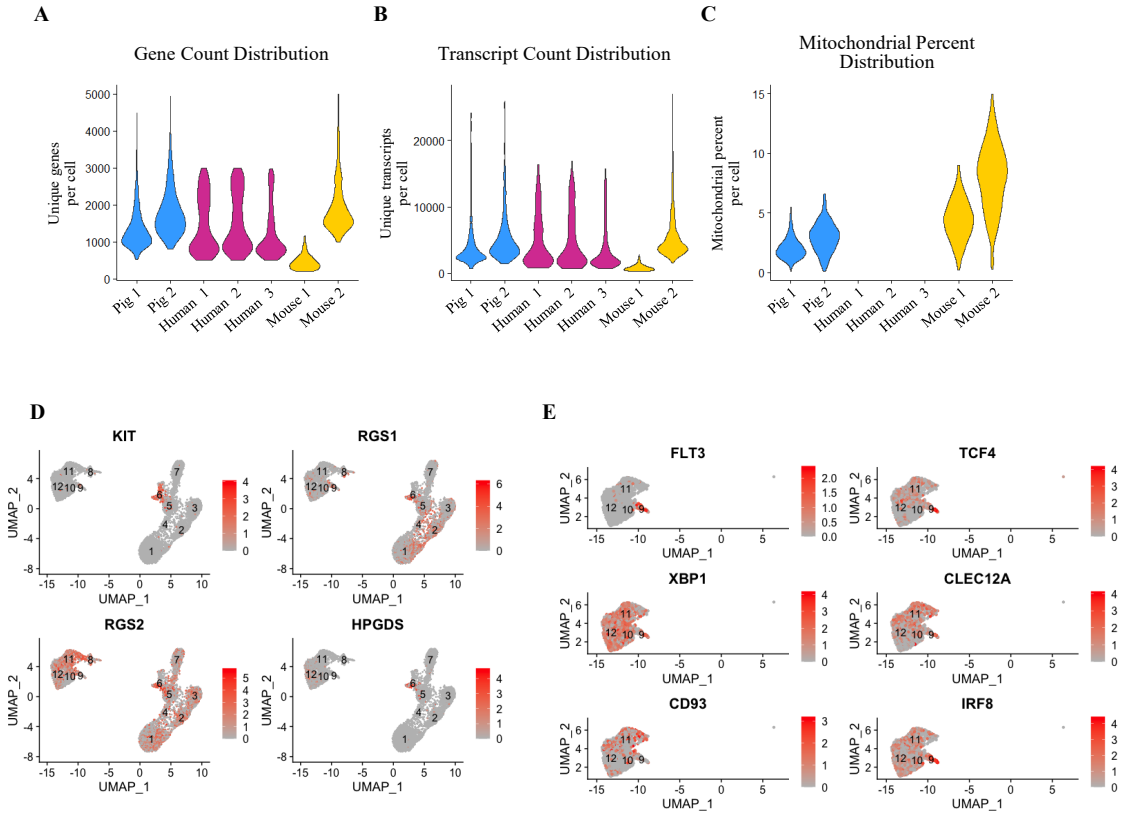

Supplementary Figure 2.3. Violin plots displaying batch-specific distributions of gene count **(A)**, transcript count **(B)**, and mitochondrial read fraction **(C)** for pig, human, and mouse datasets. Public datasets containing human (177) and mouse (193, 194) lung cell samples was used. Pig 1 and Pig 2 are the two healthy pig samples, Human 1-3 are human samples and Mouse 1 is a healthy C57BL/6J and Mouse 2 represents five pooled healthy BALB/c mice. **(D)** UMAPs displaying pig, human and mouse leukocytes overlayed with markers of mast cells (*KIT*, *RGS1*, *RGS2*, *HPGDS*). **(E)** UMAP display of the myeloid compartment of the integrated interspecies dataset overlayed with pan-dendritic cell marker *FLT3* and markers of plasmacytoid DCs.

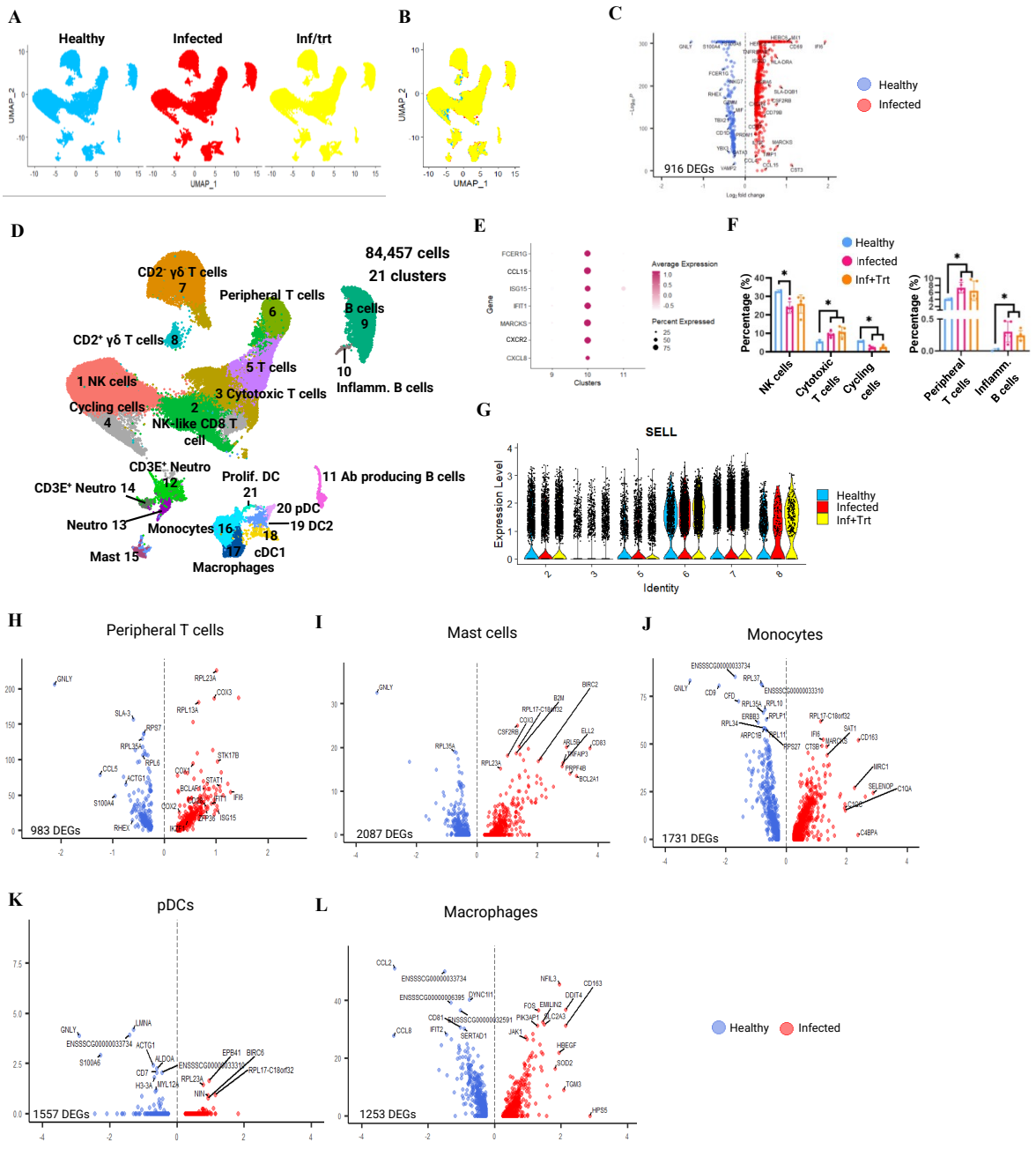
A
Healthy
Infected
Inf/trt
UMAP_1
UMAP_2
B
C
916 DEGs
Healthy
Infected
D
84,457 cells
21 clusters
CD2⁻ γδ T cells
7
Peripheral T cells
6
B cells
9
CD2⁺ γδ T cells 8
5 T cells
10
Inflamm. B cells
1 NK cells
3 Cytotoxic T cells
Cycling cells
4
2
NK-like CD8 T cell
CD3E⁺ Neutro
12
Prolif. DC
21
11 Ab producing B cells
CD3E⁺ Neutro 14
20 pDC
19 DC2
Neutro 13
Monocytes 16
18
17
cDC1
Mast 15
Macrophages
E
Average Expression
Percent Expressed
Clusters
F
Healthy
Infected
Inf+Trt
Percentage (%)
NK cells
Cytotoxic T cells
Cycling cells
Peripheral T cells
Inflamm. B cells
G
SELL
Expression Level
Identity
Healthy
Infected
Inf+Trt
H
Peripheral T cells
983 DEGs
I
Mast cells
2087 DEGs
J
Monocytes
1731 DEGs
K
pDCs
1557 DEGs
L
Macrophages
1253 DEGs
Healthy
Infected

Supplementary Figure 2.4. (A) UMAP displaying an integrative analysis of lung leukocytes isolated from Healthy, Infected, and Inf+Trt pigs using a canonical correlation approach to identify shared genes between datasets. **(B)** Same UMAP displaying the merged datasets. **(C)** Volcano plots showing differentially expressed genes between Healthy and Infected pigs. **(D)** UMAP displaying cell type clusters annotated according to canonical cell markers. **(E)** Dot plots displaying expression of pro-inflammatory genes in three B cell clusters. **(F)** Bar plots displaying the percentage of select cell subtypes for each treatment. Statistical differences were calculated by one-way ANOVA and Tukey's T test with $P<0.05$. **(G)** Violin plot of *SELL* (CD62L) in all T cell subtypes. Each dot represents one cell. **(H-L)** Volcano plots showing differentially expressed genes between Healthy and Infected pigs for peripheral T cells **(H)**, mast cells **(I)**, monocytes **(J)**, pDCs **(K)**, and macrophages **(L)**. The x-axis and y-axis represent log2 (fold change) and -log10 (p-value), respectively.

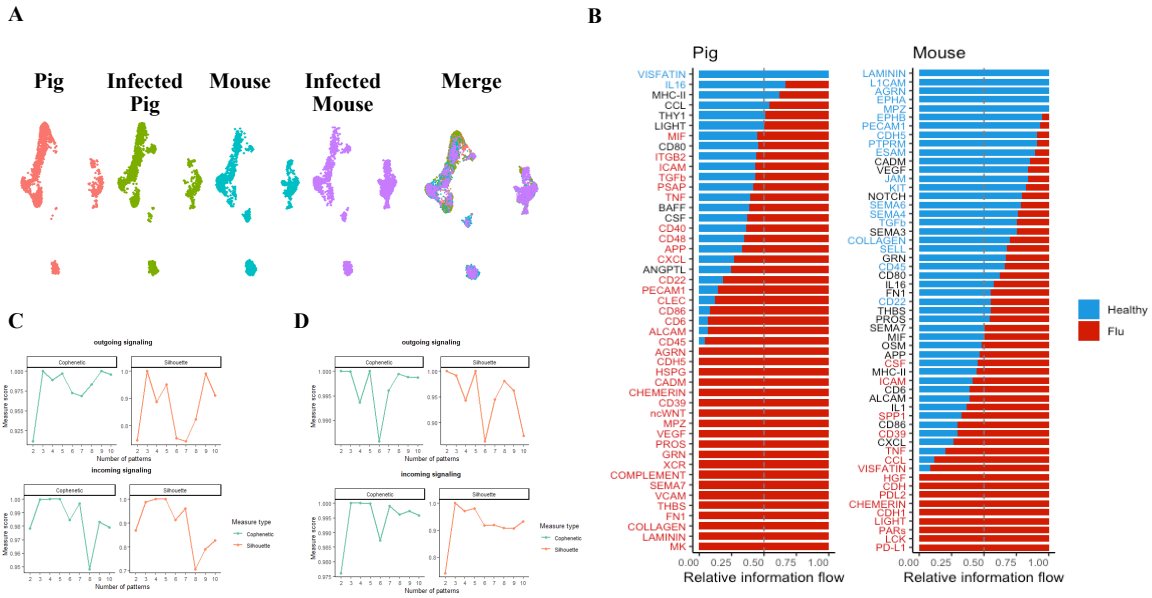

Supplementary Figure 2.5. (A) Integration of lung leukocyte datasets from healthy and influenza infected pigs and mice. Public datasets containing mouse lung cell samples was used (193, 194). **(B)** Relative information flow for individual signaling pathways of total leukocytes from healthy and influenza infected pigs and mice. Signaling pathways in blue and red are enriched in healthy and influenza-infected animals respectively. **(C)** Cophenetic and silhouette metrics for outgoing and incoming signaling in influenza-infected pigs. **(D)** Cophenetic and silhouette metrics for outgoing and incoming signaling in influenza-infected mice.

CHAPTER THREE

COMPARISON OF OSELTAMIVIR AND α-GALACTOSYLCERAMIDE FOR REDUCING DISEASE AND TRANSMISSION IN PIGS INFECTED WITH 2009 H1N1 PANDEMIC INFLUENZA VIRUS

ABSTRACT

Influenza virus infections are a major cause of respiratory disease in humans. Neuraminidase inhibitors (NAIs) are the primary antiviral medication used to treat ongoing influenza infections. However, NAIs are not always effective for controlling virus shedding and lung inflammation. Other concerns are the emergence of NAI-resistant virus strains and the risk of side effects, which are occasionally severe. Consequently, additional anti-influenza therapies to replace or combine with NAIs are desirable. Here, we compared the efficacy of the NAI oseltamivir with the invariant natural killer T (iNKT) cell superagonist, α-galactosylceramide (α-GalCer), which induces innate immune responses that inhibit influenza virus replication in mouse models. We show that oseltamivir reduced lung lesions and lowered virus titers in the upper respiratory tract of pigs infected with A/California/04/2009 (CA04) pandemic H1N1pdm09. It also reduced virus transmission to influenza-naïve contact pigs. In contrast, α-GalCer had no impact on virus replication, lung disease, or virus transmission, even when used in combination with oseltamivir. This is significant as iNKT-cell therapy has been studied as an approach for treating humans with influenza.

Keywords: α-galactosylceramide; antiviral; invariant natural killer T-cells; oseltamivir; swine; influenza.

Reference: Madrid DMC, Gu W, Artiaga BL, Yang G, Loeb J, Hawkins IK, Castleman WL, Lednicky JA, Richt JA and Driver JP. 2022. Comparison of oseltamivir and α-galactosylceramide for reducing disease and transmission in pigs infected with 2009 H1N1 pandemic influenza virus. Front. Vet. Sci. 9:999507.

INTRODUCTION

Influenza infections are a leading cause of morbidity and mortality in humans (2, 284). They also present a substantial burden for swine and poultry producers (285). Moreover, influenza infections of livestock occasionally give rise to zoonotic influenza virus strains that can be transmitted to humans and have the potential to cause human pandemics (21). Vaccination is the primary strategy for controlling influenza infections in humans and livestock. However, influenza vaccines seldom provide long-lasting protective immunity even within the same subtype and there is often insufficient time to produce vaccines against emerging strains (27). Thus, there is a need for antiviral therapies that can reduce influenza-related illness and control the spread of influenza viruses.

Oseltamivir, a neuraminidase inhibitor (NAI) (27), is the most widely prescribed influenza drug in the world and is available as an inexpensive generic medication in many countries. Although there is now strong evidence that oseltamivir shortens the duration of symptoms of influenza-like illness, the extent to which the drug impacts lung pathology, hospitalizations, and mortality due to influenza infections remains controversial (33, 34, 286-288). It has also been reported that oseltamivir may be of limited use for interrupting influenza transmission as oseltamivir treatment does not completely prevent virus shedding (289). Thus, there is a need for additional studies to clarify the efficacy of NAIs for treating human influenza infections.

The current work used pigs to evaluate oseltamivir treatment for controlling influenza infection and disease. Swine are considered a highly-reliable translational model of human influenza infections since (i) they are natural hosts for the same influenza A virus (IAV) subtypes as humans, (ii) they develop clinical disease that parallels human clinical symptoms, (iii) their

respiratory tract anatomy and physiology closely resembles that of humans, and (iv) swine anti-influenza immune responses mirror what is observed in humans (93).

In addition to the evaluation of oseltamivir, our study assessed whether influenza virus infections can be mitigated by therapeutically targeting a subset of innate T-cells known as invariant natural killer T-cells (iNKT-cells). iNKT-cells bridge the innate and adaptive immune systems and can stimulate early innate immune responses in barrier organs, including the lungs (61, 63). Unlike conventional T lymphocytes, iNKT-cells express a restricted T-cell receptor (TCR) repertoire which recognize a limited selection of lipid/glycolipid antigens presented by the MHC class-I like CD1d molecule (60). Previous studies in mice have demonstrated that administration of iNKT-cell agonist to IAV-infected mice induced antiviral immune responses that substantially reduced the severity and duration of IAV infections (66, 68, 69, 290). While these reports suggest that targeting the immunoregulatory activities of iNKT-cells may be a promising strategy to mitigate influenza infections, uncertainty remains about the clinical translatability of this approach since the average frequency of iNKT-cells in humans is significantly lower than in most inbred mouse strains (291). In the current work, our goal was to determine if iNKT-cell therapy, alone or in combination with oseltamivir, is a feasible approach to treat influenza virus infections in pigs as this species is similar to humans in regard to iNKT-cells and anti-influenza immune responses (75, 93).

MATERIALS AND METHODS

Pigs

Commercial mixed-breed pigs were obtained from the University of Florida Swine Unit and Midwest Research Swine (Gibbon, MN). The experiments were performed in compliance with guidelines from the United States Department of Agriculture and the National Research Council's Guide for the Care and Use of Laboratory Animals. The institutional animal care and use committee (IACUC) at the University of Florida approved the protocol under study number 201708209.

Experimental design

Three-week-old pigs seronegative for antibodies against H1N1, H3N2, and B influenza viruses were assigned to one of five treatment groups. At four weeks of age, the pigs were anesthetized with BAM^{TM} combination drug (Butorphanol, Azaperone, Medetomidine) at a dose rate of 1.0 ml per 75 lbs body weight and intratracheally (i.t.) inoculated with 1 x 10^6 $TCID_{50}$ 2009 pandemic H1N1 A/California/04/2009 (H1N1pdm09) influenza virus, as previously described (78). One group of pigs (αGC group) was intranasally (i.n.) administered 100 μg/kg α-galactosylceramide (α-GalCer) dissolved in 1.5 ml PBS and 2% DMSO, at the time of infection. Another group was orally administered 75 mg oseltamivir phosphate (Lupin Pharmaceuticals) twice a day during the first five days after infection (OS group). A third group of pigs received a combination of the α-GalCer and OS treatments (αGCOS group). An additional group of pigs (MC group) was mock treated with 1.5 ml of the α-GalCer vehicle solution (PBS, 2% DMSO), administered i.n. at the time of challenge. Finally, a group of control pigs (MM group) was mock

infected with virus-free Dulbecco's Modified Eagle Medium (DMEM) and mock treated with the α-GalCer vehicle solution.

Pigs were monitored daily for clinical disease as previously described (80). To quantify virus shedding, nasal swabs were collected daily from -1 to 5 days post infection (d.p.i.). Blood samples were collected on -1, 3, and 5 d.p.i. for flow cytometry. Pigs were euthanized five days after infection and tissue samples from the lung, trachea, bronchus, nasal turbinates, spleen, and bronchoalveolar lavage fluid (BALF) were collected and analyzed by virus titration, flow cytometry, and RT-qPCR, as previously described (292). The right middle lung lobe was collected for histopathology.

In another study, 16 four-week-old pigs were divided among three groups that were treated identically to the MC, OS, and αGC groups in the first study, except that two days after virus challenge five or six IAV-naïve contact pigs were co-housed with each group for three days. Additionally, BioSampler® air sampling devices (SKN, Inc.) were placed 50 cm away from two of the pens housing MC and OS groups of pigs at 3 d.p.i.. The samplers collected 720 liters of air over 90 minutes into 15 ml of PBS, which was reduced to 400 µl by centrifugation. Primary inoculated and contact pigs were necropsied at 5 d.p.i. and 5 days post contact (d.p.c.), respectively. Necropsies were performed identically to the first experiment.

Flow cytometry

Lung and spleen samples were dispersed into single cells as previously described (80). Blood and tissue samples were treated with an ammonium chloride-based erythrocyte lysis buffer (80). Cells were blocked with polyclonal rat IgG Ab, stained with tetramer and antibody reagents,

and acquired using Attune NxT flow cytometer (Thermo Fisher Scientific). Reagents used to analyze iNKT-cells, αβ and γδ T-cells, monocytes, macrophages, and granulocytes are described in Supplemental Table 3.1. Data were analyzed using FlowJo software (V 10.6.1, BD Biosciences).

Virus titers

Influenza virus encoding the original consensus sequence of the H1N1pdm09 strain A/California/04/2009 (CA04) was generated by reverse genetics as previously described (293). Viral titers were calculated as the median $TCID_{50}$, and viral titers expressed as Log_{10} $TCID_{50}$/ml or Log_{10} $TCID_{50}$/g as appropriate. $TCID_{50}$ values were determined as previously described (292).

Lung immunopathology

The right middle lung lobe was perfused with 10% neutral-buffered formalin. Four blocks were sampled and embedded in paraffin. 7µm-thick paraffin sections were stained with hematoxylin and eosin (H&E) for histopathologic analysis. The severity of bronchitis and bronchiolitis was scored according to the size of leukocyte aggregations in bronchial and bronchiolar walls, respectively. Each section was scored from 0 to 3 where a score of 0 represents no lesions; a score of 1 represents a low leukocyte density in airway walls (i.e. bronchus or bronchiole); a score of 2 represents a moderate leukocyte density in airway walls; and a score of 3 represents a high leukocyte density wrapping around the entire circumference of the airway wall. Pneumonia severity was scored according to the size of intra-alveolar lesions as follows: 0: no lesions; a score of 1 represents small areas of thickened interalveolar septa, type 2 pneumocyte hyperplasia, leukocyte septal infiltration, and low densities of intra-alveolar leukocytes; a score of

2 represents moderately-sized areas of thickened interalveolar septa, type 2 pneumocyte hyperplasia, leukocyte septal infiltration, and moderate densities of intra-alveolar leukocytes; a score of 3 represents large areas of thickened interalveolar septa, type 2 pneumocyte hyperplasia, leukocyte septal infiltration, and high densities of intra-alveolar leukocytes. The prevalence of bronchitis, bronchiolitis, and pneumonia lesions was scored from 0 to 3 as follows: 0: no lesions, 1: focal to multifocal lesions, 2: locally extensive lesions (between 20% and 45% of the section or airways), 3: diffuse or diffusely multifocal lesions throughout the section (representing greater than 45% of tissue section area). Pneumonia, bronchitis, and bronchiolitis scores were summed to calculate an overall severity score out of a maximum possible score of 12. An overall disease prevalence score was calculated by multiplying the overall severity score by the prevalence score, with a maximum possible score of 36.

RNA isolation and RT-qPCR

Cranial, middle, and caudal tissue lung samples were combined and homogenized using a Precellys homogenizer (Bertin). RNA was isolated using QIAzol Lysis Reagent (Qiagen, 79306) with the RNeasy Lipid Tissue mini kit (Qiagen, 74804) and reverse transcribed to cDNA using a Superscript VILO Master Mix (Thermo Fisher Scientific, 11755-050). cDNA was mixed with a Fast SYBR Green Master Mix (Applied Biosystems, 43-856-12). The PCR mixture was dispensed into a quantitative reverse transcriptase PCR (RT-qPCR) array (PASS-011ZF, Qiagen), which profiles 84 inflammatory cytokine/chemokines genes. The RT-qPCR reaction was carried out using a CFX Connect real-time cycler (Bio-Rad) according to the manufacturer's recommended cycling conditions. Gene expression was quantified according to standard ΔΔCt methods using the geometric mean of three housekeeping genes (*ACTG1*, *B2M, RPL13A*) that are included in each

array. A two-tailed Student's t-test was used to compare gene expression between treatments. Differentially expressed genes were subjected to a Kyoto Encyclopedia of Genes and Genomes (KEGG) pathway enrichment analysis using Database Annotation, Visualization and Integrated Discovery (DAVID) version 2021 (https://david.ncifcrf.gov/). Heatmaps were generated in GraphPad Prism using the geometric mean of the gene expression of three to six samples per treatment.

Statistical analysis

Data was graphed and analyzed using GraphPad Prism, version 9.1.0 (GraphPad Software). $TCID_{50}$ data were log transformed to address the heteroscedasticity and non-normally distributed residuals of untransformed data and analyzed using a mixed-effect model. Means were separated using Turkey's test when a main effect or interaction term was significant ($P < 0.05$). A Fisher's exact test was used to compare the proportion of infected animals between treatment groups and a Log-rank test was used to compare viral infection incidence curves. Welch's t-test was used to compare virus titers in respiratory tissues due to their unequal variances among treatment groups. Pathology scores were assessed using a one-way analysis of variance (ANOVA) followed by the Mann-Whitney U test. Flow cytometric data were analyzed on RStudio version 1.4.1103 using glm function followed by pairwise comparisons with Tukey's test.

RESULTS

Effect of oseltamivir and α-GalCer on virus shedding and replication

Virus shedding was significantly delayed and reduced in oseltamivir treated pigs (OS group) compared to mock treated pigs (MC group) (Figure 3.1). Virus positive nasal swabs were detected in 3/14 OS and 14/14 MC pigs at 4 d.p.i. when oseltamivir treatment was discontinued. An additional 3 OS pigs started shedding virus on 5 d.p.i.. Shedding was similar between MC pigs and pigs treated with α-GalCer monotherapy (αGC group). Treating pigs with the combination of α-GalCer and oseltamivir (αGCOS group) did not significantly reduce the proportion of virus-shedding pigs compared to pigs treated with oseltamivir alone. However, αGCOS pigs tended to shed less virus than OS pigs at 4 and 5 d.p.i..

Analysis of virus titers in the respiratory tissues at 5 d.p.i. found that OS pigs had reduced titers in nasal turbinates, trachea, and bronchi compared to MC pigs (Table 3.1). They also tended to have lower titers in BALF and lung tissue. Oseltamivir treatment decreased the proportion of pigs with detectable levels of virus in nasal turbinates, trachea, and BALF. The effect was less striking for lung samples as fewer MC lung samples had detectable levels of virus at 5 d.p.i. compared to the other tissues. α-GalCer monotherapy did not significantly reduce virus titers or the proportion of virus positive samples for any of the tissues tested. However, we did observe that αGC pigs tended to have lower virus titers in caudal lung samples compared to the MC pigs. αGCOS pigs were similar to OS pigs for virus titers and the proportion of virus positive samples.

In our second study which measured virus transmission, we detected virus shedding in 6/6, 5/5, and 1/5 contact pigs co-housed with MC, αGC, and OS pigs, respectively (Figure 3.2A & 3.B). All contact pigs co-housed with MC and αGC pigs shed virus by day 4 post-contact. The

single influenza positive OS contact pig began shedding low levels of virus at 3 d.p.c.. Analysis of the BioSamplers® devices detected $4.53x10^2$ infectious virions in 720 liters of air collected from the room housing MC pigs. In contrast, no infectious virus was detected in the room housing OS pigs. Analysis of the respiratory tract samples collected at 5 d.p.c. detected virus in 6/6, 5/5, and 2/5 contact pigs that were respectively co-housed with MC, αGC, and OS pigs. OS contact pigs had lower average virus titers in cranial and caudal lung, bronchi, trachea, nasal turbinates, and BALF compared to MC and αGC contact pigs (Figure 3.2C). These combined results indicate that oseltamivir treatment reduced viral replication in the respiratory tract, which decreased virus transmission. In contrast, α-GalCer had no significant impact on virus replication or shedding.

Lung pathology

Lung lesions were scored for the size and distribution of immune cell infiltrates, as described in section materials and methods. Oseltamivir monotherapy respectively reduced the severity and prevalence of pneumonia by 45 and 56 percent compared to MC pigs. OS pigs also tended to have less prevalent and less severe bronchitis and bronchiolitis compared to MC pigs. α-GalCer monotherapy did not significantly reduce lung pathology. Furthermore, combining α-GalCer and oseltamivir did not significantly reduce lung pathology compared to oseltamivir treatment alone. A comparison of the combined disease severity and prevalence scores found that OS and αGCOS pigs had fewer lesions compared to MC and αGC pigs (Figure 3.3).

Flow cytometric analysis of leukocytes

Flow cytometry was used to assess immune cell populations in the lung, BALF and spleen. No differences were detected in the frequency of total lymphocytes, DCs, or macrophages between treatments for any of these tissues (Supplemental Tables 3.2-3.4). However, the αGCOS group had a higher percentage of NK cells in BALF and spleen while OS pigs had a higher percentage of NK cells in their lungs. iNKT-cell frequencies tended to be higher in the spleens of αGC and αGCOS pigs compared to the other groups. We also observed that combination therapy lower percentage of γδ T cells in the lung and higher concentrations of CD8 cytotoxic T-cells ($CD8\alpha\beta^{+}CD4^{-}$) in all tissues.

Gene expression

An RT-qPCR array was used to compare transcript levels of 84 pro-inflammatory markers in lung tissue collected at 5 d.p.i.. Twelve genes were differentially expressed in MC compared to MM pigs (Figure 3.4A, Supplemental Table 3.5), including 5 chemokine ligands (*CCL1, CCL5, CCL17, CCL20, FASLG*), 5 chemokine/cytokine receptors (*CCR4, CXCR4, IL2RB, IL2RG, IL5RA*), the cytokine *IL16*, and the T-cell costimulatory molecule *CD70*. A KEGG pathway enrichment analysis found several of these genes were associated with cell survival (*IL2RB*, *IL2RG*, *IL4*, *IL5RA*, *FASLG*) and anti-influenza immune responses (*FASLG*, *CCL5*, *CXCL10*). To determine the effect of oseltamivir and α-GalCer on influenza-induced gene expression changes, we compared the OS, αGC, and αGCOS groups to the MC group (Figure 3.4B, Supplemental Table 3.5). The only gene differentially expressed between αGC and MC pigs was *CCL20*, which encodes a small cytokine important for the trafficking of innate immune cells into the lung (294-

296). Overall, OS and αGCOS pigs displayed a similar pattern of gene expression changes compared to the MC group. However, OS pigs expressed less *IL1A* and more *CXCR2* and *IL18* compared to MC pigs while αGCOS pigs upregulated *CCL5, CCR3, IL17A, FASLG,* and *IL2RB*. A KEGG analysis of genes that were differentially expressed between MC and αGCOS pigs at the $p < 0.1$ level found enrichment of pathways involved in T helper 17 cell differentiation (*IL1B, IL2RB, IL2RG, IL4, IL4R, IL17A, IL17F, IL21, IL23A, IL27*) and anti-influenza immune responses (*FASL, IL1, IL1B, IL12, CCL5*).

DISCUSSION

Here, we used the swine influenza challenge model to compare a single intranasal administration of α-GalCer to a 5-day course of oseltamivir for reducing the severity and transmissibility of an IAV infection. We also investigated whether combining α-GalCer and OS would act synergistically to mitigate the infection. Pigs were administered 100 μg/kg α-GalCer since a previous study found that this dose inhibited virus replication in swine (80). Oseltamivir was administered at 150 mg/day, the recommended dose for adult/adolescent humans (297).

Oseltamivir reduced virus titers in most parts of the airway, but especially the upper respiratory tract. A similar outcome was observed in oseltamivir-treated ferrets challenged with an H5N1 IAV (298). Other studies have reported inconsistent results. Sidwell et al. measured a 2-to-4-fold reduction in virus titers in the lungs of BALB/c mice administered 10 mg/kg/day of oseltamivir after infection with a lethal dose of the H1N1 strain A/NWS/33. However, the same regimen failed to inhibit the replication of two H3N2 viruses in mice (299). In another study, oseltamivir either significantly reduced or had no effect on virus titers of ferrets intranasally infected with a low ($1x10^2$ PFU) and high ($1x10^6$ PFU) dose of H1N1pdm09, respectively (300). Moreover, Govorkova et al. reported lower virus titers in the lung but not in nasal washes of oseltamivir-treated ferrets infected with H1N1pdm09 (301). Evidence supporting that oseltamivir inhibits virus replication in humans includes several reports that oseltamivir-treated influenza patients had lower virus concentrations in nasal and throat swabs compared to untreated patients (289, 302-304). A previous report which tested oseltamivir in pigs found only a modest impact on virus replication. This study differed from our own in that (i) it used 11-week-old pigs, (ii) virus inoculations were administered i.n., (iii) it used swine IAVs instead of H1N1pdm09, and (iv) oseltamivir treatment was initiated 12 h prior to infection (297).

One of our most significant findings is that oseltamivir prevented 3 of 5 contact pigs from contracting influenza virus infections, despite sharing the same pen with primary inoculated pigs during the most infectious period of disease (2-5 d.p.i.). To our knowledge, only a few ferret studies have examined the impact of oseltamivir on virus transmission (305-307). Two of these studies found that treating H1N1pdm09-infected ferrets 24 or 36 h after infection had no effect on virus transmission to contact ferrets (306, 307). However, a third study reported that administering oseltamivir to ferrets starting at 2 h after infection with human IAVs, including H1N1pdm09, significantly reduced secondary infections (305). This protocol was similar to our study as regards the short interval between infection and treatment.

Oseltamivir clearly reduced influenza-induced lung lesions. This is notable since evidence supporting that oseltamivir reduces lung immunopathology is somewhat controversial (303, 308). It was shown that influenza-infected mice and ferrets administered oseltamivir prophylactically or on the day of infection had significantly less lung consolidation compared to untreated controls (300, 301, 309). However, treating cynomolgus macaques with oseltamivir did not reduce influenza-associated acute lung injury compared to placebo-treated animals (310). There is limited evidence that oseltamivir reduces lung pneumonia in humans since influenza patients are not usually subjected to radiological examination. However, a meta-analysis of 20 randomized, placebo-controlled trials of adults and children with influenza infections found that oseltamivir had no effect on reducing hospitalizations from lower respiratory tract complications (33). In contrast, a report describing nine randomized trials, including some overlapping with the previous citation, found that oseltamivir decreased the severity of lower respiratory tract complications (311).

α-GalCer had little impact on virus shedding, virus replication, or lung immunopathology. This contrasts with previous mouse studies that showed substantially reduced virus titers and lung pathology after α-GalCer administration (66, 68, 69). The discrepancy may be due to a variety of factors, including that iNKT-cells are much less frequent in pigs than in most inbred mouse strains. Another factor is that significant differences exist in mouse and porcine antiviral immune defenses, which may affect how iNKT-cells contribute to host-pathogen interactions and to the antiviral defense system (312-314). In contrast to the current study, we previously reported that i.n. administration of 100 μg/kg α-GalCer significantly reduced virus titers and lung pathology in pigs of similar breed and age to the current work (80). This discrepancy suggests that the outcome of α-GalCer therapy in swine is unpredictable and probably depends on a variety of host and/or environmental factors. These likely include iNKT-cell frequency and/or effector functions which vary considerably among pigs and is largely controlled by genetic factors (74). Since pigs within each study were closely related, one explanation for our results may be that pigs in the previous and present studies expressed iNKT cells that were genetically similar in their proclivity to stimulate strong and weak antiviral immune responses, respectively.

In conclusion, our study demonstrated that administering oseltamivir to influenza-infected pigs significantly reduced viral replication and lung immunopathology in principal animals and virus transmission to contact pigs. These findings support the use of NAIs during influenza outbreaks, especially for reducing onward transmission of infections. In contrast, α-GalCer did not alter the course of disease, even when used in combination with oseltamivir. Since swine resemble humans for iNKT-cells and are considered a reliable translational model for human influenza infections, our work suggests that iNKT-cell therapy may not be a viable approach for treating humans with influenza virus infections.

ACKNOWLEDGMENTS

We thank the National Institutes funding this study. We thank the National Institutes of Health Tetramer Core Facility for provision of the CD1d tetramers under the contract 760 HHSN272201300006C.

Table 3.1. Virus titers of BALF and homogenized respiratory tissues at 5 d.p.i.

Tissue	MM	MC	OS	αGC	αGCOS
BALF	0/8 (0.00 ± 0.00)^{a}	**11/12 (2.39 ± 0.31)^{b}**	**4/11 (1.27 ± 0.55)^{b}**	**11/14 (2.16 ± 0.36)^{b}**	**5/8 (1.34 ± 0.52)^{b}**
Turbinate	0/8 (0.00 ± 0.00)^{a}	**7/11 (3.44 ± 0.81)^{b}**	2/11 (0.75 ± 0.51)^{ac}	**12/14 (4.27 ± 0.60)^{b}**	0/7 (0.00 ± 0.55)^{ac}
Trachea	0/8 (0.00 ± 0.00)^{a}	**11/12 (5.04 ± 0.48)^{b}**	**5/11 (2.36 ± 0.85)^{c}**	**12/14 (4.64 ± 0.55)^{bd}**	**5/8 (2.72 ± 0.81)^{cd}**
Bronchus	0/8 (0.00 ± 0.00)^{a}	**8/11 (3.78 ± 0.80)^{b}**	**4/11 (1.23 ± 0.53)^{c}**	**9/14 (3.54 ± 0.65)^{b}**	2/8 (1.17 ± 0.80)^{ac}
Cranial	0/8 (0.00 ± 0.00)^{a}	3/12 (1.96 ± 1.00)^{a}	4/11 (1.95 ± 0.83)^{a}	5/14 (1.64 ± 0.62)^{a}	1/8 (0.60 ± 0.6)^{a}
Middle	0/8 (0.00 ± 0.00)^{a}	**5/12 (2.27 ± 0.87)^{bc}**	2/11 (0.89 ± 0.60)^{ab}	**10/14 (3.90 ± 0.76)^{c}**	1/8 (0.61 ± 0.61)^{ab}
Caudal	0/8 (0.00 ± 0.00)^{a}	6/12 (2.10 ± 0.70)^{b}	3/11 (1.05 ± 0.66)^{ab}	2/14 (0.57 ± 0.39)^{ab}	1/8 (0.61 ± 0.74)^{ab}

Results are shown as the number of pigs positive for virus isolation of the total number of pigs. Numbers in parentheses indicate virus titers presented as $\log_{10}$ mean ± SEM $TCID_{50}$ per ml or g of tissue. Virus titers within tissues with no common superscripts differ significantly ($P<0.05$) when compared by Welch's t-test. Values in bold are statistically different from non-infected controls.

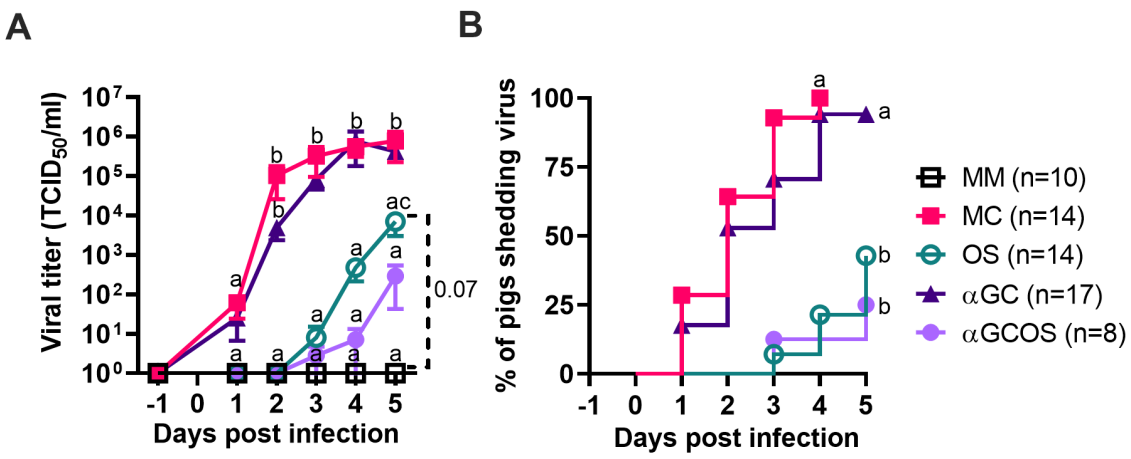

Figure 3.1. Virus levels in nasal secretions. (A) Virus titers in nasal swabs collected at -1 to 5 d.p.i. from pigs inoculated with H1N1pdm09. Data are represented as mean ± standard error of the mean (SEM). Values within days with no common superscripts differ significantly ($P<0.05$) when analyzed using Tukey's test. **(B)** Incidence of pigs shedding virus. Survival curves with no common superscripts differ significantly ($P<0.05$) when compared by the log-rank test.

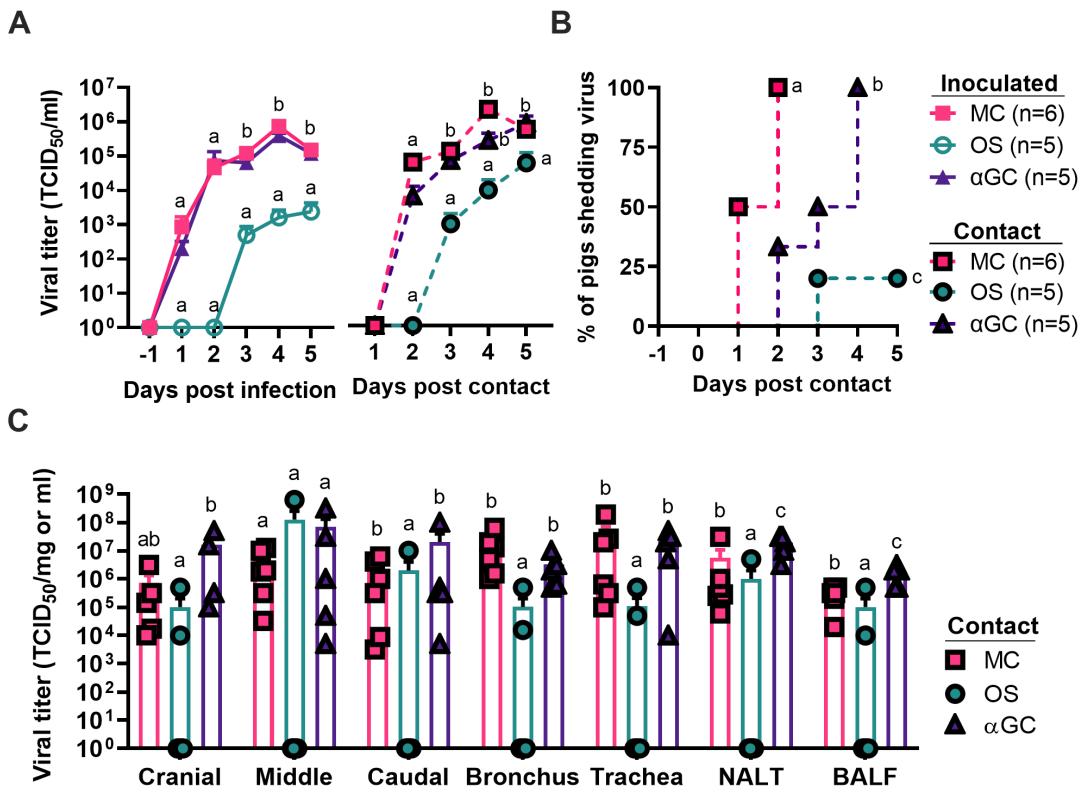

Figure 3.2. Viral load of contact pigs. (A) Virus titers in nasal swabs of principal inoculated and contact pigs during the 5-day post infection and -post contact periods, respectively. Data are represented as mean ± SEM. Values within days with no common superscripts differ significantly ($P<0.05$) when analyzed using Tukey's test. **(B)** Incidence of contact pigs shedding virus after exposure to principal infected pigs. Survival curves with no common superscripts differ significantly ($P<0.05$) when compared by the log-rank test. **(C)** Virus titers for homogenized airway tissues and bronchoalveolar lavage fluid (BALF) collected from contact pigs at 5 d.p.c.. Data are represented as mean ± SEM. Differences in BALF and airway tissue titers were compared by Welch's test. Symbols represent individual pigs.

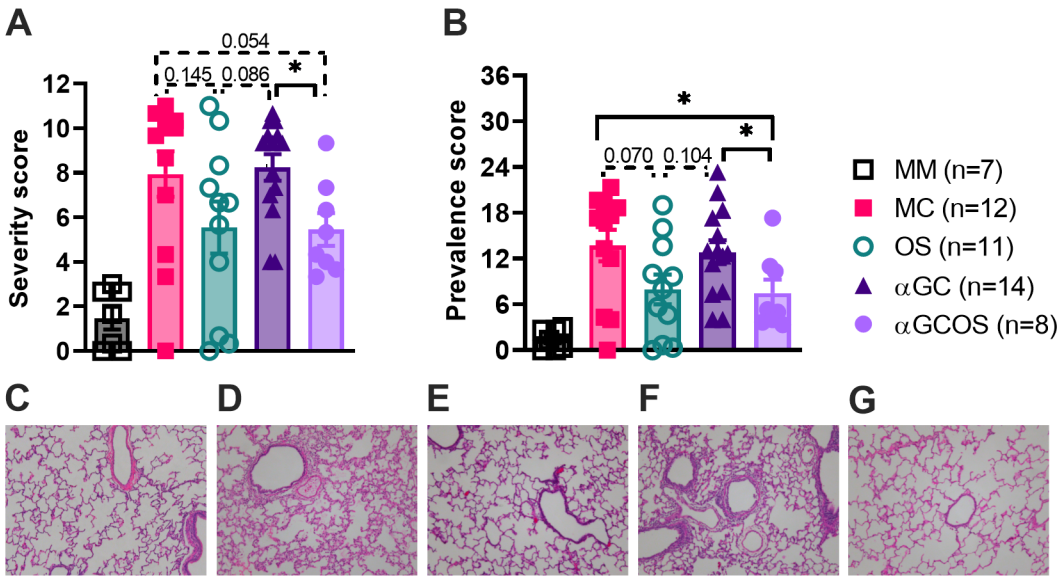

Figure 3.3. Overall severity and prevalence of lung pathology. Lung tissue from the right middle lung lobe was microscopically examined to determine the impact of oseltamivir and α-GalCer on influenza-induced immunopathology. Lung lesions were scored for the size and distribution of immune cell infiltrates, as described in section 2.5. **(A)** Pneumonia, bronchitis, and bronchiolitis scores were summed to calculate an overall severity score out of 12. **(B)** An overall disease prevalence score was calculated by multiplying the overall severity score by the prevalence score, with a maximum possible score of 36. Differences in severity and prevalence scores were compared by the Mann-Whitney test. Data are represented as mean ± SEM. * $P < 0.05$. Actual P values provided when $0.2 > P$ value > 0.05. Symbols represent individual pigs. **(C-G)** Representative transverse sections of lung tissue for the indicated treatment groups stained with H&E at 10x magnification. **(C)**: MM, **(D)**: MC, **(E)**: OS, **(F)**: αGC, and **(G)**: αGCOS. In MC and αGC groups there was mild thickening of alveolar septa by type II pneumocyte hyperplasia in peribronchiolar areas (black arrows) with small to moderate leukocyte septal infiltration, presence

of pulmonary alveolar proteinosis (asterisk), and increased numbers of alveolar macrophages (red arrows).

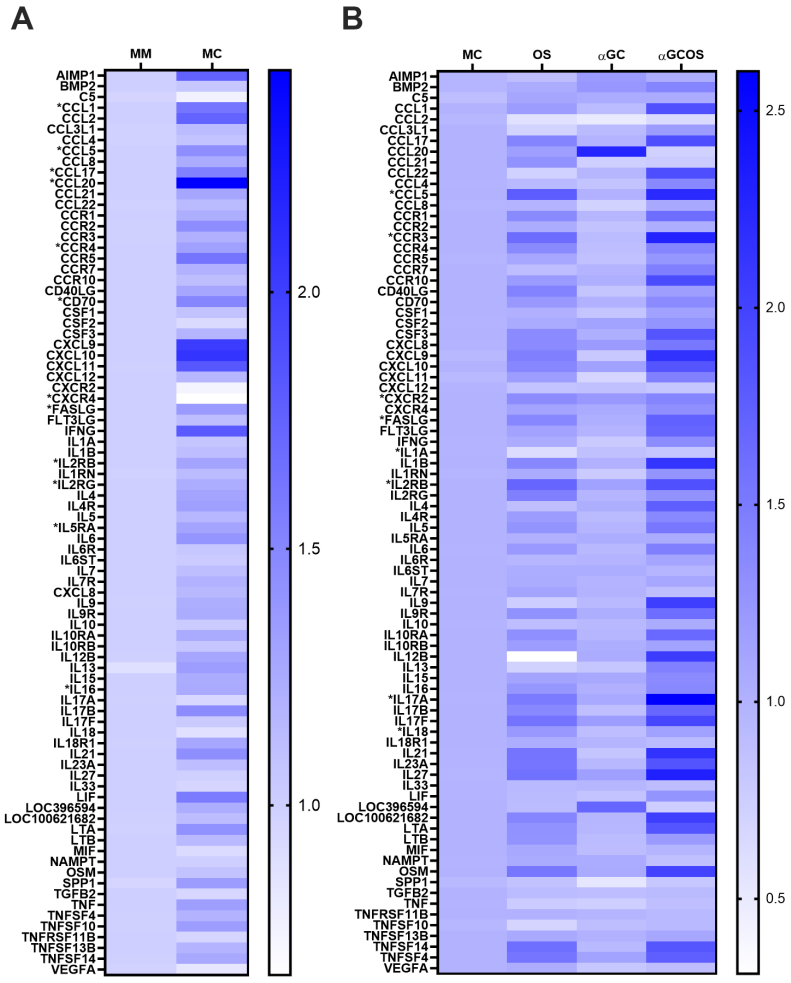

Figure 3.4. Inflammatory gene expression profile of lung tissue collected at 5 d.p.i.. Transcript levels of 84 inflammatory genes were measured in combined samples from the left cranial, middle, and caudal lung lobes of 3 MM, 6 MC, 4 OS, 6 αGC, and 4 αGCOS pigs. **(A)** Heat map representing the relative value of MC gene expression normalized to MM pigs. **(B)** Heat map representing the relative value of OS, αGC, and αGCOS gene expression normalized to MC pigs. Genes statistically different between treatments are preceded by *. See Supplemental Table 3.5 for a complete list of fold change values.

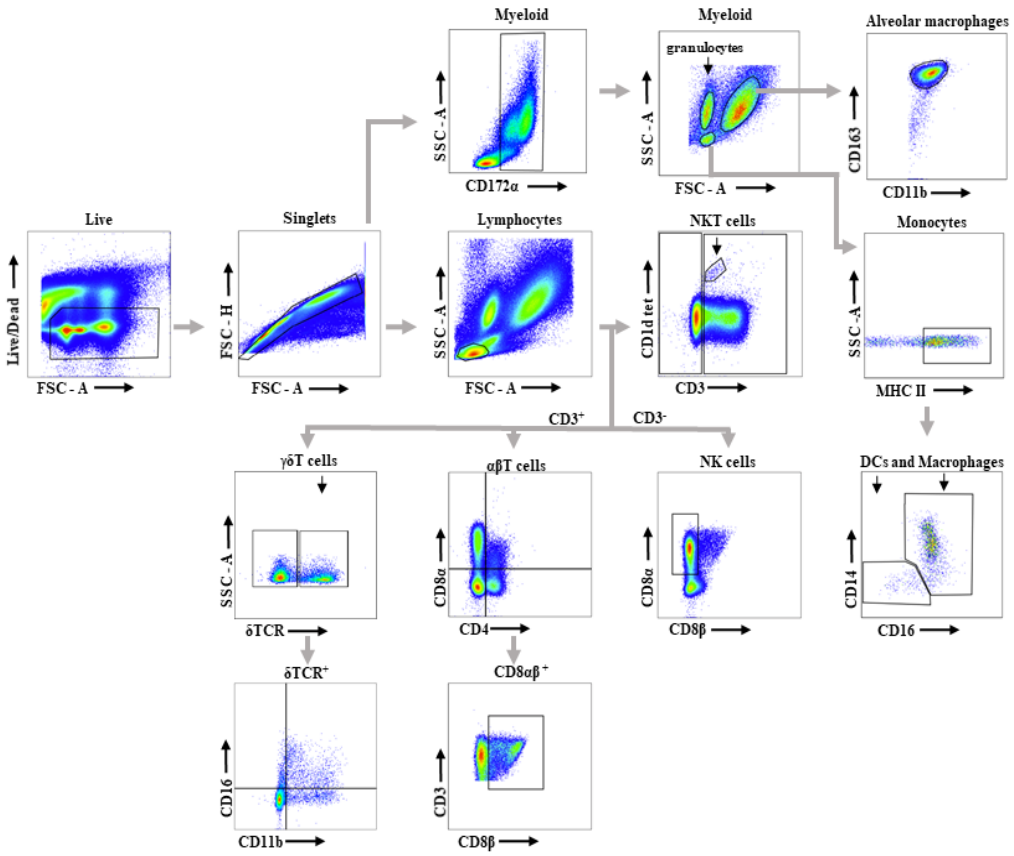

Supplemental Figure 3.1. Gating strategy to distinguish immune cell populations in blood and tissues. αβ and γδ T cells were distinguished by sequentially gating live single lymphocytes, $CD3^+$ cells, and then $CD4^+$, $CD8\alpha^+$, $CD8\beta^+$, TCR-δ^+ cells. iNKT-cells were distinguished from conventional T cells according to CD1d-tetramer staining. NK cells were identified as $CD8\alpha^+ CD3^-$ cells after first gating on single live lymphocytes. T cell and NK cell subsets were distinguished according to their surface expression of CD11b and CD16. Monocytes, macrophages, and granulocytes were identified after initially gating on live single $CD172\alpha^+$ cells. Thereafter, monocytes were identified as $MHCII^+$ $CD14^+$ cells and alveolar macrophages were identified as SCC^{high} $CD163^+$ $CD11b^+$ cells. Granulocytes were identified according to FSC and SSC. FSC, forward scatter; SSC, side scatter; A, signal area; H, signal height.

Supplemental Table 3.1. Reagents used for flow cytometry analysis of surface markers

Antigen	Clone	Isotype	Conjugation	Source
CD1d tetramer	N/A	N/A	PE	NIH Tetramer Core
Live/Dead	N/A	N/A	IR	Invitrogen
Anti-CD3ε	BB23-8E6-8C8	Mouse IgG2a κ	PE-Cy7	BD Biosciences
Anti-CD4	74-12-4	Mouse IgG2b κ	PE & Alexa647	Southern Biotech
Anti-CD8α	76-2-11	Mouse IgG2a κ	Alexa488 & Biotin	Southern Biotech
Anti-CD8*β*	PPT23	Mouse IgG1	A488	Bio-Rad
Anti-TCRδ	PGBL22A	Mouse IgG1	Alexa647	WSU mAB Center
Anti-CD14	MIL2	Mouse IgG2b	Alexa488	Bio-Rad
Anti-CD16	G7	Mouse IgG1	Biotin	BD Biosciences
Anti-CD11b	M1/70	Rat IgG2b κ	Alexa647	Biolegend
Anti-MHC class II	H42A	Mouse IgG2a κ	Alexa647	WSU mAb Center
Anti-CD163	2A10/11	Mouse IgG1	PE	Bio-Rad
Anti-CD172α	74-22-15A	Mouse IgG2b κ	PerCP	BD Biosciences

Supplemental Table 3.2. Flow cytometric analysis of immune cell populations in lung

	MM (n=6)	MC (n=10)	OS (n=8)	αGC (n=10)	αGCOS (n=8)
Lymphocytes (% of live cells)	26.6 ± 4.5[a]	28.5 ± 3.8[a]	29.3 ± 5.0[a]	26.6 ± 2.7[a]	25.8 ± 2.3[a]
Myeloid cells (% of live cells)	70.1 ± 3.3[a]	65.8 ± 2.9[ab]	57.1 ± 4.7[ab]	**63.0 ± 1.7[b]**	67.5 ± 3.2[ab]
iNKT-cells (% of $CD3^+$)	0.31±0.13[ab]	0.13±0.03[a]	0.08±0.02[a]	0.40±0.19[ab]	0.31±0.16[a]
$CD8\alpha^+CD8\beta^+CD4^-$ (% of $CD3^+$)	16.7 ± 5.8[a]	17.6 ± 4.7[a]	26.4 ± 10.8[a]	15.0 ± 3.2[a]	20.3 ± 6.2[b]
$CD8\alpha^-CD4^+$ (% of $CD3^+$)	8.15 ± 0.9[a]	7.76 ± 1.0[a]	6.09 ± 2.1[a]	9.39 ± 1.4[a]	7.69 ± 0.9[a]
δTCR^+ (% of $CD3^+$)	53.0 ± 8.7[a]	50.1 ± 7.0[a]	48.6 ± 6.4[a]	48.3 ± 5.3[a]	**30.1 ± 3.3[b]**
NK cells (% of live cells)	7.8 ± 1.8[a]	7.2 ± 1.1[a]	**8.7 ± 1.9[b]**	7.9 ± 1.2[a]	6.8 ± 0.9[a]
Alveolar macrophages (% of live cells)	36.2 ± 2.3[a]	38.5 ± 3.2[a]	32.8 ± 1.9[a]	38.1 ± 1.4[a]	40.6 ± 1.7[a]
Granulocytes (% of live cells)	18.6 ± 2.8[a]	14.3 ± 1.8[a]	20.7 ± 4.4[a]	16.7 ± 2.1[a]	19.0 ± 2.0[a]

Values expressed in means and ± SEM, $P<0.05$ calculated using R function glm followed by Tukey's test. Values within rows with no common superscript letters differ significantly. Values with the same superscript are not statistically different. Values in bold are statistically different from non-infected controls.

Supplemental Table 3.3. Flow cytometric analysis of immune cell populations in BALF

	MM (n=6)	MC (n=10)	OS (n=8)	αGC (n=10)	αGCOS (n=8)
Lymphocytes (% of live cells)	4.2 ± 0.9[a]	6.3 ± 1.6[a]	7.0 ± 1.1[a]	6.1 ±0.9[a]	7.1 ± 1.5[a]
Myeloid cells (% of live cells)	91.7 ± 0.8[a]	88.7 ± 1.5[a]	88.9 ± 1.7[a]	89.2 ± 1.2[a]	90.2 ± 1.7[a]
iNKT-cells (% of $CD3^+$)	0.57 ± 0.26[a]	0.37 ± 0.12[a]	0.13 ± 0.05[a]	0.36 ± 0.12[a]	0.57 ± 0.25[a]
$CD8\alpha^+CD8\beta^+CD4^-$ (% of $CD3^+$)	14.2 ± 3.3[ab]	14.6 ± 2.6[a]	14.4 ± 2.6[ab]	20.5 ± 4.9[ab]	**19.5 ± 3.5[b]**
$CD8\alpha^-CD4^+$ (% of $CD3^+$)	4.7 ± 1.5[a]	7.9 ± 2.0[a]	3.7 ± 1.2[a]	7.9 ± 1.7[a]	5.8 ± 2.0[a]
δTCR^+ (% of $CD3^+$)	40.8 ± 3.4[a]	37.5 ± 4.0[a]	38.6 ± 4.3[a]	44.0 ± 5.7[a]	34.4 ± 3.3[a]
NK cells (% of live cells)	5.0 ± 1.7[a]	3.9 ± 0.7[a]	4.4 ± 1.1[a]	5.3 ± 1.3[a]	**8.0 ± 1.9[b]**
Alveolar macrophages (% of live cells)	60.9 ± 4.4[a]	65.8 ± 5.8[a]	64.4 ± 2.4[a]	66.7 ± 2.4[a]	62.8 ± 3.7[a]
Granulocytes (% of live cells)	15.9 ± 3.3[a]	11.2 ± 3.1[a]	10.4 ± 1.6[a]	11.1 ± 1.2[a]	12.7 ± 1.8[a]

Values expressed in means and ± SEM, $P<0.05$ calculated using R function glm followed by Tukey's test. Values within rows with no common superscript letters differ significantly. Values with the same superscript are not statistically different. Values in bold are statistically different from non-infected controls.

Supplemental Table 3.4. Flow cytometric analysis of immune cell populations in spleen

	MM (n=6)	MC (n=10)	OS (n=8)	αGC (n=10)	αGCOS (n=8)
Lymphocytes (% of live cells)	65.9 ± 3.6[a]	63.9 ± 1.2[a]	60.2 ± 1.5[a]	61.5 ± 1.7[a]	59.7 ± 1.5[a]
Myeloid cells (% of live cells)	25.5 ± 2.5[a]	22.0 ± 1.6[a]	27.7 ± 1.6[a]	25.0 ± 1.8[a]	26.7 ± 2.7[a]
iNKT-cells (% of $CD3^+$)	0.06 ± 0.03[a]	0.08 ± 0.01[a]	0.10 ± 0.02[a]	0.36 ± 0.23[a]	0.29 ± 0.21[a]
$CD8\alpha^+CD8\beta^+CD4^-$ (% of $CD3^+$)	6.8 ± 0.7[a]	7.7 ± 0.8[a]	10.8 ± 1.4[a]	7.6 ± 0.8[a]	**12.5 ± 4.0[b]**
$CD8\alpha^-CD4^+$ (% of $CD3^+$)	22.3 ± 1.2[a]	19.5 ± 1.4[a]	21.2 ± 2.0[a]	17.30 ± 2.3[a]	14.0 ± 2.2[b]
δTCR^+ (% of $CD3^+$)	38.0 ± 3.9[a]	34.5 ± 2.2[a]	35.2 ± 3.9[a]	30.8 ± 2.1[a]	28.1 ± 2.9[a]
NK cells (% of live cells)	3.7 ± 0.6[a]	4.3 ± 1.0[a]	4.9 ± 2.0[ab]	3.7 ± 1.0[a]	**5.9 ± 2.5[b]**
Granulocytes (% of live cells)	10.2 ± 1.0[a]	7.5 ± 0.9[a]	9.4 ± 1.7[a]	9.1 ± 0.9[a]	10.2 ± 1.5[a]
Macrophages (% of live cells)	3.3 ± 0.6[a]	2.7 ± 0.3[a]	2.6 ± 0.3[a]	2.0 ± 0.2[a]	3.1 ± 0.6[a]
Dendritic cells (% of live cells)	1.3 ± 0.2[a]	1.9 ± 0.6[a]	2.1 ± 0.7[a]	2.0 ± 0.5[a]	1.1 ± 0.4[a]

Values expressed in means and ± SEM, $P<0.05$ calculated using R function glm followed by Tukey's test. Values within rows with no common superscript letters differ significantly. Values with the same superscript are not statistically different. Values in bold are statistically different from non-infected controls.

CHAPTER FOUR

SUMMARY

The lung is composed of mucosal tissue that is constantly exposed to microorganisms and environmental antigens. Therefore, the pulmonary immune system must simultaneously tolerate commensal microorganisms while providing adequate protection against infections. Due to the delicate architecture of the alveoli, the pulmonary inflammatory response must be regulated to prevent tissue damage and disruption of homeostasis.

Despite the availability of vaccines, influenza remains a viral respiratory disease that affects millions of individuals each year and contributes to pneumonia-related mortality. To better control influenza in humans, it is necessary to have a thorough understanding of the pathology that these viruses cause as well as immune responses that ameliorate or exacerbate influenza-induced disease. It is also important to understand how influenza viruses affect livestock in order to improve animal health and to prevent the occurrence of new influenza viruses capable of infecting humans.

The pig is the large animal model of choice for studying human respiratory diseases due to the resemblance between the pig and human respiratory systems. Swine are also an animal model that closely mirrors the clinical signs of human influenza infections. Furthermore, pigs can be naturally infected with the same subtypes of influenza viruses that infect humans. They are also able to transmit influenza viruses to susceptible hosts in a similar way to humans. However, many aspects of the porcine pulmonary immune system and its response to influenza infection remain unknown due to a lack of pig-specific immune reagents. Here we overcame this limitation by using

scRNA-seq to map the transcriptome of individual porcine lung leukocytes in six-weeks-old mixed breed pigs. This provided a detailed map of the pig lung, including several unconventional lymphoid cell types with innate-immune characteristics that have heretofore been poorly described. Our cross-species assessment of lung leukocytes reveals that the transcriptional profile and cellular composition of pig lungs is more comparable to that of humans than mice, in particular regarding αβ T cells, B cells, and NK cells. This finding supports that pigs are a relevant animal model to study the human pulmonary immune system. However, we also describe species-specific differences in certain cell types, such as γδ T cells, mast cells, and ILC2 cells, which may cause differences in how each species responds to influenza infections and other respiratory diseases.

My work also demonstrated that pig and mouse leukocytes present conserved and distinct cell-cell communication networks during an influenza infection. At five days post influenza infection, we show that the dominant communication hubs in pig lung leukocytes were mast cells, macrophages, monocytes, NK cells, and NK-like CD8 T cells, which coordinated a complex network for T cell co-stimulation, cytokine and chemokine signaling, and tissue remodeling. These findings are the first to describe the immune circuitry involved in an influenza immune response in pigs. The information generated provides a resource for future efforts to mitigate influenza virus infections through antiviral therapies, vaccines, and selective breeding for enhanced host immunity.

This dissertation includes a study that was performed using the swine influenza challenge model to compare the efficacy of two antiviral therapies for treating an ongoing influenza infection. One therapy was α-galactosylceramide (α-Galcer), a glycolipid molecule which activates NKT cells to release large quantities of cytokines. In mice, α-Galcer induces antiviral immune responses that inhibit influenza virus replication. The other was oseltamivir, the most

commonly prescribed influenza therapy for humans, which acts as a neuraminidase inhibitor that directly interrupts the influenza viral cycle. Although, oseltamivir is widely used, many questions about the efficacy of this drug remain, including whether it has the ability to reduce virus transmission and lung disease.

My results show that oseltamivir significantly decreased lung pathology, inhibited viral shedding, and significantly reduced virus transmission from infected to naïve pigs. These data supports using oseltamivir during influenza outbreaks in order to reduce human transmission and lung immunopathology. In contrast, α-GalCer had little impact on virus replication, virus transmission, or lung disease. Our inability to replicate previous studies showing that α-GalCer is effective at inhibiting influenza infections in mice is likely due to species differences in NKT cells and other immune cell types, and the severity of disease caused by influenza viruses, as well as other factors.

Taken together, my findings advance current knowledge about the porcine pulmonary immune cell compartment and the contribution of different cell types to the anti-influenza immune response, which is important for efforts to improve swine health. Moreover, this work will contribute to the future development of pig immune markers and immune phenotyping efforts, which are necessary to confirm that the pig is a suitable biomedical model for studying the human pulmonary immune system and human respiratory diseases, including influenza. The high degree of pig to human similarity revealed by my scRNA-seq data indicates that results obtained from studies like the antiviral experiments included in this dissertation can likely be translated to humans with high fidelity, which has important implications for using pigs to improve human health.

REFERENCES

1. Paget J, Spreeuwenberg P, Charu V, Taylor RJ, Iuliano AD, Bresee J, et al. Global mortality associated with seasonal influenza epidemics: New burden estimates and predictors from the GLaMOR Project. J Glob Health. 2019;9(2):020421.

2. Iuliano AD, Roguski KM, Chang HH, Muscatello DJ, Palekar R, Tempia S, et al. Estimates of global seasonal influenza-associated respiratory mortality: a modelling study. Lancet. 2018;391(10127):1285-300.

3. Hayward AC, Fragaszy EB, Bermingham A, Wang L, Copas A, Edmunds WJ, et al. Comparative community burden and severity of seasonal and pandemic influenza: results of the Flu Watch cohort study. Lancet Respir Med. 2014;2(6):445-54.

4. Macias AE, McElhaney JE, Chaves SS, Nealon J, Nunes MC, Samson SI, et al. The disease burden of influenza beyond respiratory illness. Vaccine. 2021;39 Suppl 1:A6-A14.

5. Lafond KE, Porter RM, Whaley MJ, Suizan Z, Ran Z, Aleem MA, et al. Global burden of influenza-associated lower respiratory tract infections and hospitalizations among adults: A systematic review and meta-analysis. PLoS Med. 2021;18(3):e1003550.

6. Wang X, Li Y, O'Brien KL, Madhi SA, Widdowson MA, Byass P, et al. Global burden of respiratory infections associated with seasonal influenza in children under 5 years in 2018: a systematic review and modelling study. Lancet Glob Health. 2020;8(4):e497-e510.

7. Hause BM, Collin EA, Liu R, Huang B, Sheng Z, Lu W, et al. Characterization of a novel influenza virus in cattle and Swine: proposal for a new genus in the Orthomyxoviridae family. mBio. 2014;5(2):e00031-14.

8. Chen R, Holmes EC. The evolutionary dynamics of human influenza B virus. J Mol Evol. 2008;66(6):655-63.

9. Fukuyama S, Kawaoka Y. The pathogenesis of influenza virus infections: the contributions of virus and host factors. Curr Opin Immunol. 2011;23(4):481-6.

10. Thompson CI, Barclay WS, Zambon MC, Pickles RJ. Infection of human airway epithelium by human and avian strains of influenza a virus. J Virol. 2006;80(16):8060-8.

11. Chan MC, Chan RW, Chan LL, Mok CK, Hui KP, Fong JH, et al. Tropism and innate host responses of a novel avian influenza A H7N9 virus: an analysis of ex-vivo and in-vitro cultures of the human respiratory tract. Lancet Respir Med. 2013;1(7):534-42.

12. Klemm C, Boergeling Y, Ludwig S, Ehrhardt C. Immunomodulatory Nonstructural Proteins of Influenza A Viruses. Trends Microbiol. 2018;26(7):624-36.

13. Matsuoka Y, Matsumae H, Katoh M, Eisfeld AJ, Neumann G, Hase T, et al. A comprehensive map of the influenza A virus replication cycle. BMC Syst Biol. 2013;7:97.

14. Steinhauer DA, Domingo E, Holland JJ. Lack of evidence for proofreading mechanisms associated with an RNA virus polymerase. Gene. 1992;122(2):281-8.

15. Both GW, Sleigh MJ, Cox NJ, Kendal AP. Antigenic drift in influenza virus H3 hemagglutinin from 1968 to 1980: multiple evolutionary pathways and sequential amino acid changes at key antigenic sites. J Virol. 1983;48(1):52-60.

16. Pauly MD, Lauring AS. Effective lethal mutagenesis of influenza virus by three nucleoside analogs. J Virol. 2015;89(7):3584-97.

17. Crotty S, Andino R. Implications of high RNA virus mutation rates: lethal mutagenesis and the antiviral drug ribavirin. Microbes Infect. 2002;4(13):1301-7.

18. Krammer F, Palese P. Advances in the development of influenza virus vaccines. Nat Rev Drug Discov. 2015;14(3):167-82.

19. Doud MB, Lee JM, Bloom JD. How single mutations affect viral escape from broad and narrow antibodies to H1 influenza hemagglutinin. Nat Commun. 2018;9(1):1386.

20. Villa M, Lässig M. Fitness cost of reassortment in human influenza. PLoS Pathog. 2017;13(11):e1006685.

21. Krammer F, Smith GJD, Fouchier RAM, Peiris M, Kedzierska K, Doherty PC, et al. Influenza. Nat Rev Dis Primers. 2018;4(1):3.

22. Yoon SW, Webby RJ, Webster RG. Evolution and ecology of influenza A viruses. Curr Top Microbiol Immunol. 2014;385:359-75.

23. Nickol ME, Kindrachuk J. A year of terror and a century of reflection: perspectives on the great influenza pandemic of 1918-1919. BMC Infect Dis. 2019;19(1):117.

24. Gomaa MR, Kandeil A, El-Shesheny R, Shehata MM, McKenzie PP, Webby RJ, et al. Evidence of infection with avian, human, and swine influenza viruses in pigs in Cairo, Egypt. Arch Virol. 2018;163(2):359-64.

25. Koopmans M, Wilbrink B, Conyn M, Natrop G, van der Nat H, Vennema H, et al. Transmission of H7N7 avian influenza A virus to human beings during a large outbreak in commercial poultry farms in the Netherlands. Lancet. 2004;363(9409):587-93.

26. Flannery B, Kondor RJG, Chung JR, Gaglani M, Reis M, Zimmerman RK, et al. Spread of Antigenically Drifted Influenza A(H3N2) Viruses and Vaccine Effectiveness in the United States During the 2018-2019 Season. J Infect Dis. 2020;221(1):8-15.

27. De Clercq E, Li G. Approved Antiviral Drugs over the Past 50 Years. Clin Microbiol Rev. 2016;29(3):695-747.

28. Hayden FG, Sugaya N, Hirotsu N, Lee N, de Jong MD, Hurt AC, et al. Baloxavir Marboxil for Uncomplicated Influenza in Adults and Adolescents. N Engl J Med. 2018;379(10):913-23.

29. Ikematsu H, Hayden FG, Kawaguchi K, Kinoshita M, de Jong MD, Lee N, et al. Baloxavir Marboxil for Prophylaxis against Influenza in Household Contacts. N Engl J Med. 2020;383(4):309-20.

30. Holmes EC, Hurt AC, Dobbie Z, Clinch B, Oxford JS, Piedra PA. Understanding the Impact of Resistance to Influenza Antivirals. Clin Microbiol Rev. 2021;34(2).

31. Welliver R, Monto AS, Carewicz O, Schatteman E, Hassman M, Hedrick J, et al. Effectiveness of oseltamivir in preventing influenza in household contacts: a randomized controlled trial. JAMA. 2001;285(6):748-54.

32. Ng S, Cowling BJ, Fang VJ, Chan KH, Ip DK, Cheng CK, et al. Effects of oseltamivir treatment on duration of clinical illness and viral shedding and household transmission of influenza virus. Clin Infect Dis. 2010;50(5):707-14.

33. Jefferson T, Jones M, Doshi P, Spencer EA, Onakpoya I, Heneghan CJ. Oseltamivir for influenza in adults and children: systematic review of clinical study reports and summary of regulatory comments. BMJ. 2014;348:g2545.

34. Santesso N, Hsu J, Mustafa R, Brozek J, Chen YL, Hopkins JP, et al. Antivirals for influenza: a summary of a systematic review and meta-analysis of observational studies. Influenza Other Respir Viruses. 2013;7 Suppl 2:76-81.

35. Aoki FY, Macleod MD, Paggiaro P, Carewicz O, El Sawy A, Wat C, et al. Early administration of oral oseltamivir increases the benefits of influenza treatment. J Antimicrob Chemother. 2003;51(1):123-9.

36. McLean HQ, Belongia EA, Kieke BA, Meece JK, Fry AM. Impact of Late Oseltamivir Treatment on Influenza Symptoms in the Outpatient Setting: Results of a Randomized Trial. Open Forum Infect Dis. 2015;2(3):ofv100.

37. Hurt AC, Ernest J, Deng YM, Iannello P, Besselaar TG, Birch C, et al. Emergence and spread of oseltamivir-resistant A(H1N1) influenza viruses in Oceania, South East Asia and South Africa. Antiviral Res. 2009;83(1):90-3.

38. Mohan T, Nguyen HT, Kniss K, Mishin VP, Merced-Morales AA, Laplante J, et al. Cluster of Oseltamivir-Resistant and Hemagglutinin Antigenically Drifted Influenza A(H1N1)pdm09 Viruses, Texas, USA, January 2020. Emerg Infect Dis. 2021;27(7):1953-7.

39. Hashimoto T, Baba K, Inoue K, Okane M, Hata S, Shishido T, et al. Comprehensive assessment of amino acid substitutions in the trimeric RNA polymerase complex of influenza A virus detected in clinical trials of baloxavir marboxil. Influenza Other Respir Viruses. 2021;15(3):389-95.

40. Ivashchenko AA, Dmitriev KA, Vostokova NV, Azarova VN, Blinow AA, Egorova AN, et al. AVIFAVIR for Treatment of Patients With Moderate Coronavirus Disease 2019 (COVID-19): Interim Results of a Phase II/III Multicenter Randomized Clinical Trial. Clin Infect Dis. 2021;73(3):531-4.

41. Miyagawa M, Akiyama T, Taoda Y, Takaya K, Takahashi-Kageyama C, Tomita K, et al. Synthesis and SAR Study of Carbamoyl Pyridone Bicycle Derivatives as Potent Inhibitors of Influenza Cap-dependent Endonuclease. J Med Chem. 2019;62(17):8101-14.

42. Credille CV, Morrison CN, Stokes RW, Dick BL, Feng Y, Sun J, et al. SAR Exploration of Tight-Binding Inhibitors of Influenza Virus PA Endonuclease. J Med Chem. 2019;62(21):9438-49.

43. White KM, Abreu P, Wang H, De Jesus PD, Manicassamy B, García-Sastre A, et al. Broad Spectrum Inhibitor of Influenza A and B Viruses Targeting the Viral Nucleoprotein. ACS Infect Dis. 2018;4(2):146-57.

44. O'Hanlon R, Shaw ML. Baloxavir marboxil: the new influenza drug on the market. Curr Opin Virol. 2019;35:14-8.

45. Lumby CK, Zhao L, Oporto M, Best T, Tutill H, Shah D, et al. Favipiravir and Zanamivir Cleared Infection with Influenza B in a Severely Immunocompromised Child. Clin Infect Dis. 2020;71(7):e191-e4.

46. Mifsud EJ, Tilmanis D, Oh DY, Ming-Kay Tai C, Rossignol JF, Hurt AC. Prophylaxis of ferrets with nitazoxanide and oseltamivir combinations is more effective at reducing the impact of influenza a virus infection compared to oseltamivir monotherapy. Antiviral Res. 2020;176:104751.

47. Chen S, Liu G, Chen J, Hu A, Zhang L, Sun W, et al. Ponatinib Protects Mice From Lethal Influenza Infection by Suppressing Cytokine Storm. Front Immunol. 2019;10:1393.

48. Walsh KB, Teijaro JR, Wilker PR, Jatzek A, Fremgen DM, Das SC, et al. Suppression of cytokine storm with a sphingosine analog provides protection against pathogenic influenza virus. Proc Natl Acad Sci U S A. 2011;108(29):12018-23.

49. Wang W, Yang P, Zhong Y, Zhao Z, Xing L, Zhao Y, et al. Monoclonal antibody against CXCL-10/IP-10 ameliorates influenza A (H1N1) virus induced acute lung injury. Cell Res. 2013;23(4):577-80.

50. Tavares LP, Garcia CC, Machado MG, Queiroz-Junior CM, Barthelemy A, Trottein F, et al. CXCR1/2 Antagonism Is Protective during Influenza and Post-Influenza Pneumococcal Infection. Front Immunol. 2017;8:1799.

51. Li C, Yang P, Zhang Y, Sun Y, Wang W, Zou Z, et al. Corticosteroid treatment ameliorates acute lung injury induced by 2009 swine origin influenza A (H1N1) virus in mice. PLoS One. 2012;7(8):e44110.

52. Ni YN, Chen G, Sun J, Liang BM, Liang ZA. The effect of corticosteroids on mortality of patients with influenza pneumonia: a systematic review and meta-analysis. Crit Care. 2019;23(1):99.

53. Lansbury L, Rodrigo C, Leonardi-Bee J, Nguyen-Van-Tam J, Lim WS. Corticosteroids as adjunctive therapy in the treatment of influenza. Cochrane Database Syst Rev. 2019;2:CD010406.

54. Zhou Y, Fu X, Liu X, Huang C, Tian G, Ding C, et al. Use of corticosteroids in influenza-associated acute respiratory distress syndrome and severe pneumonia: a systemic review and meta-analysis. Sci Rep. 2020;10(1):3044.

55. Shekhar S, Joyee AG, Yang X. Invariant natural killer T cells: boon or bane in immunity to intracellular bacterial infections? J Innate Immun. 2014;6(5):575-84.

56. Shekhar S, Joyee AG, Gao X, Peng Y, Wang S, Yang J, et al. Invariant Natural Killer T Cells Promote T Cell Immunity by Modulating the Function of Lung Dendritic Cells during Chlamydia pneumoniae Infection. J Innate Immun. 2015;7(3):260-74.

57. Ravikumar S, Win MS, Chai LY. Optimizing Outcomes in Immunocompromised Hosts: Understanding the Role of Immunotherapy in Invasive Fungal Diseases. Front Microbiol. 2015;6:1322.

58. Barthelemy A, Sencio V, Soulard D, Deruyter L, Faveeuw C, Le Goffic R, et al. Interleukin-22 Immunotherapy during Severe Influenza Enhances Lung Tissue Integrity and Reduces Secondary Bacterial Systemic Invasion. Infect Immun. 2018;86(7).

59. Pereira CS, Macedo MF. CD1-Restricted T Cells at the Crossroad of Innate and Adaptive Immunity. J Immunol Res. 2016;2016:2876275.

60. Brennan PJ, Brigl M, Brenner MB. Invariant natural killer T cells: an innate activation scheme linked to diverse effector functions. Nat Rev Immunol. 2013;13(2):101-17.

61. Mori L, Lepore M, De Libero G. The Immunology of CD1- and MR1-Restricted T Cells. Annu Rev Immunol. 2016;34:479-510.

62. Kawano T, Cui J, Koezuka Y, Toura I, Kaneko Y, Motoki K, et al. CD1d-restricted and TCR-mediated activation of valpha14 NKT cells by glycosylceramides. Science. 1997;278(5343):1626-9.

63. Van Kaer L, Parekh VV, Wu L. Invariant natural killer T cells: bridging innate and adaptive immunity. Cell Tissue Res. 2011;343(1):43-55.

64. Bendelac A, Savage PB, Teyton L. The biology of NKT cells. Annu Rev Immunol. 2007;25:297-336.

65. De Santo C, Salio M, Masri SH, Lee LY, Dong T, Speak AO, et al. Invariant NKT cells reduce the immunosuppressive activity of influenza A virus-induced myeloid-derived suppressor cells in mice and humans. J Clin Invest. 2008;118(12):4036-48.

66. Kok WL, Denney L, Benam K, Cole S, Clelland C, McMichael AJ, et al. Pivotal Advance: Invariant NKT cells reduce accumulation of inflammatory monocytes in the lungs and decrease immune-pathology during severe influenza A virus infection. J Leukoc Biol. 2012;91(3):357-68.

67. Paget C, Ivanov S, Fontaine J, Renneson J, Blanc F, Pichavant M, et al. Interleukin-22 is produced by invariant natural killer T lymphocytes during influenza A virus infection: potential role in protection against lung epithelial damages. J Biol Chem. 2012;287(12):8816-29.

68. Ishikawa H, Tanaka K, Kutsukake E, Fukui T, Sasaki H, Hata A, et al. IFN-γ production downstream of NKT cell activation in mice infected with influenza virus enhances the cytolytic activities of both NK cells and viral antigen-specific CD8+ T cells. Virology. 2010;407(2):325-32.

69. Ho LP, Denney L, Luhn K, Teoh D, Clelland C, McMichael AJ. Activation of invariant NKT cells enhances the innate immune response and improves the disease course in influenza A virus infection. Eur J Immunol. 2008;38(7):1913-22.

70. Gounder AP, Boon ACM. Influenza Pathogenesis: The Effect of Host Factors on Severity of Disease. J Immunol. 2019;202(2):341-50.

71. Bouvier NM, Lowen AC. Animal Models for Influenza Virus Pathogenesis and Transmission. Viruses. 2010;2(8):1530-63.

72. Terashima A, Watarai H, Inoue S, Sekine E, Nakagawa R, Hase K, et al. A novel subset of mouse NKT cells bearing the IL-17 receptor B responds to IL-25 and contributes to airway hyperreactivity. J Exp Med. 2008;205(12):2727-33.

73. Baranek T, Lebrigand K, de Amat Herbozo C, Gonzalez L, Bogard G, Dietrich C, et al. High Dimensional Single-Cell Analysis Reveals iNKT Cell Developmental Trajectories and Effector Fate Decision. Cell Rep. 2020;32(10):108116.

74. Artiaga BL, Whitener RL, Staples CR, Driver JP. Adjuvant effects of therapeutic glycolipids administered to a cohort of NKT cell-diverse pigs. Vet Immunol Immunopathol. 2014;162(1-2):1-13.

75. Yang G, Artiaga BL, Lomelino CL, Jayaprakash AD, Sachidanandam R, Mckenna R, et al. Next Generation Sequencing of the Pig αβ TCR Repertoire Identifies the Porcine Invariant NKT Cell Receptor. J Immunol. 2019;202(7):1981-91.

76. Kenna T, Golden-Mason L, Porcelli SA, Koezuka Y, Hegarty JE, O'Farrelly C, et al. NKT cells from normal and tumor-bearing human livers are phenotypically and functionally distinct from murine NKT cells. J Immunol. 2003;171(4):1775-9.

77. Yang G, Richt JA, Driver JP. Harnessing Invariant NKT Cells to Improve Influenza Vaccines: A Pig Perspective. Int J Mol Sci. 2017;19(1).

78. Artiaga BL, Yang G, Hackmann TJ, Liu Q, Richt JA, Salek-Ardakani S, et al. α-Galactosylceramide protects swine against influenza infection when administered as a vaccine adjuvant. Sci Rep. 2016;6:23593.

79. Gu W, Madrid DMC, Joyce S, Driver JP. A single-cell analysis of thymopoiesis and thymic iNKT cell development in pigs. Cell Rep. 2022;40(1):111050.

80. Artiaga BL, Yang G, Hutchinson TE, Loeb JC, Richt JA, Lednicky JA, et al. Rapid control of pandemic H1N1 influenza by targeting NKT-cells. Sci Rep. 2016;6:37999.

81. Ma W, Kahn RE, Richt JA. The pig as a mixing vessel for influenza viruses: Human and veterinary implications. J Mol Genet Med. 2008;3(1):158-66.

82. Abente EJ, Gauger PC, Walia RR, Rajao DS, Zhang J, Harmon KM, et al. Detection and characterization of an H4N6 avian-lineage influenza A virus in pigs in the Midwestern United States. Virology. 2017;511:56-65.

83. Powell JD, Abente EJ, Chang J, Souza CK, Rajao DS, Anderson TK, et al. Characterization of contemporary 2010.1 H3N2 swine influenza A viruses circulating in United States pigs. Virology. 2021;553:94-101.

84. He P, Wang G, Mo Y, Yu Q, Xiao X, Yang W, et al. Novel triple-reassortant influenza viruses in pigs, Guangxi, China. Emerg Microbes Infect. 2018;7(1):85.

85. Shinde V, Bridges CB, Uyeki TM, Shu B, Balish A, Xu X, et al. Triple-reassortant swine influenza A (H1) in humans in the United States, 2005-2009. N Engl J Med. 2009;360(25):2616-25.

86. Dawood FS, Jain S, Finelli L, Shaw MW, Lindstrom S, Garten RJ, et al. Emergence of a novel swine-origin influenza A (H1N1) virus in humans. N Engl J Med. 2009;360(25):2605-15.

87. Vijaykrishna D, Poon LL, Zhu HC, Ma SK, Li OT, Cheung CL, et al. Reassortment of pandemic H1N1/2009 influenza A virus in swine. Science. 2010;328(5985):1529.

88. Rajao DS, Vincent AL. Swine as a model for influenza A virus infection and immunity. ILAR J. 2015;56(1):44-52.

89. Er C, Lium B, Tavornpanich S, Hofmo PO, Forberg H, Hauge AG, et al. Adverse effects of Influenza A(H1N1)pdm09 virus infection on growth performance of Norwegian pigs - a longitudinal study at a boar testing station. BMC Vet Res. 2014;10:284.

90. Fablet C, Simon G, Dorenlor V, Eono F, Eveno E, Gorin S, et al. Different herd level factors associated with H1N1 or H1N2 influenza virus infections in fattening pigs. Prev Vet Med. 2013;112(3-4):257-65.

91. Ding F, Li Y, Huang B, Edwards J, Cai C, Zhang G, et al. Infection and risk factors of human and avian influenza in pigs in south China. Prev Vet Med. 2021;190:105317.

92. Allerson MW, Davies PR, Gramer MR, Torremorell M. Infection dynamics of pandemic 2009 H1N1 influenza virus in a two-site swine herd. Transbound Emerg Dis. 2014;61(6):490-9.

93. Starbæk SMR, Brogaard L, Dawson HD, Smith AD, Heegaard PMH, Larsen LE, et al. Animal Models for Influenza A Virus Infection Incorporating the Involvement of Innate Host Defenses: Enhanced Translational Value of the Porcine Model. ILAR J. 2018;59(3):323-37.

94. Horter DC, Yoon KJ, Zimmerman JJ. A review of porcine tonsils in immunity and disease. Anim Health Res Rev. 2003;4(2):143-55.

95. Judge EP, Hughes JM, Egan JJ, Maguire M, Molloy EL, O'Dea S. Anatomy and bronchoscopy of the porcine lung. A model for translational respiratory medicine. Am J Respir Cell Mol Biol. 2014;51(3):334-43.

96. Yang X, Steukers L, Forier K, Xiong R, Braeckmans K, Van Reeth K, et al. A beneficiary role for neuraminidase in influenza virus penetration through the respiratory mucus. PLoS One. 2014;9(10):e110026.

97. Radigan KA, Misharin AV, Chi M, Budinger GS. Modeling human influenza infection in the laboratory. Infect Drug Resist. 2015;8:311-20.

98. Humphray SJ, Scott CE, Clark R, Marron B, Bender C, Camm N, et al. A high utility integrated map of the pig genome. Genome Biol. 2007;8(7):R139.

99. Wernersson R, Schierup MH, Jørgensen FG, Gorodkin J, Panitz F, Staerfeldt HH, et al. Pigs in sequence space: a 0.66X coverage pig genome survey based on shotgun sequencing. BMC Genomics. 2005;6:70.

100. Dawson HD, Loveland JE, Pascal G, Gilbert JG, Uenishi H, Mann KM, et al. Structural and functional annotation of the porcine immunome. BMC Genomics. 2013;14:332.

101. Chevaleyre C, Riou M, Bréa D, Vandebrouck C, Barc C, Pezant J, et al. The Pig: A Relevant Model for Evaluating the Neutrophil Serine Protease Activities during Acute Pseudomonas aeruginosa Lung Infection. PLoS One. 2016;11(12):e0168577.

102. Blanc F, Prévost-Blondel A, Piton G, Bouguyon E, Leplat JJ, Andréoletti F, et al. The Composition of Circulating Leukocytes Varies With Age and Melanoma Onset in the MeLiM Pig Biomedical Model. Front Immunol. 2020;11:291.

103. Lim K, Hyun YM, Lambert-Emo K, Capece T, Bae S, Miller R, et al. Neutrophil trails guide influenza-specific $CD8^+$ T cells in the airways. Science. 2015;349(6252):aaa4352.

104. Zhu L, Liu L, Zhang Y, Pu L, Liu J, Li X, et al. High Level of Neutrophil Extracellular Traps Correlates With Poor Prognosis of Severe Influenza A Infection. J Infect Dis. 2018;217(3):428-37.

105. Kulkarni U, Zemans RL, Smith CA, Wood SC, Deng JC, Goldstein DR. Excessive neutrophil levels in the lung underlie the age-associated increase in influenza mortality. Mucosal Immunol. 2019;12(2):545-54.

106. Zarnegar B, Mendez-Enriquez E, Westin A, Söderberg C, Dahlin JS, Grönvik KO, et al. Influenza Infection in Mice Induces Accumulation of Lung Mast Cells through the Recruitment and Maturation of Mast Cell Progenitors. Front Immunol. 2017;8:310.

107. Hu Y, Jin Y, Han D, Zhang G, Cao S, Xie J, et al. Mast cell-induced lung injury in mice infected with H5N1 influenza virus. J Virol. 2012;86(6):3347-56.

108. Liu B, Meng D, Wei T, Zhang S, Hu Y, Wang M. Apoptosis and pro-inflammatory cytokine response of mast cells induced by influenza A viruses. PLoS One. 2014;9(6):e100109.

109. Murphy-Schafer AR, Paust S. Divergent Mast Cell Responses Modulate Antiviral Immunity During Influenza Virus Infection. Front Cell Infect Microbiol. 2021;11:580679.

110. O'Neill MB, Quach H, Pothlichet J, Aquino Y, Bisiaux A, Zidane N, et al. Single-Cell and Bulk RNA-Sequencing Reveal Differences in Monocyte Susceptibility to Influenza A Virus Infection Between Africans and Europeans. Front Immunol. 2021;12:768189.

111. Hoeve MA, Nash AA, Jackson D, Randall RE, Dransfield I. Influenza virus A infection of human monocyte and macrophage subpopulations reveals increased susceptibility associated with cell differentiation. PLoS One. 2012;7(1):e29443.

112. Moreno S, Alvarez B, Poderoso T, Revilla C, Ezquerra A, Alonso F, et al. Porcine monocyte subsets differ in the expression of CCR2 and in their responsiveness to CCL2. Vet Res. 2010;41(5):76.

113. Fairbairn L, Kapetanovic R, Beraldi D, Sester DP, Tuggle CK, Archibald AL, et al. Comparative analysis of monocyte subsets in the pig. J Immunol. 2013;190(12):6389-96.

114. Lin KL, Suzuki Y, Nakano H, Ramsburg E, Gunn MD. CCR2+ monocyte-derived dendritic cells and exudate macrophages produce influenza-induced pulmonary immune pathology and mortality. J Immunol. 2008;180(4):2562-72.

115. Maisonnasse P, Bouguyon E, Piton G, Ezquerra A, Urien C, Deloizy C, et al. The respiratory DC/macrophage network at steady-state and upon influenza infection in the swine biomedical model. Mucosal Immunol. 2016;9(4):835-49.

116. Bordet E, Maisonnasse P, Renson P, Bouguyon E, Crisci E, Tiret M, et al. Porcine Alveolar Macrophage-like cells are pro-inflammatory Pulmonary Intravascular Macrophages that produce large titers of Porcine Reproductive and Respiratory Syndrome Virus. Sci Rep. 2018;8(1):10172.

117. McGill J, Heusel JW, Legge KL. Innate immune control and regulation of influenza virus infections. J Leukoc Biol. 2009;86(4):803-12.

118. Koyama S, Ishii KJ, Kumar H, Tanimoto T, Coban C, Uematsu S, et al. Differential role of TLR- and RLR-signaling in the immune responses to influenza A virus infection and vaccination. J Immunol. 2007;179(7):4711-20.

119. Schneider C, Nobs SP, Heer AK, Kurrer M, Klinke G, van Rooijen N, et al. Alveolar macrophages are essential for protection from respiratory failure and associated morbidity following influenza virus infection. PLoS Pathog. 2014;10(4):e1004053.

120. Hussell T, Bell TJ. Alveolar macrophages: plasticity in a tissue-specific context. Nat Rev Immunol. 2014;14(2):81-93.

121. Kim HM, Lee YW, Lee KJ, Kim HS, Cho SW, van Rooijen N, et al. Alveolar macrophages are indispensable for controlling influenza viruses in lungs of pigs. J Virol. 2008;82(9):4265-74.

122. Crisci E, Moroldo M, Vu Manh TP, Mohammad A, Jourdren L, Urien C, et al. Distinctive Cellular and Metabolic Reprogramming in Porcine Lung Mononuclear Phagocytes Infected With Type 1 PRRSV Strains. Front Immunol. 2020;11:588411.

123. Evren E, Ringqvist E, Tripathi KP, Sleiers N, Rives IC, Alisjahbana A, et al. Distinct developmental pathways from blood monocytes generate human lung macrophage diversity. Immunity. 2021;54(2):259-75.e7.

124. DuPage M, Bluestone JA. Harnessing the plasticity of CD4(+) T cells to treat immune-mediated disease. Nat Rev Immunol. 2016;16(3):149-63.

125. Kudva A, Scheller EV, Robinson KM, Crowe CR, Choi SM, Slight SR, et al. Influenza A inhibits Th17-mediated host defense against bacterial pneumonia in mice. J Immunol. 2011;186(3):1666-74.

126. Dhume K, Finn CM, Devarajan P, Singh A, Tejero JD, Prokop E, et al. Bona Fide Th17 Cells without Th1 Functional Plasticity Protect against Influenza. J Immunol. 2022;208(8):1998-2007.

127. Sant AJ, DiPiazza AT, Nayak JL, Rattan A, Richards KA. CD4 T cells in protection from influenza virus: Viral antigen specificity and functional potential. Immunol Rev. 2018;284(1):91-105.

128. Crotty S. T follicular helper cell differentiation, function, and roles in disease. Immunity. 2014;41(4):529-42.

129. Jansen JM, Gerlach T, Elbahesh H, Rimmelzwaan GF, Saletti G. Influenza virus-specific CD4+ and CD8+ T cell-mediated immunity induced by infection and vaccination. J Clin Virol. 2019;119:44-52.

130. Sridhar S, Begom S, Bermingham A, Hoschler K, Adamson W, Carman W, et al. Cellular immune correlates of protection against symptomatic pandemic influenza. Nat Med. 2013;19(10):1305-12.

131. Hayward AC, Wang L, Goonetilleke N, Fragaszy EB, Bermingham A, Copas A, et al. Natural T Cell-mediated Protection against Seasonal and Pandemic Influenza. Results of the Flu Watch Cohort Study. Am J Respir Crit Care Med. 2015;191(12):1422-31.

132. Wang Z, Wan Y, Qiu C, Quiñones-Parra S, Zhu Z, Loh L, et al. Recovery from severe H7N9 disease is associated with diverse response mechanisms dominated by $CD8^+$ T cells. Nat Commun. 2015;6:6833.

133. Mueller SN, Gebhardt T, Carbone FR, Heath WR. Memory T cell subsets, migration patterns, and tissue residence. Annu Rev Immunol. 2013;31:137-61.

134. Schenkel JM, Masopust D. Tissue-resident memory T cells. Immunity. 2014;41(6):886-97.

135. Jameson SC, Masopust D. Understanding Subset Diversity in T Cell Memory. Immunity. 2018;48(2):214-26.

136. Zuckermann FA, Husmann RJ. Functional and phenotypic analysis of porcine peripheral blood CD4/CD8 double-positive T cells. Immunology. 1996;87(3):500-12.

137. Amezcua Vesely MC, Pallis P, Bielecki P, Low JS, Zhao J, Harman CCD, et al. Effector T. Cell. 2019;178(5):1176-88.e15.

138. Turner JS, Zhou JQ, Han J, Schmitz AJ, Rizk AA, Alsoussi WB, et al. Human germinal centres engage memory and naive B cells after influenza vaccination. Nature. 2020;586(7827):127-32.

139. Stadlbauer D, Zhu X, McMahon M, Turner JS, Wohlbold TJ, Schmitz AJ, et al. Broadly protective human antibodies that target the active site of influenza virus neuraminidase. Science. 2019;366(6464):499-504.

140. Dawson HD, Lunney JK. Porcine cluster of differentiation (CD) markers 2018 update. Res Vet Sci. 2018;118:199-246.

141. Artiaga BL, Morozov I, Ransburgh R, Kwon T, Balaraman V, Indran SV, et al. Evaluating α-galactosylceramide as an adjuvant for live attenuated influenza vaccines in pigs. Anim Dis. 2022;2(1):19.

142. Anderson RJ, Li J, Kedzierski L, Compton BJ, Hayman CM, Osmond TL, et al. Augmenting Influenza-Specific T Cell Memory Generation with a Natural Killer T Cell-Dependent Glycolipid-Peptide Vaccine. ACS Chem Biol. 2017;12(11):2898-905.

143. Forberg H, Hauge AG, Valheim M, Garcon F, Nunez A, Gerner W, et al. Early responses of natural killer cells in pigs experimentally infected with 2009 pandemic H1N1 influenza A virus. PLoS One. 2014;9(6):e100619.

144. Pommerenke C, Wilk E, Srivastava B, Schulze A, Novoselova N, Geffers R, et al. Global transcriptome analysis in influenza-infected mouse lungs reveals the kinetics of innate and adaptive host immune responses. PLoS One. 2012;7(7):e41169.

145. Cooper GE, Ostridge K, Khakoo SI, Wilkinson TMA, Staples KJ. Human CD49a. Front Immunol. 2018;9:1671.

146. Arnon TI, Achdout H, Lieberman N, Gazit R, Gonen-Gross T, Katz G, et al. The mechanisms controlling the recognition of tumor- and virus-infected cells by NKp46. Blood. 2004;103(2):664-72.

147. Arnon TI, Lev M, Katz G, Chernobrov Y, Porgador A, Mandelboim O. Recognition of viral hemagglutinins by NKp44 but not by NKp30. Eur J Immunol. 2001;31(9):2680-9.

148. Gray JD, Horwitz DA. Activated human NK cells can stimulate resting B cells to secrete immunoglobulin. J Immunol. 1995;154(11):5656-64.

149. Betakova T, Kostrabova A, Lachova V, Turianova L. Cytokines Induced During Influenza Virus Infection. Curr Pharm Des. 2017;23(18):2616-22.

150. Klose CS, Artis D. Innate lymphoid cells as regulators of immunity, inflammation and tissue homeostasis. Nat Immunol. 2016;17(7):765-74.

151. Hildreth AD, Ma F, Wong YY, Sun R, Pellegrini M, O'Sullivan TE. Single-cell sequencing of human white adipose tissue identifies new cell states in health and obesity. Nat Immunol. 2021;22(5):639-53.

152. Dadi S, Chhangawala S, Whitlock BM, Franklin RA, Luo CT, Oh SA, et al. Cancer Immunosurveillance by Tissue-Resident Innate Lymphoid Cells and Innate-like T Cells. Cell. 2016;164(3):365-77.

153. Qiu J, Zhang J, Ji Y, Sun H, Gu Z, Sun Q, et al. Tissue signals imprint Aiolos expression in ILC2s to modulate type 2 immunity. Mucosal Immunol. 2021;14(6):1306-22.

154. Vashist N, Trittel S, Ebensen T, Chambers BJ, Guzmán CA, Riese P. Influenza-Activated ILC1s Contribute to Antiviral Immunity Partially Influenced by Differential GITR Expression. Front Immunol. 2018;9:505.

155. Califano D, Furuya Y, Roberts S, Avram D, McKenzie ANJ, Metzger DW. IFN-γ increases susceptibility to influenza A infection through suppression of group II innate lymphoid cells. Mucosal Immunol. 2018;11(1):209-19.

156. Monticelli LA, Sonnenberg GF, Abt MC, Alenghat T, Ziegler CG, Doering TA, et al. Innate lymphoid cells promote lung-tissue homeostasis after infection with influenza virus. Nat Immunol. 2011;12(11):1045-54.

157. Godfrey DI, Uldrich AP, McCluskey J, Rossjohn J, Moody DB. The burgeoning family of unconventional T cells. Nat Immunol. 2015;16(11):1114-23.

158. Mair KH, Stadler M, Talker SC, Forberg H, Storset AK, Müllebner A, et al. Porcine CD3(+)NKp46(+) Lymphocytes Have NK-Cell Characteristics and Are Present in Increased Frequencies in the Lungs of Influenza-Infected Animals. Front Immunol. 2016;7:263.

159. Correia DV, Fogli M, Hudspeth K, da Silva MG, Mavilio D, Silva-Santos B. Differentiation of human peripheral blood Vδ1+ T cells expressing the natural cytotoxicity receptor NKp30 for recognition of lymphoid leukemia cells. Blood. 2011;118(4):992-1001.

160. Sagar, Pokrovskii M, Herman JS, Naik S, Sock E, Zeis P, et al. Deciphering the regulatory landscape of fetal and adult γδ T-cell development at single-cell resolution. EMBO J. 2020;39(13):e104159.

161. Li H, Xiang Z, Feng T, Li J, Liu Y, Fan Y, et al. Human Vγ9Vδ2-T cells efficiently kill influenza virus-infected lung alveolar epithelial cells. Cell Mol Immunol. 2013;10(2):159-64.

162. Wang X, Lin X, Zheng Z, Lu B, Wang J, Tan AH, et al. Host-derived lipids orchestrate pulmonary γδ T cell response to provide early protection against influenza virus infection. Nat Commun. 2021;12(1):1914.

163. Le Page L, Gillespie A, Schwartz JC, Prawits LM, Schlerka A, Farrell CP, et al. Subpopulations of swine γδ T cells defined by TCRγ and WC1 gene expression. Dev Comp Immunol. 2021;125:104214.

164. Yamagata T, Mathis D, Benoist C. Self-reactivity in thymic double-positive cells commits cells to a CD8 alpha alpha lineage with characteristics of innate immune cells. Nat Immunol. 2004;5(6):597-605.

165. Cheroutre H, Lambolez F, Mucida D. The light and dark sides of intestinal intraepithelial lymphocytes. Nat Rev Immunol. 2011;11(7):445-56.

166. Verstichel G, Vermijlen D, Martens L, Goetgeluk G, Brouwer M, Thiault N, et al. The checkpoint for agonist selection precedes conventional selection in human thymus. Sci Immunol. 2017;2(8).

167. Provine NM, Klenerman P. MAIT Cells in Health and Disease. Annu Rev Immunol. 2020;38:203-28.

168. Kjer-Nielsen L, Patel O, Corbett AJ, Le Nours J, Meehan B, Liu L, et al. MR1 presents microbial vitamin B metabolites to MAIT cells. Nature. 2012;491(7426):717-23.

169. Lamichhane R, Galvin H, Hannaway RF, de la Harpe SM, Munro F, Tyndall JD, et al. Type I interferons are important co-stimulatory signals during T cell receptor mediated human MAIT cell activation. Eur J Immunol. 2020;50(2):178-91.

170. Ussher JE, Bilton M, Attwod E, Shadwell J, Richardson R, de Lara C, et al. CD161++ CD8+ T cells, including the MAIT cell subset, are specifically activated by IL-12+IL-18 in a TCR-independent manner. Eur J Immunol. 2014;44(1):195-203.

171. Loh L, Wang Z, Sant S, Koutsakos M, Jegaskanda S, Corbett AJ, et al. Human mucosal-associated invariant T cells contribute to antiviral influenza immunity via IL-18-dependent activation. Proc Natl Acad Sci U S A. 2016;113(36):10133-8.

172. van Wilgenburg B, Loh L, Chen Z, Pediongco TJ, Wang H, Shi M, et al. MAIT cells contribute to protection against lethal influenza infection in vivo. Nat Commun. 2018;9(1):4706.

173. Meierovics A, Yankelevich WJ, Cowley SC. MAIT cells are critical for optimal mucosal immune responses during in vivo pulmonary bacterial infection. Proc Natl Acad Sci U S A. 2013;110(33):E3119-28.

174. Parrot T, Gorin JB, Ponzetta A, Maleki KT, Kammann T, Emgård J, et al. MAIT cell activation and dynamics associated with COVID-19 disease severity. Sci Immunol. 2020;5(51).

175. Xiao X, Li K, Ma X, Liu B, He X, Yang S, et al. Mucosal-Associated Invariant T Cells Expressing the TRAV1-TRAJ33 Chain Are Present in Pigs. Front Immunol. 2019;10:2070.

176. Hsia CC, Hyde DM, Weibel ER. Lung Structure and the Intrinsic Challenges of Gas Exchange. Compr Physiol. 2016;6(2):827-95.

177. Travaglini KJ, Nabhan AN, Penland L, Sinha R, Gillich A, Sit RV, et al. A molecular cell atlas of the human lung from single-cell RNA sequencing. Nature. 2020;587(7835):619-25.

178. Pabst R. The pig as a model for immunology research. Cell Tissue Res. 2020;380(2):287-304.

179. Meurens F, Summerfield A, Nauwynck H, Saif L, Gerdts V. The pig: a model for human infectious diseases. Trends Microbiol. 2012;20(1):50-7.

180. Brace CL, Hinshaw JL, Laeseke PF, Sampson LA, Lee FT. Pulmonary thermal ablation: comparison of radiofrequency and microwave devices by using gross pathologic and CT findings in a swine model. Radiology. 2009;251(3):705-11.

181. Nishikawa H, Oto T, Otani S, Harada M, Iga N, Miyoshi K, et al. Unilateral lung transplantation using right and left upper lobes: an experimental study. J Thorac Cardiovasc Surg. 2013;146(6):1534-7.

182. Steinmeyer J, Becker S, Avsar M, Salman J, Höffler K, Haverich A, et al. Cellular and acellular ex vivo lung perfusion preserve functional lung ultrastructure in a large animal model: a stereological study. Respir Res. 2018;19(1):238.

183. Lu T, Yang B, Wang R, Qin C. Xenotransplantation: Current Status in Preclinical Research. Front Immunol. 2019;10:3060.

184. Rogers CS, Abraham WM, Brogden KA, Engelhardt JF, Fisher JT, McCray PB, et al. The porcine lung as a potential model for cystic fibrosis. Am J Physiol Lung Cell Mol Physiol. 2008;295(2):L240-63.

185. Rogers CS, Stoltz DA, Meyerholz DK, Ostedgaard LS, Rokhlina T, Taft PJ, et al. Disruption of the CFTR gene produces a model of cystic fibrosis in newborn pigs. Science. 2008;321(5897):1837-41.

186. Loving CL, Brockmeier SL, Vincent AL, Palmer MV, Sacco RE, Nicholson TL. Influenza virus coinfection with Bordetella bronchiseptica enhances bacterial colonization and host responses exacerbating pulmonary lesions. Microb Pathog. 2010;49(5):237-45.

187. Reynolds JJ, Torremorell M, Craft ME. Mathematical modeling of influenza A virus dynamics within swine farms and the effects of vaccination. PLoS One. 2014;9(8):e106177.

188. Haden C, Painter T, Fangman T, Holtkamp D. Assessing Production Parameters and Economic Impact of Swine Influenza, PRRS and Mycoplasma Hyopneumoniae on Finishing Pigs in a Large Production System. American Association of Swine Veterinarians Annual Meeting (2012)2012.

189. Liao M, Liu Y, Yuan J, Wen Y, Xu G, Zhao J, et al. Single-cell landscape of bronchoalveolar immune cells in patients with COVID-19. Nat Med. 2020;26(6):842-4.

190. Zilionis R, Engblom C, Pfirschke C, Savova V, Zemmour D, Saatcioglu HD, et al. Single-Cell Transcriptomics of Human and Mouse Lung Cancers Reveals Conserved Myeloid Populations across Individuals and Species. Immunity. 2019;50(5):1317-34.e10.

191. Guo X, Zhang Y, Zheng L, Zheng C, Song J, Zhang Q, et al. Global characterization of T cells in non-small-cell lung cancer by single-cell sequencing. Nat Med. 2018;24(7):978-85.

192. Blighe K, Rana S, Lewis M. Bioconductor-EnhancedVolcano. [Available from: https://bioconductor.org/packages/release/bioc/html/EnhancedVolcano.html .

193. Steuerman Y, Cohen M, Peshes-Yaloz N, Valadarsky L, Cohn O, David E, et al. Dissection of Influenza Infection In Vivo by Single-Cell RNA Sequencing. Cell Syst. 2018;6(6):679-91.e4.

194. McGrath JJC, Vanderstocken G, Dvorkin-Gheva A, Cass SP, Afkhami S, Fantauzzi MF, et al. Cigarette smoke augments CSF3 expression in neutrophils to compromise alveolar-capillary barrier function during influenza infection. Eur Respir J. 2022;60(2).

195. Wu T, Hu E, Xu S, Chen M, Guo P, Dai Z, et al. clusterProfiler 4.0: A universal enrichment tool for interpreting omics data. Innovation (Camb). 2021;2(3):100141.

196. Jin S, Guerrero-Juarez CF, Zhang L, Chang I, Ramos R, Kuan CH, et al. Inference and analysis of cell-cell communication using CellChat. Nat Commun. 2021;12(1):1088.

197. Sheikh F, Dickensheets H, Pedras-Vasconcelos J, Ramalingam T, Helming L, Gordon S, et al. The Interleukin-13 Receptor-α1 Chain Is Essential for Induction of the Alternative Macrophage Activation Pathway by IL-13 but Not IL-4. J Innate Immun. 2015;7(5):494-505.

198. Chávez-Galán L, Olleros ML, Vesin D, Garcia I. Much More than M1 and M2 Macrophages, There are also CD169(+) and TCR(+) Macrophages. Front Immunol. 2015;6:263.

199. Zhao Y, Kilian C, Turner JE, Bosurgi L, Roedl K, Bartsch P, et al. Clonal expansion and activation of tissue-resident memory-like Th17 cells expressing GM-CSF in the lungs of severe COVID-19 patients. Sci Immunol. 2021;6(56).

200. Reyfman PA, Walter JM, Joshi N, Anekalla KR, McQuattie-Pimentel AC, Chiu S, et al. Single-Cell Transcriptomic Analysis of Human Lung Provides Insights into the Pathobiology of Pulmonary Fibrosis. Am J Respir Crit Care Med. 2019;199(12):1517-36.

201. Reinink P, Van Rhijn I. Mammalian CD1 and MR1 genes. Immunogenetics. 2016;68(8):515-23.

202. Collin M, Bigley V. Human dendritic cell subsets: an update. Immunology. 2018;154(1):3-20.

203. Auray G, Keller I, Python S, Gerber M, Bruggmann R, Ruggli N, et al. Characterization and Transcriptomic Analysis of Porcine Blood Conventional and Plasmacytoid Dendritic Cells Reveals Striking Species-Specific Differences. J Immunol. 2016;197(12):4791-806.

204. Sadik A, Somarribas Patterson LF, Öztürk S, Mohapatra SR, Panitz V, Secker PF, et al. IL4I1 Is a Metabolic Immune Checkpoint that Activates the AHR and Promotes Tumor Progression. Cell. 2020;182(5):1252-70.e34.

205. Prentzell MT, Opitz CA. cDC1 to cDC2: "Everything I do, Ido1 it for you". Immunity. 2022;55(6):967-70.

206. Parra-Sánchez H, Puebla-Clark L, Reséndiz M, Valenzuela O, Hernández J. Characterization and expression of DEC205 in the cDC1 and cDC2 subsets of porcine dendritic cells from spleen, tonsil, and submaxillary and mesenteric lymph nodes. Mol Immunol. 2018;96:1-7.

207. Sun Q, Li N, Jia L, Guo W, Jiang H, Liu B, et al. Ribosomal Protein SA-Positive Neutrophil Elicits Stronger Phagocytosis and Neutrophil Extracellular Trap Formation and Subdues Pro-Inflammatory Cytokine Secretion Against. Front Immunol. 2020;11:585399.

208. Fuchs T, Püellmann K, Scharfenstein O, Eichner R, Stobe E, Becker A, et al. The neutrophil recombinatorial TCR-like immune receptor is expressed across the entire human life span but repertoire diversity declines in old age. Biochem Biophys Res Commun. 2012;419(2):309-15.

209. Puellmann K, Kaminski WE, Vogel M, Nebe CT, Schroeder J, Wolf H, et al. A variable immunoreceptor in a subpopulation of human neutrophils. Proc Natl Acad Sci U S A. 2006;103(39):14441-6.

210. Raredon MSB, Adams TS, Suhail Y, Schupp JC, Poli S, Neumark N, et al. Single-cell connectomic analysis of adult mammalian lungs. Sci Adv. 2019;5(12):eaaw3851.

211. Li Y, Gao J, Kamran M, Harmacek L, Danhorn T, Leach SM, et al. GATA2 regulates mast cell identity and responsiveness to antigenic stimulation by promoting chromatin remodeling at super-enhancers. Nat Commun. 2021;12(1):494.

212. Inage E, Kasakura K, Yashiro T, Suzuki R, Baba Y, Nakano N, et al. Critical Roles for PU.1, GATA1, and GATA2 in the expression of human FcεRI on mast cells: PU.1 and GATA1 transactivate FCER1A, and GATA2 transactivates FCER1A and MS4A2. J Immunol. 2014;192(8):3936-46.

213. Koenitzer JR, Wu H, Atkinson JJ, Brody SL, Humphreys BD. Single-Nucleus RNA-Sequencing Profiling of Mouse Lung. Reduced Dissociation Bias and Improved Rare Cell-Type Detection Compared with Single-Cell RNA Sequencing. Am J Respir Cell Mol Biol. 2020;63(6):739-47.

214. Herrera-Uribe J, Wiarda JE, Sivasankaran SK, Daharsh L, Liu H, Byrne KA, et al. Reference Transcriptomes of Porcine Peripheral Immune Cells Created Through Bulk and Single-Cell RNA Sequencing. Front Genet. 2021;12:689406.

215. Zhang L, Zhu J, Wang H, Xia J, Liu P, Chen F, et al. A high-resolution cell atlas of the domestic pig lung and an online platform for exploring lung single-cell data. J Genet Genomics. 2021;48(5):411-25.

216. Le Page L, Baldwin CL, Telfer JC. γδ T cells in artiodactyls: Focus on swine. Dev Comp Immunol. 2022;128:104334.

217. Rogers AN, Vanburen DG, Hedblom EE, Tilahun ME, Telfer JC, Baldwin CL. Gammadelta T cell function varies with the expressed WC1 coreceptor. J Immunol. 2005;174(6):3386-93.

218. Sedlak C, Patzl M, Saalmüller A, Gerner W. CD2 and CD8α define porcine γδ T cells with distinct cytokine production profiles. Dev Comp Immunol. 2014;45(1):97-106.

219. Zhang B, Lin YY, Dai M, Zhuang Y. Id3 and Id2 act as a dual safety mechanism in regulating the development and population size of innate-like γδ T cells. J Immunol. 2014;192(3):1055-63.

220. Stepanova K, Sinkora M. Porcine γδ T lymphocytes can be categorized into two functionally and developmentally distinct subsets according to expression of CD2 and level of TCR. J Immunol. 2013;190(5):2111-20.

221. Chen YG, Tsaih SW, Serreze DV. Genetic control of murine invariant natural killer T-cell development dynamically differs dependent on the examined tissue type. Genes Immun. 2012;13(2):164-74.

222. Malhotra N, Narayan K, Cho OH, Sylvia KE, Yin C, Melichar H, et al. A network of high-mobility group box transcription factors programs innate interleukin-17 production. Immunity. 2013;38(4):681-93.

223. Spidale NA, Sylvia K, Narayan K, Miu B, Frascoli M, Melichar HJ, et al. Interleukin-17-Producing γδ T Cells Originate from SOX13. Immunity. 2018;49(5):857-72.e5.

224. Moens E, Brouwer M, Dimova T, Goldman M, Willems F, Vermijlen D. IL-23R and TCR signaling drives the generation of neonatal Vgamma9Vdelta2 T cells expressing high levels of cytotoxic mediators and producing IFN-gamma and IL-17. J Leukoc Biol. 2011;89(5):743-52.

225. Dogra P, Rancan C, Ma W, Toth M, Senda T, Carpenter DJ, et al. Tissue Determinants of Human NK Cell Development, Function, and Residence. Cell. 2020;180(4):749-63.e13.

226. Chiu C, Openshaw PJ. Antiviral B cell and T cell immunity in the lungs. Nat Immunol. 2015;16(1):18-26.

227. Shan Q, Li X, Chen X, Zeng Z, Zhu S, Gai K, et al. Tcf1 and Lef1 provide constant supervision to mature CD8. Nat Commun. 2021;12(1):5863.

228. Bertho N, Meurens F. The pig as a medical model for acquired respiratory diseases and dysfunctions: An immunological perspective. Mol Immunol. 2021;135:254-67.

229. Wiarda JE, Trachsel JM, Sivasankaran SK, Tuggle CK, Loving CL. Intestinal single-cell atlas reveals novel lymphocytes in pigs with similarities to human cells. Life Sci Alliance. 2022;5(10).

230. Szabo PA, Levitin HM, Miron M, Snyder ME, Senda T, Yuan J, et al. Single-cell transcriptomics of human T cells reveals tissue and activation signatures in health and disease. Nat Commun. 2019;10(1):4706.

231. Marques RE, Guabiraba R, Russo RC, Teixeira MM. Targeting CCL5 in inflammation. Expert Opin Ther Targets. 2013;17(12):1439-60.

232. Meermeier EW, Zheng CL, Tran JG, Soma S, Worley AH, Weiss DI, et al. Human lung-resident mucosal-associated invariant T cells are abundant, express antimicrobial proteins, and are cytokine responsive. Commun Biol. 2022;5(1):942.

233. Street K, Risso D, Fletcher RB, Das D, Ngai J, Yosef N, et al. Slingshot: cell lineage and pseudotime inference for single-cell transcriptomics. BMC Genomics. 2018;19(1):477.

234. Cao J, Spielmann M, Qiu X, Huang X, Ibrahim DM, Hill AJ, et al. The single-cell transcriptional landscape of mammalian organogenesis. Nature. 2019;566(7745):496-502.

235. Stěpánová K, Sinkora M. The expression of CD25, CD11b, SWC1, SWC7, MHC-II, and family of CD45 molecules can be used to characterize different stages of γδ T lymphocytes in pigs. Dev Comp Immunol. 2012;36(4):728-40.

236. Kavazović I, Han H, Balzaretti G, Slinger E, Lemmermann NAW, Ten Brinke A, et al. Eomes broadens the scope of CD8 T-cell memory by inhibiting apoptosis in cells of low affinity. PLoS Biol. 2020;18(3):e3000648.

237. Peng X, Moore M, Mathur A, Zhou Y, Sun H, Gan Y, et al. Plexin C1 deficiency permits synaptotagmin 7-mediated macrophage migration and enhances mammalian lung fibrosis. FASEB J. 2016;30(12):4056-70.

238. Wein AN, McMaster SR, Takamura S, Dunbar PR, Cartwright EK, Hayward SL, et al. CXCR6 regulates localization of tissue-resident memory CD8 T cells to the airways. J Exp Med. 2019;216(12):2748-62.

239. Di Pilato M, Kfuri-Rubens R, Pruessmann JN, Ozga AJ, Messemaker M, Cadilha BL, et al. CXCR6 positions cytotoxic T cells to receive critical survival signals in the tumor microenvironment. Cell. 2021;184(17):4512-30.e22.

240. Pennitz P, Kirsten H, Friedrich VD, Wyler E, Goekeri C, Obermayer B, et al. A pulmonologist's guide to perform and analyse cross-species single lung cell transcriptomics. Eur Respir Rev. 2022;31(165).

241. Zaas AK, Chen M, Varkey J, Veldman T, Hero AO, Lucas J, et al. Gene expression signatures diagnose influenza and other symptomatic respiratory viral infections in humans. Cell Host Microbe. 2009;6(3):207-17.

242. Zhang Y, Zhou L, Gu G, Feng M, Ding X, Xia Q, et al. CXCL8. Immunol Cell Biol. 2020;98(8):682-92.

243. Powell MD, Read KA, Sreekumar BK, Oestreich KJ. Ikaros Zinc Finger Transcription Factors: Regulators of Cytokine Signaling Pathways and CD4. Front Immunol. 2019;10:1299.

244. Schwickert TA, Tagoh H, Gültekin S, Dakic A, Axelsson E, Minnich M, et al. Stage-specific control of early B cell development by the transcription factor Ikaros. Nat Immunol. 2014;15(3):283-93.

245. Moore MJ, Blachere NE, Fak JJ, Park CY, Sawicka K, Parveen S, et al. ZFP36 RNA-binding proteins restrain T cell activation and anti-viral immunity. Elife. 2018;7.

246. Cannons JL, Qi H, Lu KT, Dutta M, Gomez-Rodriguez J, Cheng J, et al. Optimal germinal center responses require a multistage T cell:B cell adhesion process involving integrins, SLAM-associated protein, and CD84. Immunity. 2010;32(2):253-65.

247. Sun J, Qiu J, Yang Q, Ju Q, Qu R, Wang X, et al. Single-cell RNA sequencing reveals dysregulation of spinal cord cell types in a severe spinal muscular atrophy mouse model. PLoS Genet. 2022;18(9):e1010392.

248. Shannon I, White CL, Yang H, Nayak JL. Differences in Influenza-Specific CD4 T-Cell Mediated Immunity Following Acute Infection Versus Inactivated Vaccination in Children. J Infect Dis. 2021;223(12):2164-73.

249. Lee CM, Oh JE. Resident Memory B Cells in Barrier Tissues. Front Immunol. 2022;13:953088.

250. Barker KA, Etesami NS, Shenoy AT, Arafa EI, Lyon de Ana C, Smith NM, et al. Lung-resident memory B cells protect against bacterial pneumonia. J Clin Invest. 2021;131(11).

251. Kiefer K, Oropallo MA, Cancro MP, Marshak-Rothstein A. Role of type I interferons in the activation of autoreactive B cells. Immunol Cell Biol. 2012;90(5):498-504.

252. Domeier PP, Chodisetti SB, Schell SL, Kawasawa YI, Fasnacht MJ, Soni C, et al. B-Cell-Intrinsic Type 1 Interferon Signaling Is Crucial for Loss of Tolerance and the Development of Autoreactive B Cells. Cell Rep. 2018;24(2):406-18.

253. Man SM, Kanneganti TD. Regulation of lysosomal dynamics and autophagy by CTSB/cathepsin B. Autophagy. 2016;12(12):2504-5.

254. Hernandez-Davies JE, Dollinger EP, Pone EJ, Felgner J, Liang L, Strohmeier S, et al. Magnitude and breadth of antibody cross-reactivity induced by recombinant influenza hemagglutinin trimer vaccine is enhanced by combination adjuvants. Sci Rep. 2022;12(1):9198.

255. Lin Y, Yang X, Yue W, Xu X, Li B, Zou L, et al. Chemerin aggravates DSS-induced colitis by suppressing M2 macrophage polarization. Cell Mol Immunol. 2014;11(4):355-66.

256. Qi J, Sun H, Zhang Y, Wang Z, Xun Z, Li Z, et al. Single-cell and spatial analysis reveal interaction of FAP. Nat Commun. 2022;13(1):1742.

257. Lavelle EC, Ward RW. Mucosal vaccines - fortifying the frontiers. Nat Rev Immunol. 2022;22(4):236-50.

258. Machuca TN, Cypel M, Bonato R, Yeung JC, Chun YM, Juvet S, et al. Safety and Efficacy of Ex Vivo Donor Lung Adenoviral IL-10 Gene Therapy in a Large Animal Lung Transplant Survival Model. Hum Gene Ther. 2017;28(9):757-65.

259. Käser T. Swine as biomedical animal model for T-cell research-Success and potential for transmittable and non-transmittable human diseases. Mol Immunol. 2021;135:95-115.

260. Wang F, Ding P, Liang X, Ding X, Brandt CB, Sjöstedt E, et al. Endothelial cell heterogeneity and microglia regulons revealed by a pig cell landscape at single-cell level. Nat Commun. 2022;13(1):3620.

261. Tohyama S, Kobayashi E. Age-Appropriateness of Porcine Models Used for Cell Transplantation. Cell Transplant. 2019;28(2):224-8.

262. Rodríguez-Gómez IM, Talker SC, Käser T, Stadler M, Reiter L, Ladinig A, et al. Expression of T-Bet, Eomesodermin, and GATA-3 Correlates With Distinct Phenotypes and Functional Properties in Porcine γδ T Cells. Front Immunol. 2019;10:396.

263. Talker SC, Käser T, Reutner K, Sedlak C, Mair KH, Koinig H, et al. Phenotypic maturation of porcine NK- and T-cell subsets. Dev Comp Immunol. 2013;40(1):51-68.

264. Das G, Augustine MM, Das J, Bottomly K, Ray P, Ray A. An important regulatory role for CD4+CD8 alpha alpha T cells in the intestinal epithelial layer in the prevention of inflammatory bowel disease. Proc Natl Acad Sci U S A. 2003;100(9):5324-9.

265. Grandjean CL, Sumaria N, Martin S, Pennington DJ. Increased TCR signal strength in DN thymocytes promotes development of gut TCRαβ. Sci Rep. 2017;7(1):10659.

266. Zhu J, Peng T, Johnston C, Phasouk K, Kask AS, Klock A, et al. Immune surveillance by CD8αα+ skin-resident T cells in human herpes virus infection. Nature. 2013;497(7450):494-7.

267. Liu Q, Zhou YH, Yang ZQ. The cytokine storm of severe influenza and development of immunomodulatory therapy. Cell Mol Immunol. 2016;13(1):3-10.

268. de Prost N, Costa EL, Wellman T, Musch G, Tucci MR, Winkler T, et al. Effects of ventilation strategy on distribution of lung inflammatory cell activity. Crit Care. 2013;17(4):R175.

269. Polidoro RB, Hagan RS, de Santis Santiago R, Schmidt NW. Overview: Systemic Inflammatory Response Derived From Lung Injury Caused by SARS-CoV-2 Infection Explains Severe Outcomes in COVID-19. Front Immunol. 2020;11:1626.

270. Wang D, Ma W. Visualization of IAV Genomes at the Single-Cell Level. Trends Microbiol. 2017;25(10):781-2.

271. Hammouda MB, Ford AE, Liu Y, Zhang JY. The JNK Signaling Pathway in Inflammatory Skin Disorders and Cancer. Cells. 2020;9(4).

272. Rao J, Qian X, Li G, Pan X, Zhang C, Zhang F, et al. ATF3-mediated NRF2/HO-1 signaling regulates TLR4 innate immune responses in mouse liver ischemia/reperfusion injury. Am J Transplant. 2015;15(1):76-87.

273. Hermesh T, Moran TM, Jain D, López CB. Granulocyte colony-stimulating factor protects mice during respiratory virus infections. PLoS One. 2012;7(5):e37334.

274. Suárez-Ramírez JE, Wu T, Lee YT, Aguila CC, Bouchard KR, Cauley LS. Division of labor between subsets of lymph node dendritic cells determines the specificity of the $CD8^+$ T-cell recall response to influenza infection. Eur J Immunol. 2011;41(9):2632-41.

275. Dengler L, Kühn N, Shin DL, Hatesuer B, Schughart K, Wilk E. Cellular changes in blood indicate severe respiratory disease during influenza infections in mice. PLoS One. 2014;9(7):e103149.

276. Chien YS, Su CP, Tsai HT, Huang AS, Lien CE, Hung MN, et al. Predictors and outcomes of respiratory failure among hospitalized pneumonia patients with 2009 H1N1 influenza in Taiwan. J Infect. 2010;60(2):168-74.

277. Ferrero MR, Tavares LP, Garcia CC. The Dual Role of CCR5 in the Course of Influenza Infection: Exploring Treatment Opportunities. Front Immunol. 2021;12:826621.

278. Ferrero MR, Garcia CC, Dutra de Almeida M, Torres Braz da Silva J, Bianchi Reis Insuela D, Teixeira Ferreira TP, et al. CCR5 Antagonist Maraviroc Inhibits Acute Exacerbation of Lung Inflammation Triggered by Influenza Virus in Cigarette Smoke-Exposed Mice. Pharmaceuticals (Basel). 2021;14(7).

279. Laidlaw BJ, Cyster JG. Transcriptional regulation of memory B cell differentiation. Nat Rev Immunol. 2021;21(4):209-20.

280. Jegaskanda S, Vanderven HA, Tan HX, Alcantara S, Wragg KM, Parsons MS, et al. Influenza Virus Infection Enhances Antibody-Mediated NK Cell Functions via Type I Interferon-Dependent Pathways. J Virol. 2019;93(5).

281. Kronstad LM, Seiler C, Vergara R, Holmes SP, Blish CA. Differential Induction of IFN-α and Modulation of CD112 and CD54 Expression Govern the Magnitude of NK Cell IFN-γ Response to Influenza A Viruses. J Immunol. 2018;201(7):2117-31.

282. Muñoz-Moreno R, Martínez-Romero C, García-Sastre A. Induction and Evasion of Type-I Interferon Responses during Influenza A Virus Infection. Cold Spring Harb Perspect Med. 2021;11(10).

283. Pillai PS, Molony RD, Martinod K, Dong H, Pang IK, Tal MC, et al. Mx1 reveals innate pathways to antiviral resistance and lethal influenza disease. Science. 2016;352(6284):463-6.

284. Troeger C, Blacker B, Khalil I, Zimsen S, Albertson S, Abate D, et al. Mortality, morbidity, and hospitalisations due to influenza lower respiratory tract infections, 2017: an analysis for the Global Burden of Disease Study 2017. Lancet Respir Med. 2019;7(1):69-89.

285. Calderón Díaz JA, Fitzgerald RM, Shalloo L, Rodrigues da Costa M, Niemi J, Leonard FC, et al. Financial Analysis of Herd Status and Vaccination Practices for Porcine Reproductive and Respiratory Syndrome Virus, Swine Influenza Virus, and. Front Vet Sci. 2020;7:556674.

286. Kaiser L, Wat C, Mills T, Mahoney P, Ward P, Hayden F. Impact of oseltamivir treatment on influenza-related lower respiratory tract complications and hospitalizations. Arch Intern Med. 2003;163(14):1667-72.

287. Muthuri SG, Venkatesan S, Myles PR, Leonardi-Bee J, Al Khuwaitir TS, Al Mamun A, et al. Effectiveness of neuraminidase inhibitors in reducing mortality in patients admitted to hospital with influenza A H1N1pdm09 virus infection: a meta-analysis of individual participant data. Lancet Respir Med. 2014;2(5):395-404.

288. Whitley RJ, Boucher CA, Lina B, Nguyen-Van-Tam JS, Osterhaus A, Schutten M, et al. Global assessment of resistance to neuraminidase inhibitors, 2008-2011: the Influenza Resistance Information Study (IRIS). Clin Infect Dis. 2013;56(9):1197-205.

289. Hayden FG, Treanor JJ, Fritz RS, Lobo M, Betts RF, Miller M, et al. Use of the oral neuraminidase inhibitor oseltamivir in experimental human influenza: randomized controlled trials for prevention and treatment. JAMA. 1999;282(13):1240-6.

290. Lin KH, Liang JJ, Huang WI, Lin-Chu SY, Su CY, Lee YL, et al. In vivo protection provided by a synthetic new alpha-galactosyl ceramide analog against bacterial and viral infections in murine models. Antimicrob Agents Chemother. 2010;54(10):4129-36.

291. Montoya CJ, Pollard D, Martinson J, Kumari K, Wasserfall C, Mulder CB, et al. Characterization of human invariant natural killer T subsets in health and disease using a novel invariant natural killer T cell-clonotypic monoclonal antibody, 6B11. Immunology. 2007;122(1):1-14.

292. Gu W, Madrid DMD, Yang G, Artiaga BL, Loeb JC, Castleman WL, et al. Unaltered influenza disease outcomes in swine prophylactically treated with α-galactosylceramide. Dev Comp Immunol. 2021;114:103843.

293. Solórzano A, Webby RJ, Lager KM, Janke BH, García-Sastre A, Richt JA. Mutations in the NS1 protein of swine influenza virus impair anti-interferon activity and confer attenuation in pigs. J Virol. 2005;79(12):7535-43.

294. Demedts IK, Bracke KR, Van Pottelberge G, Testelmans D, Verleden GM, Vermassen FE, et al. Accumulation of dendritic cells and increased CCL20 levels in the airways of patients with chronic obstructive pulmonary disease. Am J Respir Crit Care Med. 2007;175(10):998-1005.

295. Hong GH, Kwon HS, Moon KA, Park SY, Park S, Lee KY, et al. Clusterin Modulates Allergic Airway Inflammation by Attenuating CCL20-Mediated Dendritic Cell Recruitment. J Immunol. 2016;196(5):2021-30.

296. Lambrecht BN, Hammad H. Taking our breath away: dendritic cells in the pathogenesis of asthma. Nat Rev Immunol. 2003;3(12):994-1003.

297. Duerrwald R, Schlegel M, Bauer K, Vissiennon T, Wutzler P, Schmidtke M. Efficacy of influenza vaccination and tamiflu® treatment--comparative studies with Eurasian Swine influenza viruses in pigs. PLoS One. 2013;8(4):e61597.

298. Boltz DA, Rehg JE, McClaren J, Webster RG, Govorkova EA. Oseltamivir prophylactic regimens prevent H5N1 influenza morbidity and mortality in a ferret model. J Infect Dis. 2008;197(9):1315-23.

299. Sidwell RW, Huffman JH, Barnard DL, Bailey KW, Wong MH, Morrison A, et al. Inhibition of influenza virus infections in mice by GS4104, an orally effective influenza virus neuraminidase inhibitor. Antiviral Res. 1998;37(2):107-20.

300. Marriott AC, Dove BK, Whittaker CJ, Bruce C, Ryan KA, Bean TJ, et al. Low dose influenza virus challenge in the ferret leads to increased virus shedding and greater sensitivity to oseltamivir. PLoS One. 2014;9(4):e94090.

301. Govorkova EA, Marathe BM, Prevost A, Rehg JE, Webster RG. Assessment of the efficacy of the neuraminidase inhibitor oseltamivir against 2009 pandemic H1N1 influenza virus in ferrets. Antiviral Res. 2011;91(2):81-8.

302. Lee N, Chan PK, Hui DS, Rainer TH, Wong E, Choi KW, et al. Viral loads and duration of viral shedding in adult patients hospitalized with influenza. J Infect Dis. 2009;200(4):492-500.

303. Nicholson KG, Aoki FY, Osterhaus AD, Trottier S, Carewicz O, Mercier CH, et al. Efficacy and safety of oseltamivir in treatment of acute influenza: a randomised controlled trial. Neuraminidase Inhibitor Flu Treatment Investigator Group. Lancet. 2000;355(9218):1845-50.

304. Whitley RJ, Hayden FG, Reisinger KS, Young N, Dutkowski R, Ipe D, et al. Oral oseltamivir treatment of influenza in children. Pediatr Infect Dis J. 2001;20(2):127-33.

305. Belser JA, Maines TR, Creager HM, Katz JM, Tumpey TM. Oseltamivir inhibits influenza virus replication and transmission following ocular-only aerosol inoculation of ferrets. Virology. 2015;484:305-12.

306. Lee LYY, Zhou J, Frise R, Goldhill DH, Koszalka P, Mifsud EJ, et al. Baloxavir treatment of ferrets infected with influenza A(H1N1)pdm09 virus reduces onward transmission. PLoS Pathog. 2020;16(4):e1008395.

307. Oh DY, Lowther S, McCaw JM, Sullivan SG, Leang SK, Haining J, et al. Evaluation of oseltamivir prophylaxis regimens for reducing influenza virus infection, transmission and disease severity in a ferret model of household contact. J Antimicrob Chemother. 2014;69(9):2458-69.

308. Treanor JJ, Hayden FG, Vrooman PS, Barbarash R, Bettis R, Riff D, et al. Efficacy and safety of the oral neuraminidase inhibitor oseltamivir in treating acute influenza: a randomized controlled trial. US Oral Neuraminidase Study Group. JAMA. 2000;283(8):1016-24.

309. Zarogiannis SG, Noah JW, Jurkuvenaite A, Steele C, Matalon S, Noah DL. Comparison of ribavirin and oseltamivir in reducing mortality and lung injury in mice infected with mouse adapted A/California/04/2009 (H1N1). Life Sci. 2012;90(11-12):440-5.

310. Nguyen CT, Suzuki S, Itoh Y, Ishigaki H, Nakayama M, Hayashi K, et al. Efficacy of neuraminidase inhibitors against H5N6 highly pathogenic avian influenza virus in a non-human primate model. Antimicrob Agents Chemother. 2020.

311. Dobson J, Whitley RJ, Pocock S, Monto AS. Oseltamivir treatment for influenza in adults: a meta-analysis of randomised controlled trials. Lancet. 2015;385(9979):1729-37.

312. Grimm D, Staeheli P, Hufbauer M, Koerner I, Martínez-Sobrido L, Solórzano A, et al. Replication fitness determines high virulence of influenza A virus in mice carrying functional Mx1 resistance gene. Proc Natl Acad Sci U S A. 2007;104(16):6806-11.

313. Tumpey TM, Szretter KJ, Van Hoeven N, Katz JM, Kochs G, Haller O, et al. The Mx1 gene protects mice against the pandemic 1918 and highly lethal human H5N1 influenza viruses. J Virol. 2007;81(19):10818-21.

314. Dawson HD, Smith AD, Chen C, Urban JF. An in-depth comparison of the porcine, murine and human inflammasomes; lessons from the porcine genome and transcriptome. Vet Microbiol. 2017;202:2-15.

VITA

Darling Melany de Carvalho Madrid was born in Goiânia, state of Goiás, located in the center of Brazil. Since very young, Melany dedicated a lot of her time caring for animals and decided to join and contribute to the advancement of veterinary medicine. In 2009 she began her studies in the School of Veterinary Medicine and Animal Sciences at the Federal University of Goiás (EVZ/UFG). Throughout her undergraduate work, she was involved in several internships in small animal clinics. In 2012 she was awarded a one year scholarship to study abroad by CAPES/Brafagri, a foundation within the Brazilian Minsitry of Education. From August 2012 to July 2013 she studied at the veterinary school ONIRIS, in Nantes, France, where she also completed her clinical rotations. Returning to Brazil, Melany got involved with microbiology and animal infectious diseases research and completed her senior year in veterinary medicine, graduating in July 2014. In 2015, the Brazilian government awarded her with a two-year scholarship for a Master of Science program in Animal Sciences at the Federal University of Goiás under the supervision of Dr Valéria de Sá Jayme. Her research focused on cattle parasitology and disease control, completing the program and graduating in August 2017. In 2018 she began her PhD in Animal Molecular and Cellular Biology at the University of Florida under the supervision of Dr. John Driver. Her research focused on swine immunology, antiviral strategies and the use of the pig as a model for respiratory infectious diseases. Melany transfered to the University of Missouri in January 2022 to finish her PhD degree in Animal Sciences under the mentorship of the same advisor. This dissertation is the result of that research program and was defended in November of 2022.